

**A MATHEMATICAL STUDY OF THE EFFECT  
OF A MOVING BOUNDARY AND A  
THERMAL BOUNDARY LAYER ON  
DROPLET HEATING AND EVAPORATION**

**IVAN GUSEV**

**PHD**

**2012**

**A MATHEMATICAL STUDY OF THE EFFECT  
OF A MOVING BOUNDARY AND A  
THERMAL BOUNDARY LAYER ON  
DROPLET HEATING AND EVAPORATION**

**IVAN GUSEV**

A thesis submitted in partial fulfilment of the  
requirements of the University of Brighton  
for the degree of Doctor of Philosophy

February 2012

Sir Harry Ricardo Laboratories  
The University of Brighton

## Abstract

Two new solutions to the heat conduction equation, describing transient heating of an evaporating droplet, are suggested. Both solutions take into account the effect of the reduction of the droplet radius due to evaporation, assuming that this radius is a linear function of time. It has been pointed out that the new approach predicts lower droplet surface temperatures and slower evaporation rates compared with the traditional approach. New solutions to the heat conduction equation, describing transient heating of an evaporating droplet, are suggested, assuming that the time evolution of droplet radius  $R_d(t)$  is known. The results of calculations are compared with the results obtained using the previously suggested approach, when the droplet radius was assumed to be a linear function of time during individual time steps, for typical Diesel engine-like conditions. Both solutions predict the same results which indicates that both models are likely to be correct.

Two new solutions to the equation, describing the diffusion of species during multi-component droplet evaporation, are suggested. The first solution is the explicit analytical solution to this equation while the second one reduces the solution of the differential species diffusion equation to the solution of the Volterra integral equation of the second kind. Both solutions take into account the effect of the reduction of the droplet radius due to evaporation, assuming that this radius is a linear function of time. The analytical solution has been incorporated into a zero dimensional CFD code and applied to the analysis of bi-component (50% ethanol – 50% acetone mixture) droplet evaporation at atmospheric pressure.

The transient heat conduction equation, describing heating of a body immersed into gas with inhomogeneous temperature distribution, is solved analytically, assuming that, at a certain distance from the body, gas temperature remains constant. The solution is applied to modelling of body heating in conditions close to those observed in Diesel engines. In the long time limit, the distribution of temperature in the body and gas practically does not depend on the initial distribution of gas temperature.

# Contents

<b>Abstract</b>	<b>i</b>
<b>Contents</b>	<b>ii</b>
<b>List of Tables</b>	<b>iii</b>
<b>List of Figures</b>	<b>iv</b>
<b>Acknowledgements</b>	<b>ix</b>
<b>Declaration</b>	<b>x</b>
<b>Nomenclature</b>	<b>xi</b>
<b>1 Introduction</b>	<b>1</b>
1.1 Motivation . . . . .	1
1.2 Background research . . . . .	2
1.3 Structure of the thesis . . . . .	6
<b>2 Transient heating of an evaporating droplet when droplet is a linear function of time</b>	<b>8</b>
2.1 Introduction of Chapter 2 . . . . .	8
2.2 Basic equations and approximations . . . . .	10
2.3 Analysis of the equations . . . . .	13
2.3.1 Preliminary analysis . . . . .	13
2.3.2 Analytical solution . . . . .	15
2.3.3 Analysis of the general case . . . . .	20
2.4 Analysis of the solutions . . . . .	22

2.5	Numerical vs analytical solutions . . . . .	30
2.6	Conclusions of Chapter 2 . . . . .	33
<b>3</b>	<b>Transient heating of an evaporating droplet with presumed time evolution of its radius</b>	<b>35</b>
3.1	Introduction of Chapter 3 . . . . .	35
3.2	Solution for the case of arbitrary $R_d(t)$ but $T_{d0}(R) = \text{const}$ . . . . .	36
3.3	Solution for the case of arbitrary $R_d(t)$ and $T_{d0}(R)$ . . . . .	38
3.4	Implementation of the new solutions into a numerical code . . . . .	41
3.5	Results . . . . .	41
3.6	Conclusions of Chapter 3 . . . . .	52
<b>4</b>	<b>New solutions to the species diffusion equation inside droplets in the presence of the moving boundary</b>	<b>54</b>
4.1	Introduction of Chapter 4 . . . . .	54
4.2	Basic equations for multi-component droplets . . . . .	55
4.3	Analytical solution of Equation (4.1) . . . . .	58
4.4	Application to bi-component droplets . . . . .	66
4.4.1	Effect of species diffusion . . . . .	66
4.4.2	Combined effects of species and thermal diffusion . . . . .	70
4.5	Conclusions of Chapter 4 . . . . .	75
<b>5</b>	<b>Transient heating of a semitransparent spherical body immersed into a gas with inhomogeneous temperature distribution</b>	<b>78</b>
5.1	Introduction of Chapter 5 . . . . .	78
5.2	Basic equations and assumptions . . . . .	79
5.3	The analytical solution . . . . .	81
5.4	Analysis . . . . .	82
5.5	Conclusions of Chapter 5 . . . . .	87
<b>6</b>	<b>Conclusions</b>	<b>89</b>
	<b>References</b>	<b>93</b>
	<b>Appendices</b>	<b>107</b>

# List of Tables

4.1	Approximations of acetone, ethanol and their mixtures' droplet velocities. . . . .	70
4.2	The measured initial values of droplet temperature, diameter, ambient gas temperature and distance parameter for the same cases as in Table 4.1. . . . .	71

# List of Figures

2.1	A schematic presentation of the plot $R_d$ versus $t$ for an evaporating droplet (solid); approximation of this plot using the conventional approach assuming that $R_d = \text{const}$ during the time step (dotted); approximation of this plot using the new approach assuming that $R_d$ is the linear function of $t$ during each time step (dashed). . . . .	9
2.2	The plots of $\alpha$ versus droplet surface temperature $T_s$ for $M_a = 29$ kg/kmole, $M_f = 170$ kg/kmole ( $\text{C}_{12}\text{H}_{26}$ ), $p = 3000$ kPa, $a = 15.5274$ , $b = 5383, 59$ , $T_g = 1000$ K, and droplet initial radii $5 \mu\text{m}$ (a) and $50 \mu\text{m}$ (b). . . . .	23
2.3	The plots of $T$ versus $\xi = R/R_d$ for the same values of parameters as in Fig. 2.2 and various times (indicated near the curves). The calculations were performed using the new model, taking into account the evaporation process (solid), and ignoring the effects of evaporation (dotted) for $R_{d0} = 5 \mu\text{m}$ (a) and $R_{d0} = 50 \mu\text{m}$ (b). . . . .	25
2.4	The plots of $T_s$ versus time (a) and $R_d$ versus time (b) for heated and evaporating droplets using the conventional (dotted), and new (solid) approaches for $T_g = 1000$ K and $R_{d0} = 5 \mu\text{m}$ . . . . .	26
2.5	The same as Fig. 2.4 but for $R_{d0} = 10 \mu\text{m}$ . . . . .	27
2.6	The same as Fig. 2.4 but for $R_{d0} = 50 \mu\text{m}$ . . . . .	28
2.7	The values of $\Delta \equiv (t_e(\text{new}) - t_e(\text{conventional}))/t_e(\text{new})$ versus $T_g$ for $T_g = 1000$ K and $R_{d0} = 5 \mu\text{m}$ . . . . .	29
2.8	The values of $\text{Error} = \frac{t_e(\text{time step}) - t_e(\text{time step}=0.003 \text{ ms})}{t_e(\text{time step}=0.003 \text{ ms})}$ versus time step for the conventional and new approaches for $T_g = 1000$ K and $R_{d0} = 5 \mu\text{m}$ . . . . .	30

2.9	Comparison of $\theta_s$ vs. $t$ obtained using three different methods: the box scheme (solid); the method developed in this chapter (dotted); and the conventional method for which $R(t)$ is piecewise constant in time (dashed). . . . .	31
2.10	Comparison of $\tilde{R}$ vs. $t$ obtained using three different methods: the box scheme (solid); the method developed in this chapter (dotted); and the conventional method for which $R(t)$ is piecewise constant in time (dashed). . . . .	32
3.1	The plots of $T_s$ versus time (a) and $R_d$ versus time (b) using the conventional model (thick solid), integral model based on Equation (3.11) (dashed) and linear model (thin solid) for a stationary n-dodecane ( $M_f = 170$ kg/kmole) droplet with an initial radius $5 \mu\text{m}$ , evaporating in ambient air at a pressure of $p = 30$ atm = 3000 kPa and temperature 1000 K. . . . .	42
3.2	The same as Fig. 3.1 but for different numbers of iterations in the integral solution. . . . .	44
3.3	The same as Fig. 3.1 but for a droplet with initial radius $50 \mu\text{m}$ . . . .	45
3.4	The same as Figs. 3.1 and 3.3 but for a droplet with initial radius $100 \mu\text{m}$ . . . . .	46
3.5	The same as Fig. 3.1 but for an ambient gas temperature equal to 800 K. . . . .	48
3.6	The same as Figs. 3.1 and 3.5 but for an ambient gas temperature equal to 1200 K. . . . .	49
3.7	The plots of $T$ versus $\xi = R/R_d$ for a stationary n-dodecane ( $M_f = 170$ kg/kmole) droplet with initial radius $5 \mu\text{m}$ , evaporating in ambient air at a pressure of $p = 30$ atm = 3000 kPa and temperature 1000 K. The moments of time are indicated near the curves. The calculations were performed based on Equations (3.11) (derived for constant initial distribution of temperatures inside droplets) and (3.23) (derived for the general case of the arbitrary distribution of the initial temperature inside the droplet). . . . .	50

3.8	The same as Fig. 3.7 but for the general solution (Equation (3.23) applied to the case when the initial distribution of temperature inside the droplet is given by Equation (3.24)). . . . .	51
4.1	The plots of ethanol mass fraction $Y_{\text{eth}}$ versus $\xi = R/R_d$ , as predicted by the conventional model (dashed) and the new model, taking into account the effect of the moving boundary (solid), for times 0.001 s, 0.01 s and 0.03 s. We consider an initial 50% ethanol – 50% acetone mixture and droplets with initial diameter equal to 142.7 $\mu\text{m}$ . . . . .	67
4.2	The plots of $Y_{\text{eth}}(\xi = 1)$ versus time, as predicted by the conventional model (dashed) and the new model, taking into account the effect of the moving boundary (solid). . . . .	68
4.3	The plots of droplet radius $R_d$ versus time, as predicted by the conventional model (dashed) and the new model, taking into account the effect of the moving boundary (solid). . . . .	68
4.4	The plots of Spalding mass transfer number $B_M$ versus time, as predicted by the conventional model (dashed) and the new model, taking into account the effect of the moving boundary (solid). . . . .	69
4.5	The time evolution of droplet surface, average and centre temperatures ( $T_s$ , $T_{\text{av}}$ and $T_c$ ), predicted by the one-way Solution A for the non-ideal model, taking and not taking into account the effects of the moving boundary during individual time steps (moving and stationary boundaries) on the solutions to both heat transfer and species diffusion equations for the 25% ethanol – 75% acetone mixture droplets with the values of the initial parameters, droplet velocity and gas temperature given in Tables 4.1 and 4.2 (a); the same as (a) but for the 50% ethanol – 50% acetone mixture droplets (b). . . . .	72

4.6	The time evolution of droplet surface temperatures ( $T_s$ ) and radius ( $R_d$ ), predicted by the one-way Solution A for the non-ideal model, taking and not taking into account the effects of the moving boundary during individual time steps on the solutions to the heat transfer equation only, species diffusion equation only and both heat transfer and species diffusion equations for the 50% ethanol – 50% acetone mixture droplets with the values of the initial parameters, and gas temperature given in Table 4.2, assuming that the droplet velocity is constant and equal to 12.71 m/s. . . . .	73
4.7	The same as Fig. 4.6 but for the gas temperature equal to 1000 K. . . . .	75
4.8	The same as Fig. 4.7 but for the mass fraction of ethanol at the surface of the droplet. . . . .	76
5.1	A schematic presentation of a spherical body of radius $R_b$ immersed in the center of a gaseous sphere of radius $R_g$ . . . . .	79
5.2	The plots of $\hat{T} \equiv (T_{g0}(R_g) - T(R, t)) / (T_{g0}(R_g) - T_{b0})$ versus $r = R/R_b$ for $r_g \equiv R_g/R_b = 3.301$ and four Fo (indicated near the curves). Solid curves refer to the initial distribution (5.15), while dashed curves refer to the initial distribution (5.14). The thickness of the curves is inversely proportionate to Fo. . . . .	84
5.3	The same as Fig. 5.2 but for $r_g = 11.337$ . . . . .	85
5.4	The plots of $\hat{T}_s \equiv (T_{g0}(R_g) - T_s(R, t)) / (T_{g0}(R_g) - T_{b0})$ versus Fo for $r_g = 3.301$ and distribution (5.15) (solid), $r_g = 11.337$ and distribution (5.15) (dashed-dotted), $r_g = 3.301$ and distribution (5.14) (thick dashed), $r_g = 11.337$ and distribution (5.14) (thin dashed). . . . .	86
5.5	The plots of $\chi$ versus Fo for four $r_g$ (indicated near the curves). Solid curves refer to the initial distribution (5.15). while dashed curves refer to the initial distribution (5.14). . . . .	87

# Acknowledgements

First of all I would like to thank my supervisors Prof. Sergei Sazhin and Prof. Morgan Heikal for their support during my work on this project. Also I am grateful to Dr. Pavel Krutitskii, Dr. Michael Vynnycky, Dr. Sarah Mitchell, Dr. Elena Sazhina, Dr. Guillaume Castanet, Prof. Fabrice Lemoine and Mr. Ahmed Elwardany for their criticism, support and valuable contributions to this work.

Last, but not least, I would like to thank my family and friends who gave me much inspiration and a moral boost.

Finally I am grateful to the European Regional Development Fund Franco-British INTERREG IVA (Project C5, Reference 4005) for the financial support of this project.

# Declaration

I declare that the research contained in this thesis, unless otherwise formally indicated within the text, is the original work of the author. The thesis has not been previously submitted to this or any other university for a degree, and does not incorporate any material already submitted for a degree.

Signed:

Dated:

# Nomenclature

$a, b$	coefficients introduced in Equation (2.7) or $1/\sqrt{\kappa}$
$a_{b,g}$	coefficients introduced in Eq. (5.9) ( $\sqrt{s}/m$ )
$b$	weight (see Appendix 7) [ $J/(m^3 K)$ ]
$A$	function defined by Eq. (A711)
$B$	function defined by Eq. (A711)
$B_M$	Spalding mass transfer number
$c$	specific heat capacity [ $J/(kg K)$ ]
$c_0$	parameter defined by (A13)
$C_F$	friction drag coefficient
$D$	diffusion coefficient [ $m^2/s$ ]
$f$	function defined in (2.32) or in (4.30)
$F(t, \xi)$	$u(t, R)$ or function introduced in Equations (4.11) or (4.14)
$Fo$	Fourier number
$G$	function introduced in Equation (2.49),(3.5) or (4.51)
$h$	convective heat transfer coefficient [ $W/(m^2 K)$ ]
$h_0$	$\frac{h(t)}{k_l} R_d(t) - 1 - \frac{R'_d(t) R_d(t)}{2\kappa}$
$h_1$	function introduced in Equation (4.48)
$H$	variable introduced in Equation (2.13) or (4.18)
$k$	thermal conductivity [ $W/(m K)$ ]
$L$	specific heat of evaporation [ $J/kg$ ]
$Le$	Lewis number
$m$	mass [ $kg$ ]
$M$	molar mass [ $kg/kmole$ ]
$M(t)$	variable introduced in Equation (2.11)
$Nu$	Nusselt number

$p$	pressure [Pa] or parameter introduced in Equation (4.23)
$p_n(t)$	functions introduced in Eq. (5.9) [K m/s]
$P$	thermal radiation power density [K/s]
$Pr$	Prandtl number
$q$	function introduced in Equation (2.33)
$q''$	heat flux [W/m <sup>2</sup> ]
$\dot{q}$	heat rate [W]
$q_n$	parameter introduced in Equation (4.31)
$q_K$	function introduced in Equation (2.19)
$r_{(g)}$	$R_{(g)}/R_b$
$R$	distance from the center [m]
$\tilde{R}$	$\frac{R_d}{R_{d0}}$
$R_{d,b}$	droplet radius [m]
$R_g$	radius of the gaseous sphere [m]
$R_u$	universal gas constant [J/(K mole)]
Re	Reynolds number
Sc	Schmidt number
Sh	Sherwood number
$t$	time (s)
$t_0$	beginning of the timestep
$t_{00}$	parameter introduced in Equation (A18)
$T$	temperature [K]
$\tilde{T}_{(b,gs)}$	$T_{(b_0,g_0)}(R, t)/T_{g_0}(R_g)$
$\hat{T}_{(s)}$	$(T_{g_0}(R_g) - T_{(s)}(R, t))/(T_{g_0}(R_g) - T_{b_0})$
$u$	$TR$ or $(T - T_{g_0}(R_g))R$
$U(t, R)$	function defined by Equation (3.13)
$U_s$	maximal surface velocity [m/s]
$v$	$u - RT_{d0}$ or function defined by Equation (3.17)
$v_n$	functions introduced in Equations (2.25) or (5.10) or (4.23)
$\ v_n\ ^2$	norm of $v_n$ [J/(m <sup>2</sup> K)]
$V$	function introduced by Equation (2.23) or (4.20)
$\mathcal{V}$	function introduced in Equation (2.49) or (4.51)

$W$	function introduced by Equation (2.17) or (4.14)
$X$	molar fraction
$Y$	mass fraction

### Greek symbols

$\alpha$	evaporation rate introduced in Equation (2.8)
$\alpha_m$	parameter defined by Equation (4.3)
$\delta_{T0}$	thermal ‘film’ thickness [m]
$\Delta$	$(t_{e \text{ (new)}} - t_{e \text{ (conventional)}})/t_{e \text{ (new)}}$
$\Delta t$	time step [s]
$\Delta T$	$T_g - T_s$ [K]
$\gamma$	activity coefficient
$\epsilon$	evaporation rate
$\Theta$	function defined by Equation (2.25) or (A61) or (4.22)
$\theta_s$	$\frac{T_s - T_0}{\Delta T}$
$\check{\Theta}$	function defined by Equation (4.44)
$\kappa$	thermal diffusivity (m <sup>2</sup> /s)
$\lambda, \lambda_n$	eigenvalues defined by Equations (2.28),(4.26),(4.28) or (5.11)
$\mu(t)$	variable introduced by Equation (2.13) or (4.18)
$\hat{\mu}_0(t)$	variable introduced in Equation (4.49)
$\nu(t)$	function defined by Equation (3.5) or kinematic viscosity
$\omega(t, \tau)$	function defined in Appendix 3
$\Omega(t, \tau)$	function defined in Appendix 3
$\xi$	$R/R_d(t)$
$\chi$	parameter defined by Eq. (5.19)
$\chi_Y$	parameter defined by Equation (4.6)
$\rho$	density [kg/ m <sup>3</sup> ]
$\psi(t)$	$W(t, 1)$

### Subscripts

$a$	air
amb	ambient

<i>b</i>	body or boiling
<i>d</i>	droplet
<i>e</i>	evaporation
<i>eff</i>	effective
<i>eth</i>	ethanol
<i>f</i>	fuel
<i>g</i>	gas
<i>i</i>	species
<i>iso</i>	isolated
<i>l</i>	liquid
<i>n</i>	timesteps in the integration
<i>p</i>	constant pressure
<i>part</i>	particular
<i>s</i>	surface
<i>v</i>	vapour
0	initial
$\infty$	ambient conditions

# Chapter 1

## Introduction

### 1.1 Motivation

The problem of the modelling of droplet heating and evaporation has attracted considerable attention in the research community and a number of advanced models have been suggested and developed [1]. Most of these models have been based on the hydrodynamic approximation, but kinetic models and even models based on molecular dynamic simulation have also been developed [2–8]. At the same time, practically none of these advanced models have been widely used in the engineering community where the problem of droplet heating and evaporation constitutes a relatively small part of the multi-dimensional modelling of complex processes involving the effects of 3D geometry, chemical reactions, turbulence and so on. In most cases, this modelling has been performed based on commercial or research computational fluid dynamics (CFD) codes. A typical example of this type of modelling is the simulation of the processes in Diesel engines described in [9, 10]. In this case, the models of droplet heating and evaporation are typically based on a number of rather restrictive assumptions, including the assumption that the thermal conductivity of droplets is infinitely large and, in the case of multi-component droplets, the diffusivity of species within them is infinitely large or small [11–13]. Kinetic effects have been ignored. In most recent developments, the effects of finite thermal conductivity and recirculation in droplets was taken into account in the modelling of droplet heating and evaporation [14–18]. In contrast to the previously developed models, the approach suggested in these papers is based on the analytical solution to the

heat conduction equation inside droplets. It was shown that this approach is more efficient, compared with the one based on the numerical solution to this equation, both from the point of view of accuracy and of CPU efficiency [16].

In this thesis, a number of new models of droplet heating and evaporation have been developed, where these effects have been taken into account alongside new ones such as those of the moving boundary of droplets, due to evaporation, and the effect of the thermal boundary layer around droplets. As in the case of the previously developed models (for example [14–18]) the new models are based either on the analytical solutions of the underlying heat transfer or species diffusion equations or on the reduction of these equations to the integral equations. The format of most of these models is such that they can be incorporated into CFD codes and used for modelling real-life engineering processes. Here lies the main motivation for this work: the development of new mathematical tools, combining high accuracy and CPU efficiency, for engineering applications. These applications are primarily focused on modelling the processes in Diesel engines, although a much wider range of applications is anticipated in the future.

The results of the thesis have been presented in the following papers published in international refereed journals [19–24] and refereed conference proceedings [25–33].

## 1.2 Background research

The problem of the modelling of droplet or solid body heating/cooling and evaporation has been discussed in numerous papers (for example [15, 34]) and the results have been summarised in a number of reviews and monographs, including [1, 35–37] (see [19, 20, 38] for the most recent developments in this area).

The importance of accurately modelling these processes in engineering applications is widely accepted (for example [36]). In Diesel engine combustion, for example, this has a significant effect on the prediction of the ignition delay period and combustion processes [9, 10]. These in turn affect emission formation and fuel consumption.

Following [11] the models of droplet heating can be subdivided into the following groups in order of ascending complexity:

- 1) models based on the assumption that the droplet surface temperature is uniform and does not change with time;
- 2) models based on the assumption that there is no temperature gradient inside droplets (infinite thermal conductivity of liquid);
- 3) models taking into account finite liquid thermal conductivity, but not the re-circulation inside droplets (conduction limit);
- 4) models taking into account both finite liquid thermal conductivity and the re-circulation inside droplets via the introduction of a correction factor to the liquid thermal conductivity (effective conductivity models);
- 5) models describing the re-circulation inside droplets in terms of vortex dynamics (vortex models);
- 6) models based on the full solution of the Navier-Stokes equations.

The first group allows the reduction of the dimensions of the system via the complete elimination of the equation for droplet temperature. This appears to be particularly attractive for the analytical studies of droplet evaporation and thermal ignition of fuel vapour/air mixture (see [39–43]). This group of models, however, appears to be too simplistic for application in most computational fluid dynamics (CFD) codes. Groups (5) and (6) have not been used and are not expected to be used in these codes in the foreseeable future due to their complexity. These models are widely used for validation of more basic models of droplet heating, or for in-depth understanding of the underlying physical processes (see [11, 35, 44–46]). Traditionally, in most CFD codes, droplet heating has been modelled assuming that the thermal conductivity of droplets is infinitely large, and there is no temperature gradient inside droplets (second group of models)(for example [42, 47]). This assumption contradicts direct measurements of the temperature distribution inside droplets [14, 38, 48–50]. Bertoli and Migliaccio [51] were perhaps the first to draw attention to the fact that taking into account the temperature gradient inside droplets can considerably increase the accuracy of CFD modelling of combustion processes in Diesel engines. The analysis by these authors was based on the numerical solution of the heat conduction equation inside droplets. However, this approach led to a considerable increase in the required computational time – a serious drawback. Also, the effects of internal liquid recirculation inside droplets were ignored in [51]. An alter-

native approach was suggested and developed in [1, 15–17, 52]. In these papers both finite liquid thermal conductivity and recirculation inside droplets (via the effective thermal conductivity (ETC) model [44]) were taken into account by incorporating the analytical solution to the heat conduction equation inside the droplet into a numerical scheme. The liquid thermal conductivity inside droplets was replaced by the effective thermal conductivity to take into account liquid recirculation [44]. The temperature distribution inside droplets at the end of the integration time step, predicted by the analytical solution, was used as the initial condition for the next time step. This approach was shown to be considerably more efficient (both from the point of view of accuracy and of computer efficiency) than the one used in [51] (see [16]).

The models for droplet heating used in [15–17, 51] were implicitly based on the assumptions that the evaporation rate of droplets is small and the value of droplet radius does not change during any time step (although this radius changes from one step to another). This means that the effect of a moving boundary on droplet heating was ignored. This is a well known approach used in all available CFD codes (for example [42, 47]).

The species diffusion equation in liquids and gases, describing the dynamics of multi-component systems, has been widely discussed in the literature [53]. One of the most important applications of this equation is that to the analysis of heating and evaporation of multi-component droplets [1, 54]. In realistic moving droplets, species diffusion takes place alongside species convection when Hill-type vortices are formed inside droplets [55]. In most practically relevant cases, however, the details of species distribution inside droplets are not important and the effects of species diffusion and convection can be described in terms of the spherically symmetric effective diffusivity model [1] in which the actual diffusivity of liquid species is replaced by the effective diffusivity. The models of multi-component droplet heating and evaporation are generally subdivided into two main groups: those based on the analysis of individual components [55–61], applicable in the case when a small number of components needs to be taken into account, and those based on the probabilistic analysis of a large number of components [62–65]. In the second family of models a number of additional simplifying assumptions were used, including the

assumption that species inside droplets mix infinitely quickly. Models containing features of both these groups of models have been suggested in [66]. Most of the models belonging to the first group are based on the numerical solution to the species diffusion equation inside droplets. At the same time the analysis of [38, 50] was based on the analytical solution to this equation. The model in [38] was applied to the analysis of heating and evaporation of bi-component ethanol/acetone droplets. The authors of [38] based their analysis on the analytical solution to the species diffusion equation, which was incorporated into the numerical code. This approach is expected to be more CPU efficient and accurate compared with the one based on the conventional approach [50]. The model described in [38] has been generalised in [50] to take into account coupling between droplets and gas. None of these models took into account the effects of the moving boundary due to evaporation on the species diffusion equation.

Most of the models of droplet heating and evaporation suggested so far are based on the assumption that gas in computational cells is always homogeneous and the gas temperature in the immediate vicinity of the droplet surface is the same as in the rest of the cell [1, 37]. The droplet heating in this case is described based on Newton's law with gas ambient temperature assumed equal to gas temperature at any point of the cell. The validity of this approach has been investigated in [52], where the effects of a sudden immersion of a body into a homogeneous gas have been studied. In the model, described in [52], gas temperature was fixed at a certain distance from the surface of the body and assumed equal to the ambient temperature, while gas temperature near the body was allowed to change with time alongside the temperature inside the body. As follows from the analysis of [52], noticeable deviations from the predictions of the conventional Newton's law, used in CFD codes, were observed. At the initial stage, the body was heated up (or cooled down) much more quickly than predicted by Newton's law, while at the final stages the body heating/cooling followed Newton's law, but with the values of the heat transfer coefficient smaller or larger than predicted by the conventional model, depending on the thickness of the region where gas temperature was allowed to change. In the limit of an infinitely large gaseous area around the body the predictions of [52] turned out to be identical with the predictions based on the

model described in [67]. The latter model is based on an approach which differs from the one used in [52]. One of the main limitations of the model described in [52] is that it was based on the assumption that initially gas temperature was homogeneous in the whole domain. This imposes a serious limitation for practical applications of this model in a realistic environment when the ambient temperature can vary with time.

Near-critical and supercritical droplet heating and evaporation was covered in relatively recent reviews [68, 69], and [64]. Analysis of the interaction between droplets, collisions, coalescence, atomization, oscillations (including instabilities of evaporating droplets) and size distribution were considered in [70–85]). The problem of heating and evaporation of droplets on heated surfaces was considered in [82, 86]. The problem of droplet heating and evaporation is related to spray combustion (see [9, 10, 87–89]). Two groups of models for radiative heating of droplets have been considered: the one based on the assumption that droplets are opaque grey spheres [42, 47, 90], and the one based on the assumption that droplets are semi-transparent for thermal radiation [91–97]. The first approach is the one used in all CFD codes which are known to us, while the second one is much more appropriate from the point of view of underlying physics. The Soret effect describes the flow of matter caused by a temperature gradient (thermal diffusion), while the Dufour effect describes the flow of heat caused by concentration gradients. The two effects occur simultaneously. Both effects are believed to be small in most cases although sometimes their contribution may be significant (see [98–102]). Kinetic and molecular dynamics effects on droplet heating and evaporation were considered in [2–5, 7, 103, 104]. All effects mentioned in this paragraph will be ignored in our analysis.

### 1.3 Structure of the thesis

In Chapter 2 a model for mono-component droplet heating and evaporation, based on the assumption that droplet radius is a linear function of time during time steps, is presented and discussed. A more general model, based on the assumption that droplet radius is an *a priori* known function of time, is discussed in Chapter 3.

In Chapter 4 the effects of the moving boundary on the solution to the species diffusion equation in multi-component droplets are discussed. A model for body heating/cooling, when this body is immersed into an ambient gas with temperature varying with distance from the surface of the body, is presented in Chapter 5. The main results of the thesis are summarised in Chapter 6.

# Chapter 2

## Transient heating of an evaporating droplet when droplet is a linear function of time

### 2.1 Introduction of Chapter 2

Taking into account the effect of receding droplet radius on droplet heating and evaporation leads to the well known Stefan problem, which has been widely discussed in the literature (e.g. [105]-[54]), but has been rarely applied to engineering sprays, due to the complex structure. Hence, a substantial gap has developed between mathematical and engineering research in this field. The main objective of this work is to fill this particular gap. This will include the development of an appropriate mathematical model for specific spray applications, and the actual application of this model to simulate droplet heating and evaporation processes in Diesel engine-like conditions. There has been no previous research in this direction to the best of our knowledge.

The essence of the difference between the new approach to the modelling of droplet heating and evaporation, suggested in this chapter, and the traditional approach is schematically illustrated in Fig. 2.1. As follows from this figure, the approximation of the reduction of the droplet radius during the time step by the linear function is noticeably much more accurate than the approximation based on the assumption that the droplet radius is constant during the time step (the conventional approach

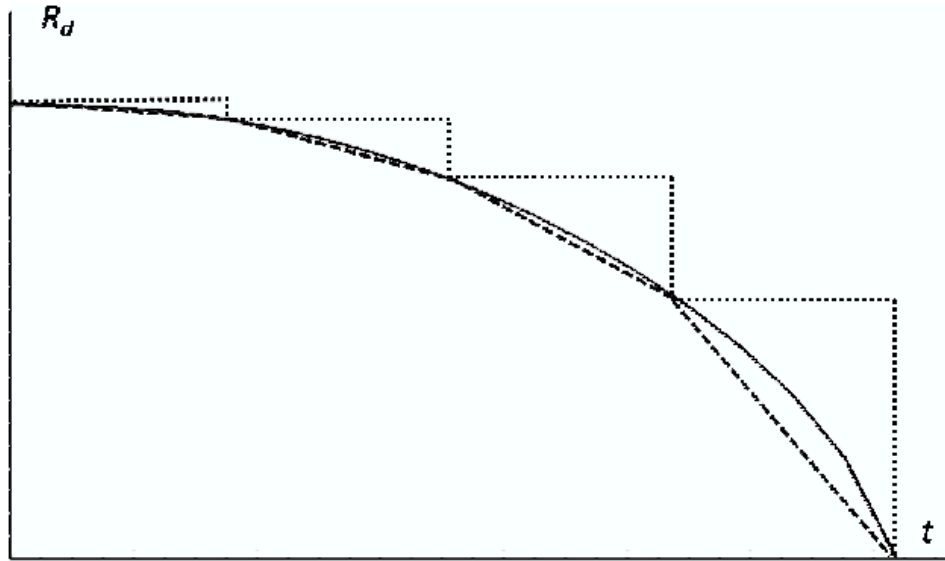


Figure 2.1: A schematic presentation of the plot  $R_d$  versus  $t$  for an evaporating droplet (solid); approximation of this plot using the conventional approach assuming that  $R_d = \text{const}$  during the time step (dotted); approximation of this plot using the new approach assuming that  $R_d$  is the linear function of  $t$  during each time step (dashed).

used in CFD codes). This difference, however, can be mitigated by choosing sufficiently small time steps (more time steps would be required in the case when the reduction of droplet radius during the time step is ignored than in the case when it is taken into account). A more important implication of the new approach, compared with the traditional one, however, is that the effect of the reduction of droplet radius on droplet heating is explicitly taken into account in the new approach at every time step. This leads to the prediction of temperatures different compared with the ones predicted by the traditional approach, regardless of how many time steps are used in the analysis. These differences in droplet temperatures lead to different time dependencies of droplet radii. These effects will be illustrated in this chapter using examples of fuel droplet heating and evaporation in Diesel engine-like conditions.

The basic equations and approximations of the new model are described in Section 2. The analysis and solutions of these basic equations are given in Section 3. In Section 4, one of these solutions is analysed for the values of parameters typical for Diesel engines. The main results of the chapter are summarised in Section 5.

## 2.2 Basic equations and approximations

Let us assume that an evaporating droplet is immersed into a homogeneous hot gas at constant temperature  $T_g$ . The droplet is heated by convection, with the convection heat transfer coefficient  $h(t)$  depending on time  $t$  and droplet radius  $R_d(t)$ , and cools down due to evaporation.  $R_d(t)$  is a continuously differentiable function of time in the range  $0 \leq t \leq t_e$ , where  $t_e$  is the evaporation time. Both  $R_d(t)$  and  $h(t)$  are assumed to be known. Effects of thermal radiation are taken into account. The changes in the droplet temperature ( $T \equiv T(t, R)$ ) are described by the heat conduction equation in the form [105, 106]:

$$\frac{\partial T}{\partial t} = \kappa \left( \frac{\partial^2 T}{\partial R^2} + \frac{2}{R} \frac{\partial T}{\partial R} \right) + P(R) \quad (2.1)$$

for  $0 \leq t < t_e$ ,  $0 \leq R < R_d(t)$ , where  $\kappa$  is liquid thermal diffusivity ( $\kappa = k_l / (c_l \rho_l) = \text{const}$ ),  $k_l$  is the liquid thermal conductivity,  $c_l$  is the liquid specific heat capacity,  $\rho_l$  is the liquid density,  $R$  is the distance from the centre of the droplet.

The term  $P(R)$  takes into account the effects of thermal radiation, assuming that droplets are semi-transparent (radiation can penetrate inside droplets). Various approximations for  $P(R)$  were suggested in [91]–[107].

Remembering the physical background of the problem, we look for the solution of this equation in the form of a twice continuously differentiable function  $T \equiv T(t, R)$  for  $0 \leq t < t_e$ ,  $0 \leq R < R_d(t)$ . This solution should satisfy the boundary condition:

$$\left( k_l \frac{\partial T}{\partial R} + hT \right) \Big|_{R=R_d(t)} = hT_g + \rho_l L \dot{R}_d(t), \quad (2.2)$$

$T$  is finite and continuous at  $R \rightarrow +0$ ,  $T_s = T(R_d(t), t)$  is the droplet's surface temperature,  $L$  is the specific heat of evaporation. We took into account that  $\dot{R}_d(t) \equiv dR_d/dt \leq 0$ . Effects of swelling are ignored. Equation (2.2) is just the energy balance condition at  $R = R_d(t)$ . The initial condition is taken in the form:

$$T(t=0) = T_0(R), \quad (2.3)$$

where  $0 \leq R \leq R_{d0} = R_d(t=0)$ .

The value of  $R_d(t)$  is controlled by fuel vapour diffusion from the droplet surface, and can be found from the equation [1]:

$$\dot{R}_d = - \frac{k_g \ln(1 + B_M)}{\rho_l c_{pg} R_d}, \quad (2.4)$$

where

$$B_M = \frac{Y_{vs} - Y_{v\infty}}{1 - Y_{vs}}, \quad (2.5)$$

is the Spalding mass transfer number,  $Y_{fs}$  is the mass fraction of fuel vapour near the droplet surface:

$$Y_{fs} = \left[ 1 + \left( \frac{p}{p_{fs}} - 1 \right) \frac{M_a}{M_f} \right]^{-1}, \quad (2.6)$$

$Y_{v\infty}$  is the mass fraction of fuel vapour in ambient gas (in our analysis we assume  $Y_{v\infty} = 0$ ),

$p$  and  $p_{fs}$  are ambient pressure and the pressure of saturated fuel vapour near the surface of the droplet respectively,  $M_a$  and  $M_f$  are molar masses of air and fuel;  $p_{fs}$  is calculated from the Clausius-Clapeyron equation presented in the form:

$$p_{fs} = \exp \left[ a - \frac{b}{T_s - 43} \right], \quad (2.7)$$

$a$  and  $b$  are constants to be specified for specific fuels,  $T_s$  is the surface temperature of fuel droplets in K;  $p_{fs}$  predicted by Equation (2.7) is in kPa.

In [15] it was assumed that  $R_d = \text{const}$ , while the contribution of  $\dot{R}_d$  was taken into account by replacing gas temperature with the so called effective temperature. It was assumed that this approach is applicable when used during relatively short times (time steps in computational fluid dynamics (CFD) codes), but it has never been rigorously justified. The focus of this chapter is on the effects of changing droplet radius during the time step on the heating of droplets.

The current state of the development of mathematical tools for the solution of this type of problem is described by Kartashov [105]. In the following analysis, some of the results described in [105] will be adapted to the investigation of our problem.

A number of simplifying assumptions will be made. Firstly, the contribution of thermal radiation will be ignored ( $P(R) = 0$ ). Secondly, we assume that  $R_d(t)$  is the linear function of  $t$ :

$$R_d(t) = R_{d0}(1 + \alpha t). \quad (2.8)$$

Remembering (2.4), the explicit expression for  $\alpha$  can be presented as:

$$\alpha = - \frac{k_g \ln(1 + B_M)}{\rho_l c_{pg} R_{d0}^2}. \quad (2.9)$$

The effect of thermal radiation on droplet heating and evaporation in Diesel engine-like conditions has been considered in a number of papers including [96,

108]. As follows from the analysis of [96], in the case when external temperature, responsible for radiative heating, is about or less than 1000 K the effect of radiation on droplet evaporation is less than about 1% (see Fig. 2.3 of [96]). This justifies our assumption that  $P(R) = 0$ .

The second assumption is justified if the results are applied to a relatively short period of time, when  $R_d(t)$  can be expanded into a Taylor series in time and only the first two terms are retained (in our previous analyses and in all CFD codes known to us, only the zeroth terms were used). In this case,  $t = 0$  will refer to the beginning of the time step  $t_0$ ,  $t_e$  will refer to  $t_0 + \Delta t$ , where  $\Delta t$  is the time step.

Note that Brenn [54], considering a different problem of calculating the concentration field in evaporating droplets, assumed that  $R_d^2$ , rather than  $R_d$ , is a linear function of time during the whole evaporation process:

$$R_d^2(t) = R_{d0}^2 - \alpha' t. \quad (2.10)$$

This could be justified by Eq. (2.4) assuming that  $B_M = \text{const}$ . In our case this assumption can be made during the time step but not during the whole evaporation process. For sufficiently small time steps, both approaches lead to identical results since:

$$R_d = R_{d0} \sqrt{1 - \alpha' t / R_{d0}^2} \approx R_{d0} (1 + \alpha t),$$

where  $\alpha = -\alpha' / (2R_{d0}^2)$ .

The problem considered in [54] is more general compared with the one considered in this chapter, as the 3D effects on species concentrations were taken into account in that paper. If only the radial dependence of this concentration is taken into account, Eq. (1) of [54] would have exactly the same structure as Eq. (2.1) in this chapter. However, the solution of his equation cannot be used for our equation due to different boundary conditions used in our papers.

Among other assumptions used in our analysis we mention that the effects of the interaction between droplets were ignored. This can be justified when the distance parameter (ratio of the distance between droplets to their diameters) is large (see [49] for details).

## 2.3 Analysis of the equations

### 2.3.1 Preliminary analysis

Let us rewrite boundary condition (2.2) in the form:

$$\left(\frac{\partial T}{\partial R} + \frac{h}{k_l}T\right)\Big|_{R=R_d(t)} = \frac{h}{k_l}T_g + \frac{\rho_l}{k_l}L\dot{R}_d(t) \equiv M(t), \quad (2.11)$$

and introduce the new variable  $u = TR$ . Using this new variable, we can rewrite Equation (2.1) as:

$$\frac{\partial u}{\partial t} = \kappa \frac{\partial^2 u}{\partial R^2}, \quad (2.12)$$

for  $t \in [0, t_e]$  (or  $t \in [t_0, t_0 + \Delta t]$ ),  $R \in [0, R_d(t)]$  with the boundary conditions:

$$\left(\frac{\partial u}{\partial R} + H(t)u\right)\Big|_{R=R_d(t)} = \mu(t), \quad (2.13)$$

$$u|_{R=0} = 0, \quad (2.14)$$

where:

$$H(t) = \frac{h(t)}{k_l} - \frac{1}{R_d(t)}, \quad \mu(t) = M(t)R_d(t)$$

for  $t \in [0, t_e]$  (or  $t \in [t_0, t_0 + \Delta t]$ ).

The initial condition is:

$$u(t, R)|_{t=0} = RT_0(R) \quad (2.15)$$

for  $R \in [0, R_{d0}]$ .

Following Kartashov [105], we introduce a new variable

$$\xi = R/R_d(t),$$

and a new function

$$F(t, \xi) = u(t, R).$$

This new variable allows us to reduce the problem with a moving boundary to the one with a stationary boundary, since:

$$0 \leq \xi \leq 1 \quad \text{when} \quad 0 \leq R \leq R_d(t).$$

Since

$$u'_t = F'_t + F'_\xi \xi'_t = F'_t - \xi \frac{R'_d(t)}{R_d(t)} F'_\xi; \quad u'_R = F'_\xi \xi'_R = \frac{F'_\xi}{R_d(t)}; \quad u''_{RR} = \frac{F''_{\xi\xi}}{R_d^2(t)},$$

we can rewrite Equation (2.12) as

$$R_d^2(t)F_t' = \kappa F_{\xi\xi}'' + \xi R_d'(t)R_d(t)F_\xi'. \quad (2.16)$$

Equation (2.16) is identical to the one studied in [109], where the distribution of temperature in the melting region was considered (plane problem).

Equation (2.16) is to be solved for  $t \in [0, t_e]$  (or  $t \in [t_0, t_0 + \Delta t]$ ) and  $0 \leq \xi \leq 1$ . Initial and boundary conditions for this equation can be presented as:

$$F|_{t=0} = R_{d0}\xi T_0(\xi R_{d0}), \quad 0 \leq \xi \leq 1,$$

$$F|_{\xi=0} = 0, \quad (F_\xi' + \tilde{H}(t)F)|_{\xi=1} = \tilde{\mu}(t), \quad 0 \leq t \leq t_e \quad (\text{or } t \in [t_0, t_0 + \Delta t]),$$

where  $\tilde{H}(t) = H(t)R_d(t)$ ,  $\tilde{\mu}(t) = M(t)R_d^2(t)$ .

Following Kartashov [105], we introduce the new unknown function  $W(t, \xi)$  via the relation:

$$F(t, \xi) = \frac{1}{\sqrt{R_d(t)}} \exp\left[-\frac{R_d'(t)R_d(t)}{4\kappa}\xi^2\right] W(t, \xi). \quad (2.17)$$

From Equation (2.17) we obtain the following expressions for the derivatives:

$$\begin{aligned} F_t' &= \left\{ -\left[ \frac{1}{2}R_d^{-3/2}(t)R_d'(t) + R_d^{-1/2}(t) \left( \frac{(R_d'(t))^2 + R_d(t)R_d''(t)}{4\kappa}\xi^2 \right) \right] W(t, \xi) \right. \\ &\quad \left. + R_d^{-1/2}(t)W_t'(t, \xi) \right\} \exp\left[-\frac{R_d'(t)R_d(t)}{4\kappa}\xi^2\right], \\ F_\xi' &= \left\{ -\frac{2\xi R_d'(t)R_d(t)}{4\sqrt{R_d(t)}\kappa} W(t, \xi) + \frac{1}{\sqrt{R_d(t)}} W_\xi'(t, \xi) \right\} \exp\left[-\frac{R_d'(t)R_d(t)}{4\kappa}\xi^2\right], \\ F_{\xi\xi}'' &= \left\{ \frac{2}{\sqrt{R_d(t)}} \left[ -\frac{R_d(t)R_d'(t)}{4\kappa} + 2\xi^2 \left( \frac{R_d(t)R_d'(t)}{4\kappa} \right)^2 \right] W(t, \xi) \right. \\ &\quad \left. - \frac{4\xi}{\sqrt{R_d(t)}} \frac{R_d(t)R_d'(t)}{4\kappa} W_\xi'(t, \xi) + \frac{1}{\sqrt{R_d(t)}} W_{\xi\xi}''(t, \xi) \right\} \exp\left[-\frac{R_d'(t)R_d(t)}{4\kappa}\xi^2\right]. \end{aligned}$$

Remembering Equation (2.8), we can see that  $d^2R_d/dt^2 = 0$ . Keeping in mind this condition, the substitution of the above-mentioned expressions for the derivatives into Equation (2.16) gives:

$$R_d^2(t)W_t'(t, \xi) = \kappa W_{\xi\xi}''(t, \xi), \quad (2.18)$$

where  $t \in [0, t_e]$  (or  $t \in [t_0, t_0 + \Delta t]$ ),  $0 \leq \xi \leq 1$ .

In the case of non-zero  $d^2 R_d/dt^2$  and  $P(R)$ , Eq. (2.18) would need to be replaced by the following equation (cf. Equation (8.149) in [105]):

$$R_d^2(t)W_t'(t, \xi) = \kappa W_{\xi\xi}''(t, \xi) + \left[ \frac{\xi^2}{4\kappa} \right] R_d^3 \frac{d^2 R_d}{dt^2} W(t, \xi) + \frac{R_d^2 R}{q_K(\xi, t)} P(R), \quad (2.19)$$

where

$$q_K(\xi, t) = \frac{1}{\sqrt{R_d(t)}} \exp \left[ -\frac{R_d'(t)R_d(t)}{4\kappa} \xi^2 \right].$$

Equation (2.19) reduces to Equation (2.18) in the limit when  $d^2 R_d/dt^2 = 0$  and  $P(R) = 0$ .

Equation (2.18) is to be solved subject to initial and boundary conditions:

$$W(t, \xi)|_{t=0} = W_0(\xi) \equiv R_{d0}^{3/2} \xi T_0(\xi R_{d0}) \exp \left[ \frac{R_d'(0)R_{d0}}{4\kappa} \xi^2 \right], \quad (2.20)$$

$$0 \leq \xi \leq 1,$$

$$W(t, \xi)|_{\xi=0} = 0, \quad (2.21)$$

$$t \in [0, t_e], \quad (\text{or } t \in [t_0, t_0 + \Delta t])$$

$$\left[ W_\xi'(t, \xi) + H_0(t)W(t, \xi) \right] \Big|_{\xi=1}$$

$$= \mu_0(t) \equiv \tilde{\mu}(t) \sqrt{R_d(t)} \exp \left[ \frac{R_d'(t)R_d(t)}{4\kappa} \right], \quad (2.22)$$

$$t \in [0, t_e] \quad (\text{or } t \in [t_0, t_0 + \Delta t]),$$

where:

$$H_0(t) = \tilde{H}(t) - \frac{R_d'(t)R_d(t)}{2\kappa} = \frac{h(t)}{k_l} R_d(t) - 1 - \frac{R_d'(t)R_d(t)}{2\kappa}.$$

### 2.3.2 Analytical solution

Let us now simplify the problem further by assuming that  $H_0(t) \equiv h_0 = \text{const} > -1$ . Remembering that  $h = k_g/R_d(t)$  for stationary droplets, the term

$$\frac{h(t)}{k_l} R_d(t)$$

can be simplified to  $k_g/k_l$ , and this ratio does not depend on  $t$ . Except at the final stage of droplet evaporation, in Diesel engine-like conditions it is typically much larger than

$$\frac{R_d'(t)R_d(t)}{2\kappa}.$$

Hence the time dependence of  $H_0(t)$  during the time step in this case can be ignored. This assumption will be relaxed later.

Our next goal is to find such change of variables that the inhomogeneous boundary condition (2.22) is replaced by the homogeneous one. This is achieved by the introduction of the new function  $V(t, \xi)$  via the relation:

$$W(t, \xi) = V(t, \xi) + \frac{\mu_0(t)}{1 + h_0} \xi, \quad (2.23)$$

Equation (2.23) allows us to rearrange Equation (2.18) to:

$$R_d^2(t) V_t'(t, \xi) = \kappa V_{\xi\xi}''(t, \xi) - \frac{\mu_0'(t)}{1 + h_0} R_d^2(t) \xi, \quad (2.24)$$

$$t \in [0, t_e] \quad (\text{or } t \in [t_0, t_0 + \Delta t]), \quad 0 \leq \xi \leq 1.$$

The initial and boundary conditions for Equation (2.24) can be presented as:

$$\begin{aligned} V(t, \xi)|_{t=0} &= W_0(\xi) - \frac{\mu_0(0)}{1 + h_0} \xi, \quad 0 \leq \xi \leq 1, \\ V(t, \xi)|_{\xi=0} &= 0, \quad [V_\xi'(t, \xi) + h_0 V(t, \xi)]|_{\xi=1} = 0, \\ t &\in [0, t_e] \quad (\text{or } t \in [t_0, t_0 + \Delta t]). \end{aligned}$$

In the absence of thermal radiation, Equation (2.24) is identical to Equation (12) in [15]. Following the analysis presented in that paper we look for the solution of Equation (2.24) in the form:

$$V(t, \xi) = \sum_{n=1}^{\infty} \Theta_n(t) v_n(\xi), \quad (2.25)$$

where functions  $v_n(\xi)$  form the full set of non-trivial solutions of the equation:

$$\frac{d^2 v}{d\xi^2} + \lambda^2 v = 0, \quad 0 \leq \xi \leq 1, \quad (2.26)$$

subject to boundary conditions:

$$v|_{\xi=0} = \left( \frac{dv}{d\xi} + h_0 v \right) \Big|_{\xi=1} = 0.$$

The general solution to Equation (2.26):

$$v(\xi) = A \cos \lambda \xi + B \sin \lambda \xi \quad (2.27)$$

satisfies the boundary conditions when  $A = 0$  and

$$\lambda \cos \lambda + h_0 \sin \lambda = 0. \quad (2.28)$$

The solution to Equation (2.28) gives a set of positive eigenvalues  $\lambda_n$  numbered in ascending order ( $n = 1, 2, \dots$ ). If  $h_0 = 0$ , then  $\lambda_n = \pi(n - \frac{1}{2})$ . Assuming that  $B = 1$ , expressions for eigenfunctions  $v_n(\xi)$  can be written as:

$$v_n(\xi) = \sin \lambda_n \xi \quad (n = 1, 2, \dots). \quad (2.29)$$

The solution  $\lambda = 0$  is excluded as it leads to a trivial solution  $v_n(\xi) = 0$ .

The value of  $B$  is implicitly accounted for by the coefficients  $\Theta_n(t)$  in Series (2.25). The functions  $v_n(\xi)$  form a full set of eigenfunction functions which are orthogonal for  $\xi \in [0, 1]$ . The orthogonality of functions  $v_n(\xi)$  follows from the relation:

$$\int_0^1 v_n(\xi)v_m(\xi)d\xi = \delta_{nm} \|v_n\|^2, \quad (2.30)$$

where:

$$\delta_{nm} = \begin{cases} 0 & n \neq m \\ 1 & n = m \end{cases}, \quad (2.31)$$

$$\|v_n\|^2 = \frac{1}{2} \left(1 - \frac{\sin 2\lambda_n}{2\lambda_n}\right) = \frac{1}{2} \left(1 + \frac{h_0}{h_0^2 + \lambda_n^2}\right).$$

It is easy to see that the expression for  $V(t, \xi)$  in the form (2.25) with  $v_n(\xi)$  defined by Equation (2.29) satisfies the boundary conditions for Equation (2.24).

The orthogonality of the functions  $v_n(\xi)$  allows us to expand known functions in Equation (2.24), and the initial conditions in the series:

$$f(\xi) \equiv -\xi/(1 + h_0) = \sum_{n=1}^{\infty} f_n v_n(\xi), \quad (2.32)$$

$$W_0(\xi) = \sum_{n=1}^{\infty} q_n v_n(\xi), \quad (2.33)$$

where:

$$f_n = \frac{1}{\|v_n\|^2} \int_0^1 f(\xi)v_n(\xi)d\xi = -\frac{\sin \lambda_n}{\|v_n\|^2 \lambda_n^2},$$

$$q_n = \frac{1}{\|v_n\|^2} \int_0^1 W_0(\xi)v_n(\xi)d\xi.$$

Although both Series (2.32) and (2.33) converge, the speed of convergence of series (2.32) can be slow. This can create a problem with applications of the new approach to practical engineering problems.

If  $T_0(R)$  is a twice continually differentiable function (this was assumed at the very beginning of the analysis) then this property is retained by function  $W_0(\xi)$ . In

this case one can show that [15]:

$$|q_n| < \frac{\text{const}}{\lambda_n^2}. \quad (2.34)$$

Remembering Equations (2.25) and (2.32), Equation (2.24) can be rewritten as:

$$\sum_{n=1}^{\infty} \left( R_d^2(t) \frac{d\Theta_n(t)}{dt} + \Theta_n(t) \kappa \lambda_n^2 \right) v_n(\xi) = \sum_{n=1}^{\infty} \left( f_n R_d^2(t) \frac{d\mu_0(t)}{dt} \right) v_n(\xi). \quad (2.35)$$

Both sides of Equation (2.35) are Fourier series with respect to functions  $v_n(\xi)$ . Two Fourier series are equal if, and only if, their coefficients are equal. This implies that:

$$R_d^2(t) \frac{d\Theta_n(t)}{dt} + \Theta_n(t) \kappa \lambda_n^2 = f_n R_d^2(t) \frac{d\mu_0(t)}{dt}. \quad (2.36)$$

Equation (2.36) is to be solved subject to the initial condition:

$$\Theta_n(0) = q_n + \mu_0(0) f_n. \quad (2.37)$$

To simplify the notation, hence-forward it is assumed that  $t_0 = 0$ .

The general solution to the homogeneous equation:

$$R_d^2(t) \frac{d\Theta_n(t)}{dt} + \Theta_n(t) \kappa \lambda_n^2 = 0 \quad (2.38)$$

can be presented as:

$$\ln(\Theta_n(t)/\Theta_n(0)) = -\kappa \lambda_n^2 \int_0^t \frac{dt}{R_d^2(t)}. \quad (2.39)$$

The initial condition (2.37) was used. Assuming that  $R_d(t)$  is a linear function of  $t$  given by Equation (2.8), Solution (2.39) can be presented in a more explicit form:

$$\Theta_n(t) = \Theta_n(0) \exp \left[ \frac{\kappa \lambda_n^2}{\alpha R_{d0}^2} \left( \frac{1}{1 + \alpha t} - 1 \right) \right]. \quad (2.40)$$

One can see that the following function:

$$\Theta_{n(\text{part})}(t) = f_n \int_0^t \frac{d\mu_0(\tau)}{d\tau} \exp \left[ \frac{\kappa \lambda_n^2}{\alpha R_{d0}^2} \left( \frac{1}{1 + \alpha t} - \frac{1}{1 + \alpha \tau} \right) \right] d\tau \quad (2.41)$$

satisfies Equation (2.36). Hence, this function can be considered as a particular solution to Equation (2.36). Integration by parts in (2.41) allows us to present  $\Theta_{n(\text{part})}(t)$  as:

$$\Theta_{n(\text{part})}(t) = f_n \left\{ \mu_0(t) - \mu_0(0) \exp \left[ -\frac{\kappa \lambda_n^2 t}{R_{d0} R_d(t)} \right] \right\}$$

$$- \exp \left[ \frac{\kappa \lambda_n^2}{\alpha R_{d0} R_d(t)} \right] \int_0^t \frac{\mu_0(\tau) \kappa \lambda_n^2}{R_d^2(\tau)} \exp \left[ -\frac{\kappa \lambda_n^2}{\alpha R_{d0} R_d(\tau)} \right] d\tau \Big\}. \quad (2.42)$$

Remembering Equations (2.40) and (2.41), the solution to Equation (2.36) can be presented as:

$$\begin{aligned} \Theta_n(t) &= \Theta_n(0) \exp \left[ \frac{\kappa \lambda_n^2}{\alpha R_{d0}^2} \left( \frac{1}{1 + \alpha t} - 1 \right) \right] \\ &+ f_n \int_0^t \frac{d\mu_0(\tau)}{d\tau} \exp \left[ \frac{\kappa \lambda_n^2}{\alpha R_{d0}^2} \left( \frac{1}{1 + \alpha t} - \frac{1}{1 + \alpha \tau} \right) \right] d\tau. \end{aligned} \quad (2.43)$$

Remembering (2.42) and (2.37) we can write an alternative formula for  $\Theta_n(t)$ :

$$\begin{aligned} \Theta_n(t) &= q_n \exp \left[ -\frac{\kappa \lambda_n^2 t}{R_{d0} R_d(t)} \right] + f_n \mu_0(t) \\ &- f_n \kappa \lambda_n^2 \int_0^t \frac{\mu_0(\tau)}{R_d^2(\tau)} \exp \left[ \frac{\kappa \lambda_n^2}{\alpha R_{d0}} \left( \frac{1}{R_d(t)} - \frac{1}{R_d(\tau)} \right) \right] d\tau. \end{aligned} \quad (2.44)$$

Note that  $\Theta_n(t)$  in the form (2.43) satisfies Equation (2.36), while  $\Theta_n(t)$  in the form (2.44) does not satisfy it. This is related to the fact that Equation (2.36) was derived under the assumption that Series (2.25), after being substituted into Equation (2.24), can be differentiated term by term (derivative of the series is equal to the series of derivatives). This assumption is valid when  $\Theta_n(t)$  is taken the form (2.43), but it is not valid when  $\Theta_n(t)$  is taken the form (2.44), as

$$\mu_0(t) \frac{d^2}{d\xi^2} \left( \sum_{n=1}^{\infty} f_n v_n \right) \neq \mu_0(t) \sum_{n=1}^{\infty} f_n \frac{d^2 v_n}{d\xi^2}$$

(the last series diverges). Note that Series (2.25) satisfies Equation (2.24) regardless of whether  $\Theta_n(t)$  is taken in the form (2.43) or in the form (2.44).

In the limit  $\alpha t \ll 1$  Equation (2.43) reduces to Equation (A11) of [15] if the effects of thermal radiation are ignored. The latter equation was derived assuming a stationary droplet boundary during the time step of integration.

Having substituted (2.43) or (2.44) into Equation (2.25) we obtain the required solution for  $V(t, \xi)$ . Remembering that exponential terms are less or equal to 1, the definition of  $f_n$ , and condition (2.34), we can see that series (2.25) converges absolutely and uniformly, since  $\lambda_n^{-2} < n^{-2}$  for  $n > 1$  (see [15]).

The final equation for temperature distribution inside the droplet can be presented as

$$T(R) = \frac{1}{R \sqrt{R_d(t)}} \exp \left[ -\frac{\alpha R_{d0} R^2}{4 \kappa R_d(t)} \right] \left[ \sum_{n=1}^{\infty} \Theta_n(t) \sin \left( \lambda_n \frac{R}{R_d(t)} \right) + \frac{\mu_0(t)}{1 + h_0} \frac{R}{R_d(t)} \right], \quad (2.45)$$

where  $\Theta_n$  are given by Equations (2.43) or (2.44).

Note that strictly speaking Equation (2.45) is an implicit function of droplet temperature since  $\alpha$  depends on droplet surface temperature  $T_s$  (see Fig. 2.2). Hence, the iteration process would be required. However, as follows from our calculations (see Figs. 2.2 and 2.4-2.6), except at the very final stage of droplet evaporation, for sufficiently small time steps, the value of  $T_s$  can be taken equal to the one obtained at the end of the previous time step. This allows us to consider Equation (2.45) as an explicit formula for  $T(R)$ .

### 2.3.3 Analysis of the general case

Let us now relax our assumption that  $H_0(t) \equiv h_0 = \text{const} > -1$  and assume that:

$$H_0(t) = h_0 + h_1(t), \quad (2.46)$$

where  $h_0 = \text{const} > -1$ . Note that many of the following equations would be greatly simplified in the case when  $h_0 = 0$ . In view of (2.46) we can rewrite the boundary condition at  $\xi = 1$  for Equation (2.18) in the form:

$$\left[ W'_\xi(t, \xi) + h_0 W(t, \xi) \right] \Big|_{\xi=1} = \mu_0(t) - h_1(t) W(t, 1) \equiv \hat{\mu}_0(t). \quad (2.47)$$

Assuming that  $\hat{\mu}_0(t)$  is known, we can formally use the previously obtained solutions (2.23) and (2.25) to present the solution to Problem (2.18)–(2.22) in the form:

$$\begin{aligned} W(t, \xi) &= \frac{\hat{\mu}_0(t)}{1 + h_0} \xi + V(t, \xi) = \sum_{n=1}^{\infty} \sin(\lambda_n \xi) q_n \exp \left[ -\frac{\kappa \lambda_n^2 t}{R_{d0} R_d(t)} \right] \\ &- \sum_{n=1}^{\infty} \sin(\lambda_n \xi) f_n \kappa \lambda_n^2 \int_0^t \frac{\hat{\mu}_0(\tau)}{R_d^2(\tau)} \exp \left[ \frac{\kappa \lambda_n^2}{\alpha R_{d0}} \left( \frac{1}{R_d(t)} - \frac{1}{R_d(\tau)} \right) \right] d\tau. \end{aligned} \quad (2.48)$$

In contrast to the previous case of  $H_0(t) = \text{const}$ , Equation (2.48) does not give us an explicit solution for  $W(t, \xi)$  since  $\hat{\mu}_0(t)$  depends on  $W(t, 1)$ .

Equation (2.48) can be presented in a more compact form:

$$W(t, \xi) = \mathcal{V}(t, \xi) - \int_0^t \hat{\mu}_0(\tau) G(t, \tau, \xi) d\tau, \quad (2.49)$$

where

$$\mathcal{V}(t, \xi) = \sum_{n=1}^{\infty} \sin(\lambda_n \xi) q_n \exp \left[ -\frac{\kappa \lambda_n^2 t}{R_{d0} R_d(t)} \right]$$

$$G(t, \tau, \xi) = - \sum_{n=1}^{\infty} \sin(\lambda_n \xi) \frac{\kappa \sin(\lambda_n)}{R_d^2(\tau) \|v_n\|^2} \exp \left[ \frac{\kappa \lambda_n^2}{\alpha R_{d0}} \left( \frac{1}{R_d(t)} - \frac{1}{R_d(\tau)} \right) \right].$$

Explicit expressions for  $f_n$  have been used in these formulae. Both functions  $\mathcal{V}(t, \xi)$  and  $G(t, \tau, \xi)$  are assumed to be known.

Remembering (2.47), we can rewrite Equation (2.49) as:

$$W(t, \xi) = \mathcal{V}(t, \xi) - \int_0^t [\mu_0(\tau) - h_1(\tau)W(\tau, 1)] G(t, \tau, \xi) d\tau. \quad (2.50)$$

This is an integral representation for a solution to Problem (2.18)–(2.22) for time dependent  $H_0(t)$  given by Equation (2.46). For  $\xi = 1$ , integral representation (2.50) reduces to the Volterra integral equation of the second kind for function  $W(t, 1)$ :

$$W(t, 1) = \mathcal{V}(t, 1) - \int_0^t [\mu_0(\tau) - h_1(\tau)W(\tau, 1)] G(t, \tau, 1) d\tau. \quad (2.51)$$

One can show that (see Equation (28) of [15]):

$$\sin^2 \lambda_n = \frac{\lambda_n^2}{\lambda_n^2 + h_0^2}. \quad (2.52)$$

Remembering Equations (2.31) and (2.52) we obtain:

$$G(t, \tau, 1) = - \frac{2\kappa}{R_d^2(\tau)} \sum_{n=1}^{\infty} \frac{\lambda_n^2}{h_0^2 + h_0 + \lambda_n^2} \exp \left[ \frac{\kappa \lambda_n^2}{\alpha R_{d0}} \left( \frac{1}{R_d(t)} - \frac{1}{R_d(\tau)} \right) \right]. \quad (2.53)$$

Let us now introduce a new function  $G_1(t, \tau, \xi)$  defined as:

$$G_1(t, \tau, \xi) = R_d^2(\tau) G(t, \tau, \xi), \quad (2.54)$$

where  $0 \leq \tau \leq t$ .

The convergence of the series in  $G_1(t, \tau, \xi)$  for  $(t - \tau) \in [\delta, -1/\alpha)$ , where  $\delta$  is an arbitrary small positive number, is proven in Appendix 1. Moreover, in the same appendix the validity of the estimate

$$|G_1(t, \tau, \xi)| \leq \tilde{c}/\sqrt{t - \tau}, \quad t - \tau \in (0, t_0] \quad (2.55)$$

is shown, where  $\tilde{c}$  is a constant, and  $t_0$  is an arbitrary fixed time in the range  $(0, t_e)$  (or  $(0, \Delta t)$ ).

All results in Appendix 1 are applicable to the first series in Equation (2.48) if we assume that  $\tau = 0$ .

Equation (2.51) has a unique solution, although this solution cannot be found in an explicit form. The numerical solution can be found as described in Appendix 2.

Once the solution to this equation has been found we can substitute it into integral representation (2.50) and find the required solution to the initial and boundary value problem (2.18) – (2.22). The required distribution of  $T$  is found to be:

$$T(t, R) = \frac{1}{R\sqrt{R_d(t)}} \exp\left[-\frac{R'_d(t)R^2}{4\kappa R_d(t)}\right] W(t, R/R_d(t)). \quad (2.56)$$

In the case when  $h_1(t) = 0$  and  $\alpha t \ll 1$  this solution reduces to that given by Equation (16) of [15]. Note that in the case of  $h_0 = 0$  we have  $\lambda_n = \pi(n - (1/2))$  and  $\|v_n\|^2 = 1/2$  in all equations.

## 2.4 Analysis of the solutions

As follows from the previous analysis, the importance of the effects described by the new model depends on the value of the coefficient  $\alpha$  given by Equation (2.9). The plots of  $\alpha$  versus droplet surface temperature  $T_s$  for the same values of parameters as in [15] (see their Fig. 2.2) ( $M_a = 29$  kg/kmole,  $M_f = 170$  kg/kmole ( $C_{12}H_{26}$ ),  $p = 3000$  kPa,  $a = 15.5274$ ,  $b = 5383, 59$ ), and for droplet initial radii  $5 \mu\text{m}$  and  $50 \mu\text{m}$  are shown in Fig. 2.2. As follows from this figure, for both initial droplet radii the values of  $\alpha$  can be considered negligibly small when  $T_s < 450$  K. In this case the conventional approach based on the assumption that  $R_d = \text{const}$  during the time step can be accurate enough for practical applications. However, for larger temperatures the absolute values of  $\alpha$  start to increase rapidly, and the effects of non zero  $\alpha$  can no longer be neglected.

The plots of  $T$  versus  $\xi = R/R_d$  for the same values of parameters as above are shown in Fig. 2.3 for various moments of time (indicated near the curves). The calculations have been performed using the new model, both taking into account the evaporation process, and ignoring the effects of evaporation. In both cases, the gas temperature was equal to 1000 K. As one can see from this figure, at times less than about 0.15 ms for  $R_{d0} = 5 \mu\text{m}$  and less than about 15 ms for  $R_{d0} = 50 \mu\text{m}$ , the effects of evaporation on the distribution of temperature inside droplets can be ignored. At longer times, the effects of evaporation lead to the reduction of droplet temperature, especially in the areas near the surface. In the case without evaporation, the predictions of the new model coincide with the predictions of the model described in [15], as expected. Apart from the plots shown in Fig. 2.3, we

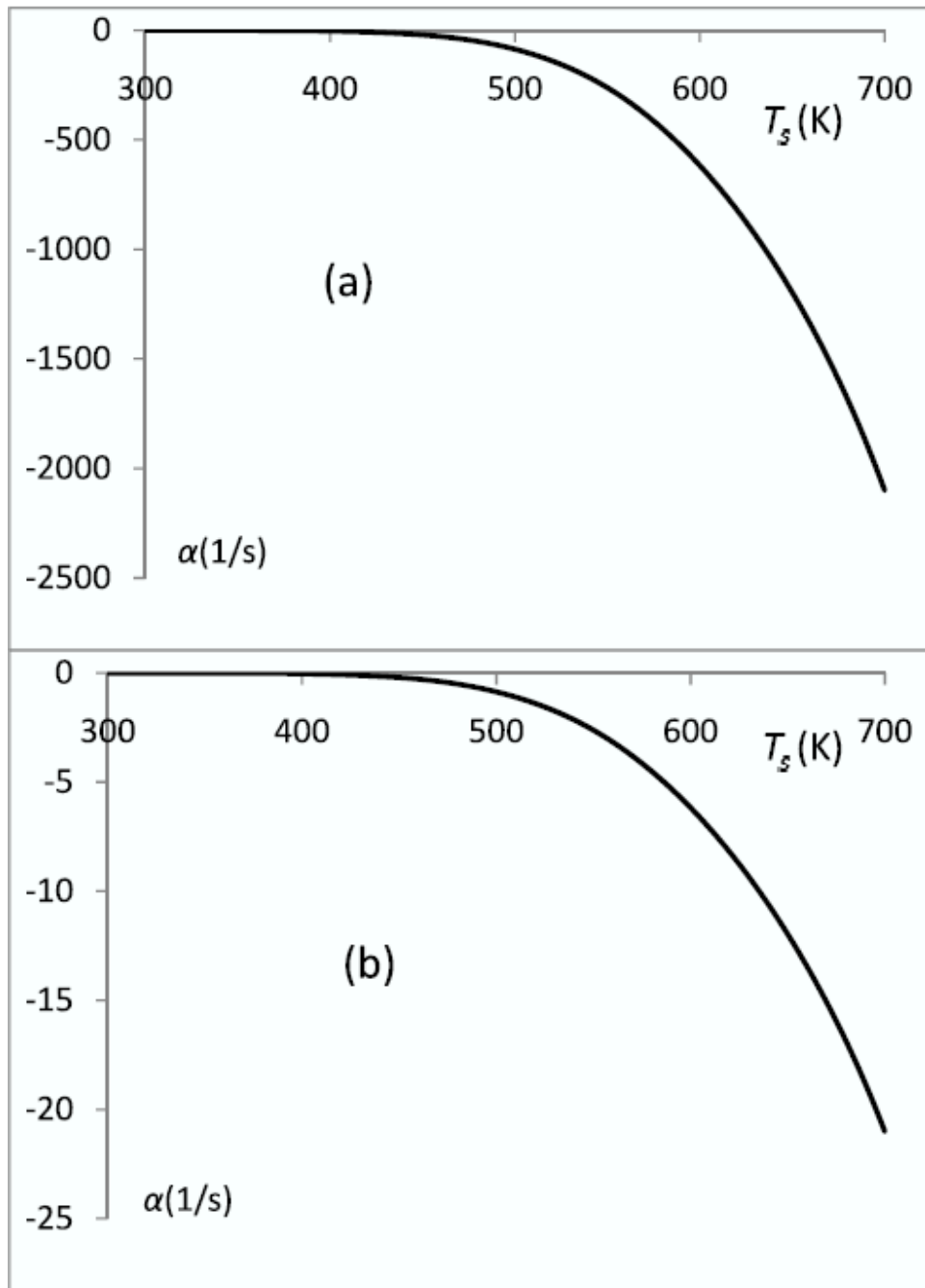


Figure 2.2: The plots of  $\alpha$  versus droplet surface temperature  $T_s$  for  $M_a = 29$  kg/kmole,  $M_f = 170$  kg/kmole ( $C_{12}H_{26}$ ),  $p = 3000$  kPa,  $a = 15.5274$ ,  $b = 5383, 59$ ,  $T_g = 1000$  K, and droplet initial radii  $5 \mu m$  (a) and  $50 \mu m$  (b).

have performed similar calculations but for  $T_g = 2000$  K (not shown). The plots without evaporation for  $R_{d0} = 50 \mu\text{m}$  in this case coincided with the ones shown in Fig. 2.2 of [15], obtained using the conventional approach.

In Fig. 2.4 we compared the results of calculations of droplet surface temperatures, taking into account the effects of evaporation, using the new and conventional approaches. Ambient conditions were the same as in Fig. 2.3, and the initial droplet radius was assumed equal to  $5 \mu\text{m}$  (typical values for Diesel engine-like conditions). Over 1000 time steps were used for both approaches. As can be seen from this figure, the new approach predicts slightly smaller droplet surface temperatures and slightly longer evaporation times compared with the conventional approach. The evaporation time predicted by the new model turned out to be more than 4% longer than with the conventional approach ( $\Delta \equiv (t_{e(\text{new})} - t_{e(\text{conventional})})/t_{e(\text{new})} = 4.32\%$ ). This increase in the evaporation time is certainly large enough to warrant taking into account the effect considered in this chapter in practical modelling of droplet heating and evaporation for engineering applications (including Diesel engines).

In Figs. 2.5 and 2.6 the same plots as in Fig. 2.4 are shown but for initial droplet radii equal to  $10 \mu\text{m}$  and  $50 \mu\text{m}$  respectively. About the same number of time steps as in Fig. 2.4 were used. As one can see from these figures, the same effect of lower surface temperature and longer evaporation times, predicted by the new model, compared with the conventional one, as shown in Fig. 2.4, can be observed for larger droplets. Interestingly, the relative increase in the evaporation time ( $\Delta$ ), predicted by the new model, remained equal to 4.32% for all droplets under consideration.

The values of  $\Delta \equiv (t_{e(\text{new})} - t_{e(\text{conventional})})/t_{e(\text{new})}$  versus  $T_g$  for  $R_d = 10 \mu\text{m}$  are shown in Fig. 2.7. The calculations were performed for  $T_g = 800$  and  $1200$  K apart from already presented results for  $T_g = 1000$  K. As one can see from this figure,  $\Delta$  is an almost linear function of  $T_g$  in the range of  $T_g$  under consideration. For gas temperatures less than about  $800$  K, the effect considered in this chapter can be ignored in most practical engineering applications. Note that the absence of any noticeable dependence of  $\Delta$  on  $R_d$  was observed for  $T_g = 1200$  K (similarly to the case of  $T_g = 1000$  K). Finally, the dependence of the results on the choice of time steps has been investigated. For  $R_d = 10 \mu\text{m}$  and  $T_g = 1000$ , the predicted temperatures and evaporation times changed slightly with decreasing time steps until the value

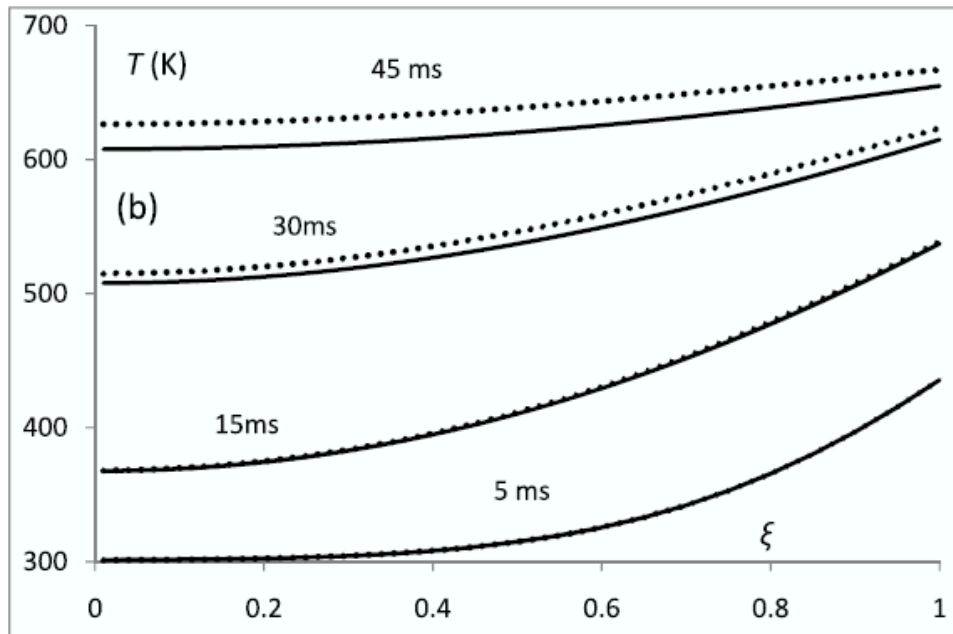
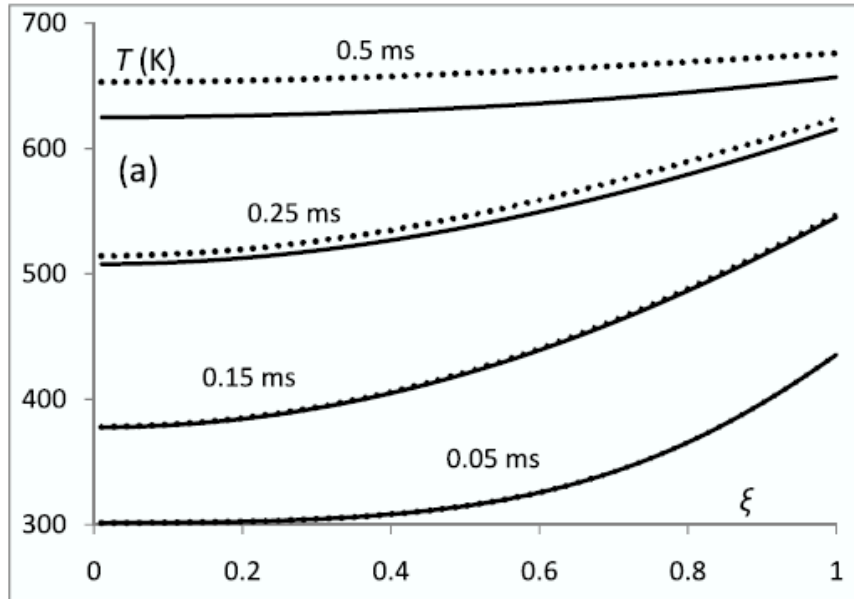


Figure 2.3: The plots of  $T$  versus  $\xi = R/R_d$  for the same values of parameters as in Fig. 2.2 and various times (indicated near the curves). The calculations were performed using the new model, taking into account the evaporation process (solid), and ignoring the effects of evaporation (dotted) for  $R_{d0} = 5 \mu\text{m}$  (a) and  $R_{d0} = 50 \mu\text{m}$  (b).

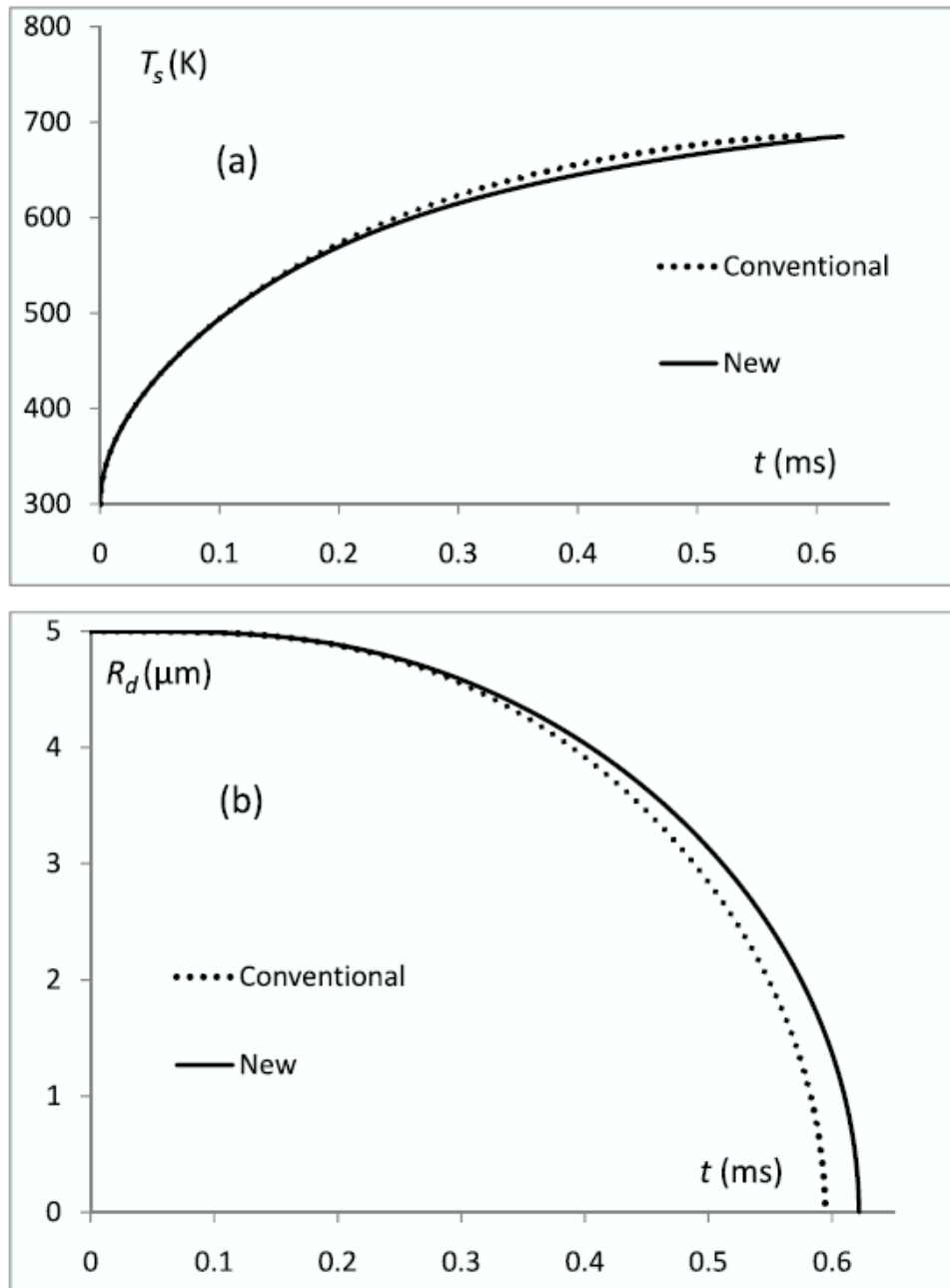


Figure 2.4: The plots of  $T_s$  versus time (a) and  $R_d$  versus time (b) for heated and evaporating droplets using the conventional (dotted), and new (solid) approaches for  $T_g = 1000$  K and  $R_{d0} = 5 \mu\text{m}$ .

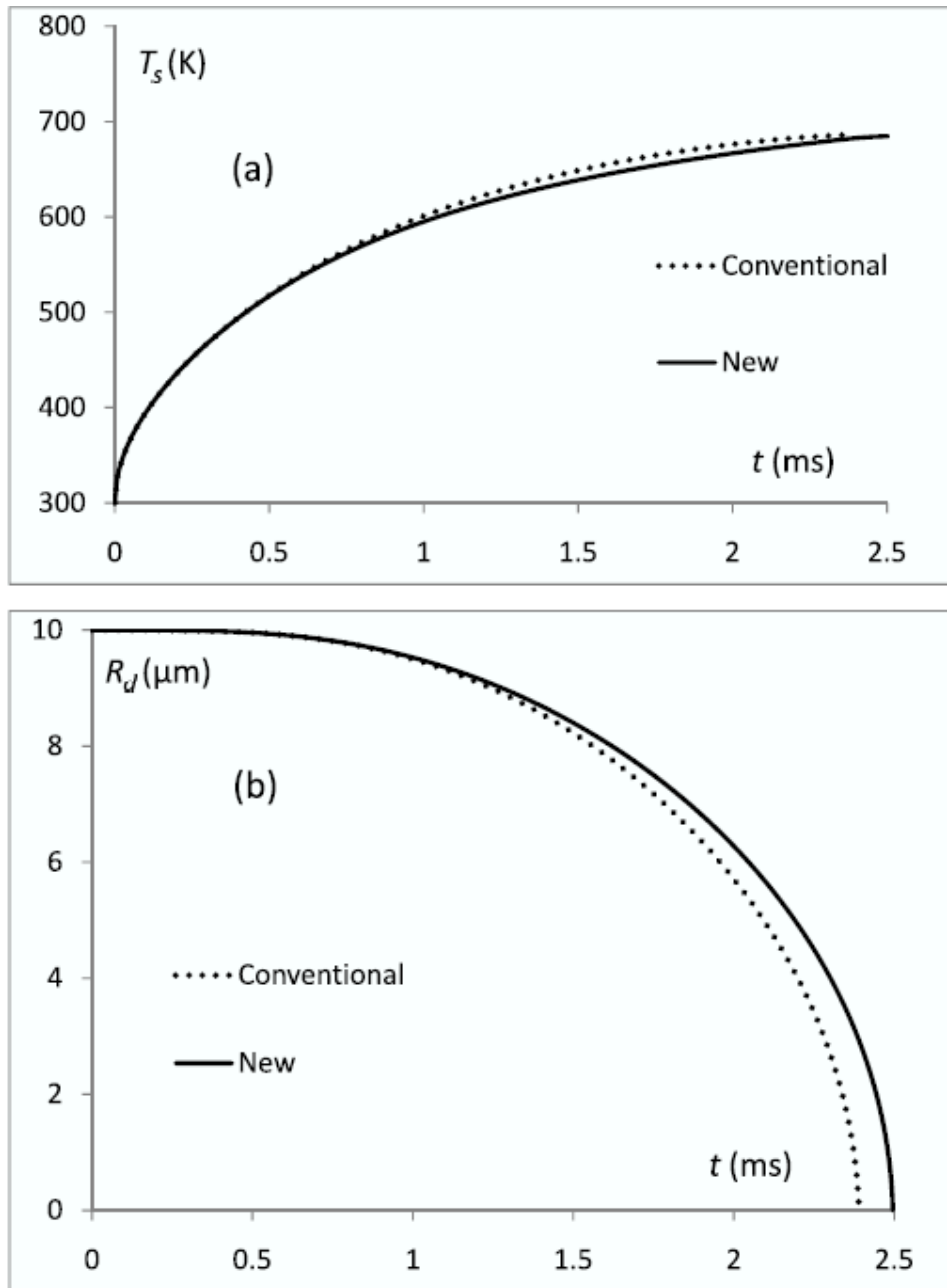


Figure 2.5: The same as Fig. 2.4 but for  $R_{d0} = 10 \mu\text{m}$ .

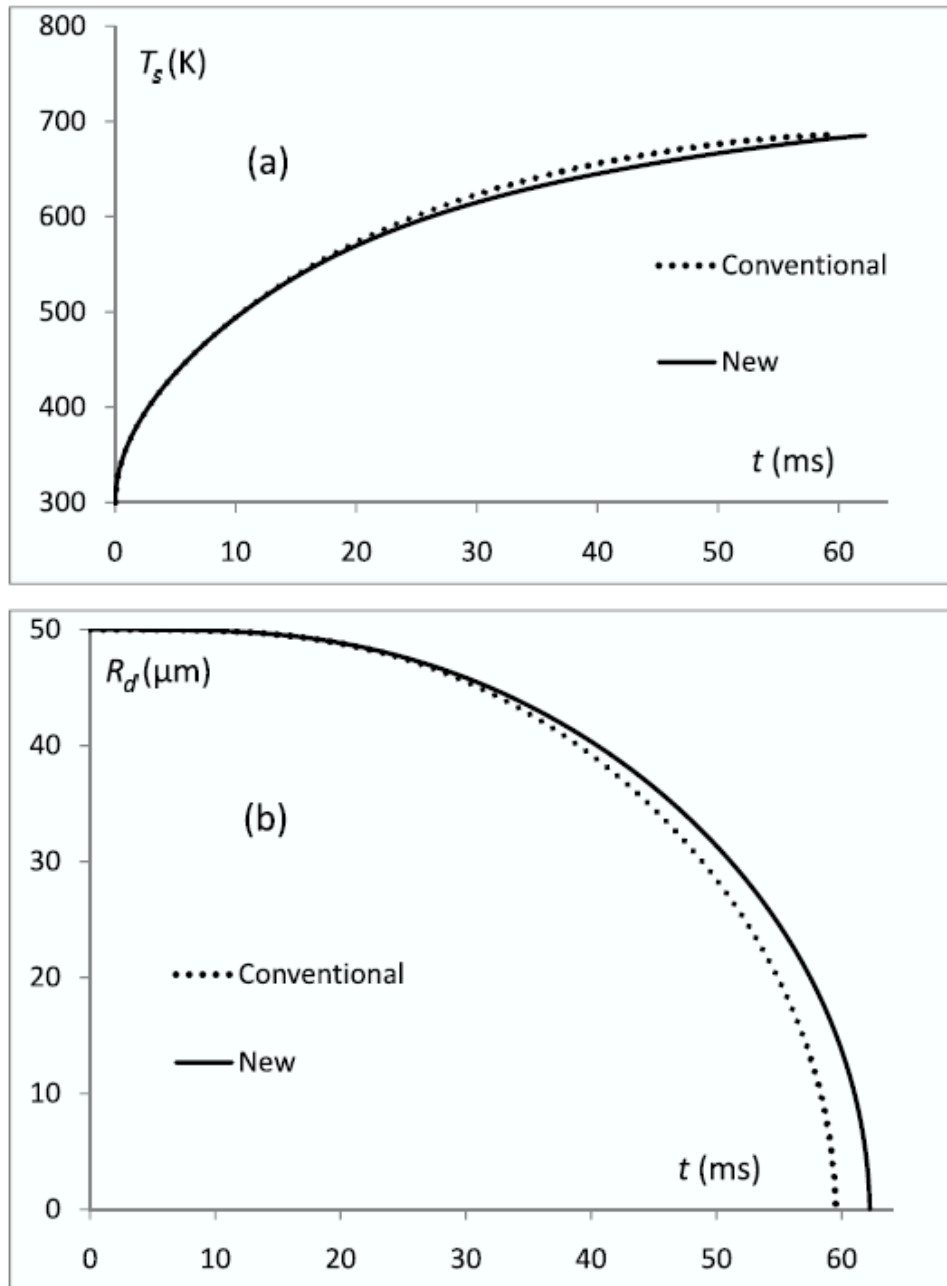


Figure 2.6: The same as Fig. 2.4 but for  $R_{d0} = 50 \mu\text{m}$ .

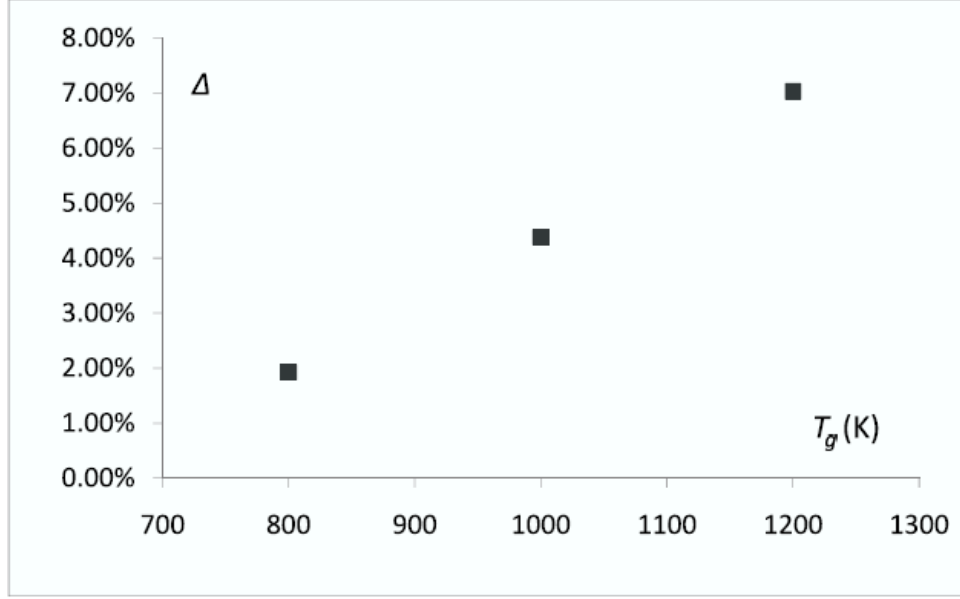


Figure 2.7: The values of  $\Delta \equiv (t_{e(\text{new})} - t_{e(\text{conventional})})/t_{e(\text{new})}$  versus  $T_g$  for  $T_g = 1000$  K and  $R_{d0} = 5 \mu\text{m}$ .

of the time step reached about 0.003 ms. Further reduction in the time steps has practically no effect on the results. Assuming that the true evaporation time for both conventional and new approaches is predicted for the time step 0.003 ms, we calculated errors which result from the choice of larger time steps as:

$$\text{Error} = \frac{t_e(\text{time step}) - t_e(\text{time step} = 0.003 \text{ ms})}{t_e(\text{time step} = 0.003 \text{ ms})}.$$

The values of errors versus time steps for new and conventional approaches are shown in Fig. 2.8. For the time step equal to 0.003 ms errors predicted by both models are equal to zero by definition. For larger time steps, the conventional approach always leads to larger errors compared with the new approach. In other words, a given error of calculation of the evaporation time can be associated with longer time steps in the case of the new model than in the case of the conventional one. These errors differ by a factor of approximately 2. Note that a serious restriction on the choice of the time step used in calculations, based on the new approach, is imposed by the requirement that  $h_0$  should be constant during the time step to enable us to use the analytical solution of the heat conduction equation.

It does not seem easy to explain the physical meaning of the effect of a moving droplet surface on droplet heating and evaporation, as the non-zero values of  $\alpha$  affect the solution in various ways. It would be difficult to relate it to the reduction in the

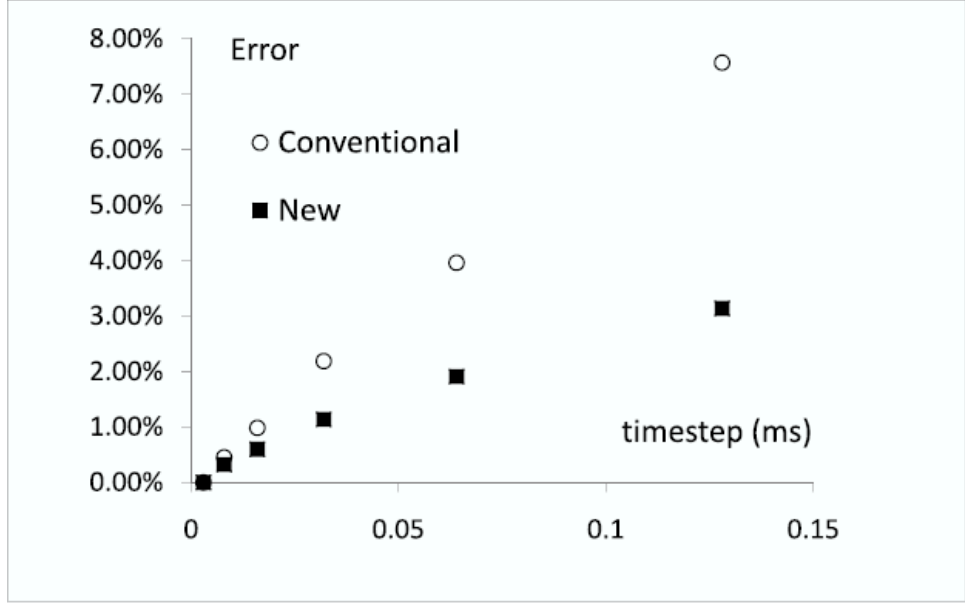


Figure 2.8: The values of  $\text{Error} = \frac{t_e(\text{time step}) - t_e(\text{time step}=0.003 \text{ ms})}{t_e(\text{time step}=0.003 \text{ ms})}$  versus time step for the conventional and new approaches for  $T_g = 1000 \text{ K}$  and  $R_{d0} = 5 \mu\text{m}$ .

kinetic energy of molecules hitting the receding wall, as the velocities of molecules and droplet surface differ by about 5 orders of magnitude.

## 2.5 Numerical vs analytical solutions

Although a few analytic solutions to Stefan problems are known, it is more common to apply numerical methods [110] to the problems with a moving boundary. Amongst these methods are the boundary immobilization method [111–117], the enthalpy method [118, 119], the variable space grid method [114, 118], the finite element numerical method [120], the nodal integral method [121] and the heat balance integral method [119, 122–129].

From amongst all of the above methods, the boundary immobilization method coupled to a Keller Box discretization scheme of the one-phase one-dimensional time-dependent governing equations appears to perform best as regards order of accuracy and computational efficiency [116]. This algorithm is implicit, therefore not having any limitation on the time step size, and was in addition shown to be second-order accurate in the time and space variables. All of the methods cited above are either of indeterminate accuracy or no higher than first-order accurate in time.

To compare results obtained using different methods dimensionless variables are used:  $\tilde{R} = \frac{R_d}{R_{d0}}$ ,  $\theta_s = \frac{T_s - T_0}{\Delta T}$ , where we have chosen the temperature scale  $\Delta T = L/c_l$  from the boundary condition (2.2).

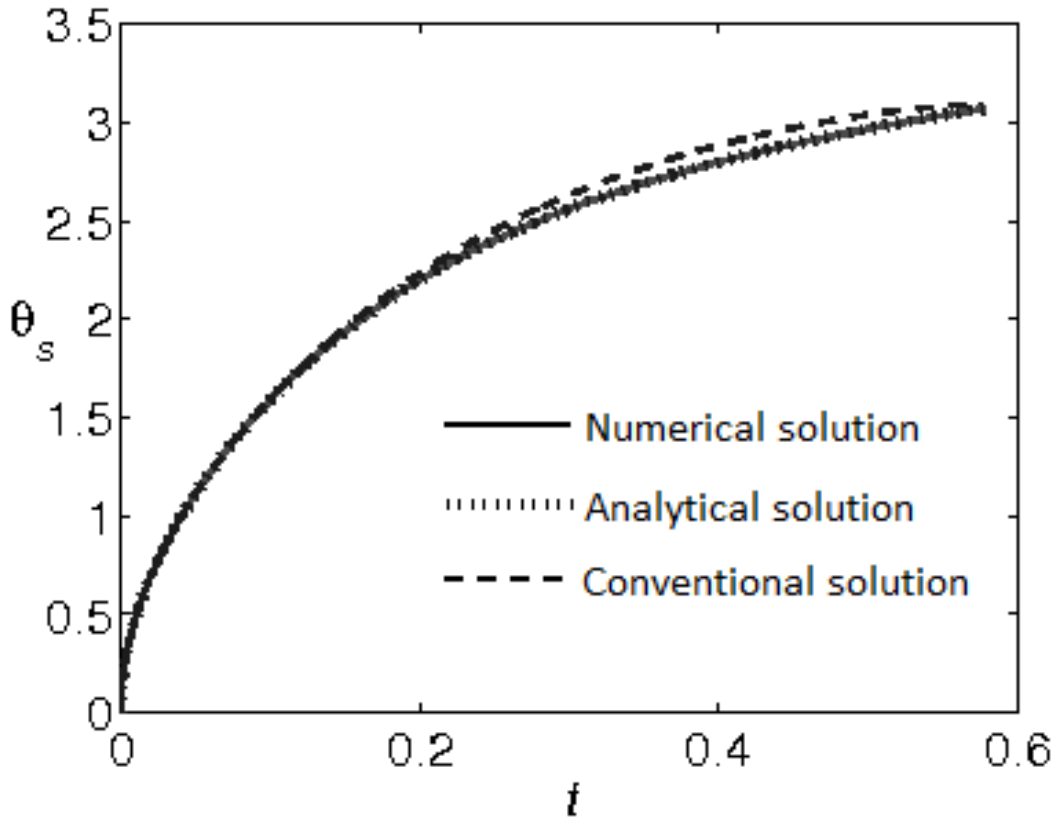


Figure 2.9: Comparison of  $\theta_s$  vs.  $t$  obtained using three different methods: the box scheme (solid); the method developed in this chapter (dotted); and the conventional method for which  $R(t)$  is piecewise constant in time (dashed).

Fig. 2.9 (reproduced from [23]) compares the numerical result for  $\theta_s$  from [23] with the solution provided in this chapter. Fig. 2.9 also displays the result obtained using the conventional numerical method, for which  $R(t)$  is assumed to be piecewise constant in time. There is a clear discrepancy between this result and the others. The result, predicted by the numerical solution, however, coincides within the accuracy of plotting with the one predicted by the model described in this chapter.

The same comparison as in Fig. 2.9 but for the normalised radius is shown in Fig. 2.10 (reproduced from [23]). As in Fig. 2.9, there is a clear discrepancy between

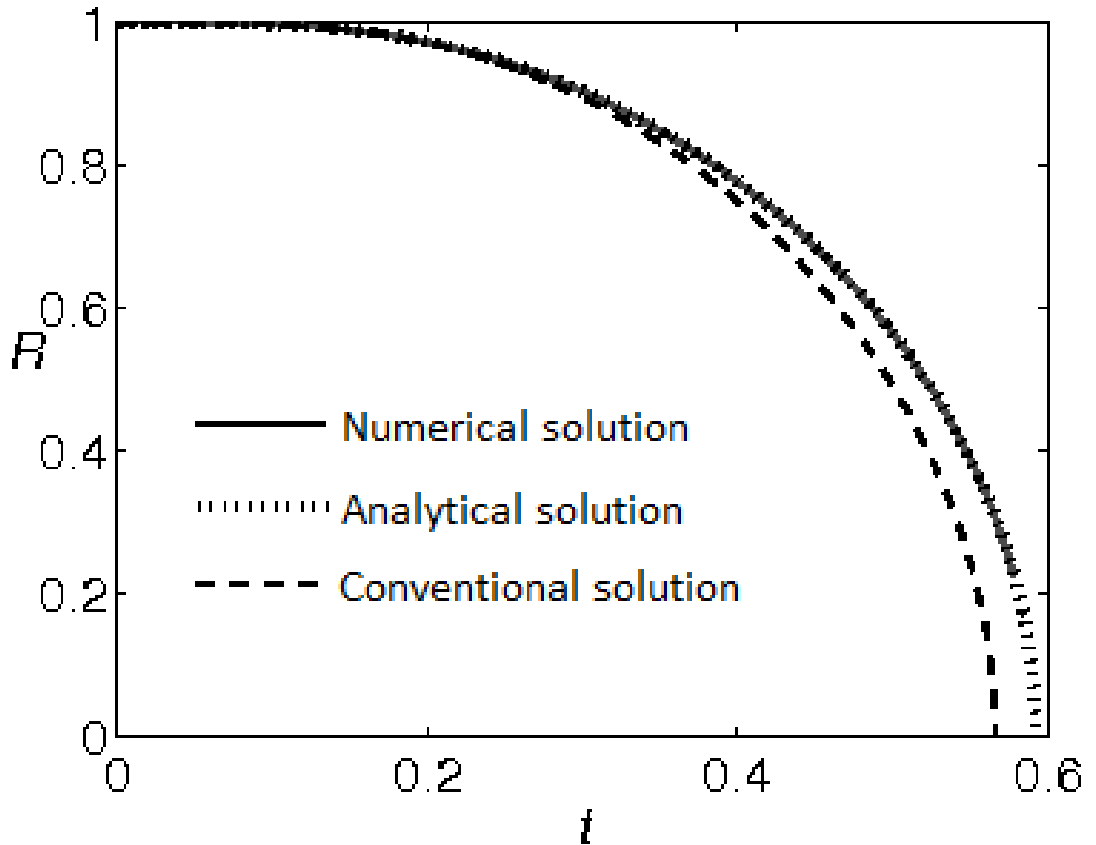


Figure 2.10: Comparison of  $\tilde{R}$  vs.  $t$  obtained using three different methods: the box scheme (solid); the method developed in this chapter (dotted); and the conventional method for which  $R(t)$  is piecewise constant in time (dashed).

the result obtained, assuming that  $R(t)$  is piecewise constant in time, and the results taking into account the changes of  $R(t)$  during time steps. The results predicted by the numerical solution coincides within the accuracy of plotting with the one predicted by the model described in this chapter (as in the case shown in Fig. 2.9).

It is indicated in [23] that, for given values of  $T_0$  and  $T_g$ , the maximum surface temperature reached is always the same, regardless of the initial droplet radius. Note that this maximal temperature (wet-bulb temperature) is asymptotically approached only in the case when the contribution of thermal radiation is ignored; when this contribution is taken into account, the droplet temperature reaches its maximal temperature, which is greater than the wet-bulb temperature, and then decreases, approaching the wet-bulb temperature from above [44]. Fortunately, for the case of

negligible thermal radiation, we are able to investigate this further analytically, as shown in [23]. In brief, an analytical solution can be found as  $t \rightarrow t_e$ , and from this we are able to find the maximum surface temperature. For the same parameter values as were used in this chapter, we obtain 685.79 K, which is in excellent agreement with the value of 685.68 K obtained in numerical solution and that of 685.29 K obtained in analytical solution from this chapter.

## 2.6 Conclusions of Chapter 2

New solutions to the heat conduction equation, describing transient heating of an evaporating droplet, are suggested. These solutions take into account the effect of the reduction of the droplet radius due to evaporation, assuming that this radius is a linear function of time. The latter assumption does not allow us to apply these solutions to describe the whole process, from the start of evaporation, until the moment in time when the droplet completely evaporates. However, these solutions are expected to be used to describe droplet heating and evaporation over a small time step when other parameters, except droplet radius and temperature, can be assumed constant. In this case they can be considered as generalisations of the approach currently used in all research and commercial computational fluid dynamics (CFD) codes known to us (KIVA, FLUENT, PHOENICS etc.), in which it is assumed that droplet radius is constant during the time step.

The solution is presented in the explicit analytical form in the case when parameter  $h_0$  can be assumed to be constant greater than  $-1$  during the time step. In the general case of a time dependent  $h_0$  the solution of the differential heat conduction equation is reduced to the solution of the Volterra integral equation of the second kind.

The analytical solution has been incorporated into the zero dimensional CFD code and applied to the analysis of Diesel fuel droplet heating and evaporation in typical engine conditions. Effects of droplets on gas have been ignored at this stage. The results have been compared with those which follow from the conventional (traditional) approach to modelling droplet heating and evaporation, based on the assumption that the droplet radius is constant over the time step (but changes from

one time step to another). It has been pointed out that the new approach leads to the prediction of lower droplet temperatures and longer evaporation times than the traditional method. For typical Diesel engine-like conditions and  $T_g = 1000$  K, the evaporation time predicted by the new approach turned out to be about 4.5% longer compared with the conventional method regardless of the value of the initial droplet radius, and this needs to be taken into account in practical engineering applications. This difference increased to about 7% for  $T_g = 1200$  K, and decreased to about 2% for  $T_g = 800$  K.

Larger time steps can be used in the case of the new approach compared with the conventional one to achieve the same accuracy of calculation.

The boundary immobilization method was considered, in tandem with the Keller box finite-difference scheme, for the accurate numerical solution of the problem. An important component of this was the use of variable transformations that must be built into the numerical algorithm in order to preserve second-order accuracy in both time and space for the temperature and the heat flux. This solution was found to agree well with that obtained using an algorithm described earlier in this Chapter.

# Chapter 3

## Transient heating of an evaporating droplet with presumed time evolution of its radius

### 3.1 Introduction of Chapter 3

As mentioned in Chapter 2, the conventional approach to the modelling of droplet heating and evaporation is based on the assumption that droplet radius remains constant during each time step, but changes from one time step to another due to the evaporation process [1, 44]. In Chapter 2 we took into account the time evolution of droplet radius  $R_d(t)$  assuming that  $R_d(t)$  is a linear function of time during the time step. It was shown that this approach not only allows the reduction of the number of time steps required for the calculation, but also leads to the prediction of lower droplet temperatures and longer evaporation times compared with the conventional approach. These new and in practice important results encouraged us to investigate this problem further and relax our assumption that  $R_d(t)$  is a linear function of time. The results of our investigation are presented in this chapter. Some preliminary results and their analysis were presented in [29].

Basic equations and approximations used in the analysis are the same as in Chapter 2.

## 3.2 Solution for the case of arbitrary $R_d(t)$ but

$$T_{d0}(R) = \text{const}$$

The analysis of this Chapter is based on the assumption that  $T_{d0}(R) = T_{d0} = \text{const}$ . In this case we can introduce the new variable  $v = u - RT_{d0}$  and rearrange Equation (2.12) as:

$$\frac{\partial v}{\partial t} = \kappa \frac{\partial^2 v}{\partial R^2} \quad (3.1)$$

for  $t \in (0, t_e)$  and  $R \in (0, R_d(t))$  with the boundary conditions

$$\left( \frac{\partial v}{\partial R} + H(t)v \right) \Big|_{R=R_d(t)} = \mu_0(t), \quad (3.2)$$

$$v|_{R=0} = 0 \quad (3.3)$$

for  $t \in (0, t_e)$  and the initial condition

$$v|_{t=0} = 0 \quad (3.4)$$

for  $R \in (0, R_d(t))$ , where

$$\mu_0(t) = -T_{d0} - H(t)R_d(t)T_{d0} + \mu(t) = -\frac{h(t)}{k_l}R_d(t)T_{d0} + \mu(t).$$

We look for the solution to the problem (3.1) – (3.4) in the form:

$$v(R, t) = \int_0^t \nu(\tau)G(t, \tau, R)d\tau, \quad (3.5)$$

where

$$G(t, \tau, R) = G_0(t - \tau, R - R_d(\tau)) - G_0(t - \tau, R + R_d(\tau)),$$

$$G_0(t, x) = \frac{\sqrt{\kappa}}{2\sqrt{\pi t}} \exp \left[ -\frac{x^2}{4\kappa t} \right].$$

Function  $G(t, \tau, R)$  can be presented in an alternative form:

$$G(t, \tau, R) = \frac{\sqrt{\kappa}}{2\sqrt{\pi(t-\tau)}} \left\{ \exp \left[ -\frac{(R - R_d(\tau))^2}{4\kappa(t-\tau)} \right] - \exp \left[ -\frac{(R + R_d(\tau))^2}{4\kappa(t-\tau)} \right] \right\}. \quad (3.6)$$

Note that  $G(t, \tau, R = 0) = 0$ .  $\nu(t)$  is an unknown continuous function to be found later from one of the boundary conditions. Function  $v(R, t)$  is known as a single layer heat potential and it has the following properties for any continuous function  $\nu(t)$  [105, 130]:

- 1) It satisfies Equation (3.1) for  $0 < t < t_e$  and  $0 < R < R_d(t)$ ;

- 2) It satisfies Conditions (3.3) and (3.4);
- 3) It is continuous at  $R \rightarrow R_d - 0$ ;
- 4) For the derivative  $\partial v(R, t)/\partial R$  the following limiting formula is valid:

$$\left. \frac{\partial v(R, t)}{\partial R} \right|_{R \rightarrow R_d(t)-0} = \frac{\nu(t)}{2} + \int_0^t \nu(\tau) \left[ \frac{\partial G(t, \tau, R)}{\partial R} \right] \Big|_{R=R_d(t)} d\tau. \quad (3.7)$$

This means that for any continuous function  $\nu(t)$  the potential  $v(R, t)$  satisfies Equation (3.1) and boundary and initial conditions (3.3) and (3.4). Choice of the function  $\nu(t)$ , satisfying integral Equation (3.7), should be made in such a way that the remaining boundary condition (3.2) is satisfied as well.

From Equation (3.6) it follows that

$$\begin{aligned} \left. \frac{\partial G(t, \tau, R)}{\partial R} \right|_{R=R_d(t)} &= -\frac{1}{4\sqrt{\pi\kappa}(t-\tau)^{3/2}} \\ &\times \left\{ (R_d(t) - R_d(\tau)) \exp \left[ -\frac{(R_d(t) - R_d(\tau))^2}{4\kappa(t-\tau)} \right] \right. \\ &\left. - (R_d(t) + R_d(\tau)) \exp \left[ -\frac{(R_d(t) + R_d(\tau))^2}{4\kappa(t-\tau)} \right] \right\}. \end{aligned} \quad (3.8)$$

Since  $R_d(t)$  is a continuously differentiable function, we obtain in the limit  $\tau \rightarrow t-0$ :

$$\left. \frac{\partial G(t, \tau, R)}{\partial R} \right|_{R=R_d(t)} \propto O\left(\frac{1}{\sqrt{t-\tau}}\right). \quad (3.9)$$

It follows from this equation, that there is an improper integral on the right hand side of Equation (3.7).

In view of Equations (3.7) and (3.5) we can rewrite the boundary condition (3.2) as:

$$\frac{\nu(t)}{2} + \int_0^t \nu(\tau) \left[ \frac{\partial G(t, \tau, R)}{\partial R} \right] \Big|_{R=R_d(t)} d\tau + H(t) \int_0^t \nu(\tau) G(t, \tau, R_d(t)) d\tau = \mu_0(t),$$

or

$$\frac{\nu(t)}{2} + \int_0^t \nu(\tau) \left\{ \left[ \frac{\partial G(t, \tau, R)}{\partial R} \right] \Big|_{R=R_d(t)} + H(t) G(t, \tau, R_d(t)) \right\} d\tau = \mu_0(t), \quad (3.10)$$

where  $G(t, \tau, R)$  and its derivative with respect to  $R$  are defined by Equations (3.6) and (3.8).

As follows from the definition of  $G(t, \tau, R_d(t))$  (see Equation (3.6)), in the limit  $\tau \rightarrow t-0$  this function has the singularity:

$$G(t, \tau, R_d(t)) \propto O\left(\frac{1}{\sqrt{t-\tau}}\right)$$

(cf. Equation (3.9)). Therefore, the integral in Equation (3.10) is defined as an improper integral.

Equation (3.10) is an integral equation of Volterra type. It has a unique continuous solution. A scheme for its numerical solution is described in Appendix 3. This solution is then substituted into Equation (3.5). The final distribution of temperature inside the droplet can be calculated from the following expression:

$$T(t, R) = T_{d0} + \frac{\sqrt{\kappa}}{2R\sqrt{\pi}} \int_0^t \frac{\nu(\tau)}{\sqrt{t-\tau}} \left\{ \exp \left[ -\frac{(R-R_d(\tau))^2}{4\kappa(t-\tau)} \right] - \exp \left[ -\frac{(R+R_d(\tau))^2}{4\kappa(t-\tau)} \right] \right\} d\tau. \quad (3.11)$$

Details of the numerical calculation of the integral on the right hand side of Equation (3.11) are given in Appendix 4.

### 3.3 Solution for the case of arbitrary $R_d(t)$ and $T_{d0}(R)$

Let us assume that an arbitrary twice continuously differentiable function  $T_{d0}(R)$  is defined for  $0 \leq R \leq R_{d0}$ . This definition is extended for the whole range  $0 \leq R < \infty$ :

$$T_{d0}(R) = \begin{cases} T_{d0}(R) & \text{when } 0 \leq R \leq R_{d0} \\ T_{\text{out}}(R) & \text{when } R_{d0} < R \leq R_{\text{eff}} \\ 0 & \text{when } R > R_{\text{eff}}, \end{cases} \quad (3.12)$$

where

$$T_{\text{out}}(R) = \frac{1}{R} \left\{ R_{d0} T_{d0}(R_{d0}) + (R - R_{d0}) \left[ (RT_{d0}(R))' \Big|_{R=R_{d0}} \right] \right\},$$

$R_{\text{eff}}$  is the effective outer radius such that  $R_{\text{eff}} > R_{d0}$ . Function  $T_{d0}(R)$  defined by Equation (3.12) is continuously differentiable in the range  $0 \leq R \leq R_{\text{eff}}$ .

Let us now introduce a new function  $U(t, R)$  defined as:

$$U(t, R) = \int_0^{R_{\text{eff}}} (\zeta T_{d0}(\zeta)) G_1(t, R, \zeta) d\zeta, \quad (3.13)$$

where

$$G_1(t, R, \zeta) = \frac{1}{\kappa} [G_0(t, R - \zeta) - G_0(t, R + \zeta)],$$

$G_0(t, x)$  is the same as in Equation (3.5). Remembering the latter equation, the expression for  $G_1(t, R, \zeta)$  can be presented in an alternative form:

$$G_1(t, R, \zeta) = \frac{1}{2\sqrt{\pi t \kappa}} \left\{ \exp \left[ -\frac{(R-\zeta)^2}{4\kappa t} \right] - \exp \left[ -\frac{(R+\zeta)^2}{4\kappa t} \right] \right\}. \quad (3.14)$$

Note that  $G_1(t, R = 0, \zeta) = 0$ .

Function  $U(t, R)$  has the following properties [105, 130]:

- 1) It satisfies Equation (3.1) for  $0 < t < t_e$  and  $0 < R < \infty$ ;
- 2) It satisfies the boundary Condition (3.3) for  $0 < t < t_e$ ;
- 3) It satisfies the initial condition

$$U(t, R)|_{t=+0} = \begin{cases} RT_{d0}(R) & \text{when } 0 \leq R \leq R_{\text{eff}} \\ 0 & \text{when } R > R_{\text{eff}}. \end{cases} \quad (3.15)$$

The latter relation follows from the property of the delta-function:

$$\lim_{\alpha_{\text{delta}} \rightarrow \infty} \frac{\alpha_{\text{delta}}}{\sqrt{\pi}} \exp(-\alpha_{\text{delta}}^2 x^2) = \delta(x). \quad (3.16)$$

We look for the solution to Equation (2.12) in the form:

$$u(t, R) = U(t, R) + v(t, R). \quad (3.17)$$

Having substituted Equation (3.17) into Equation (2.12) and boundary and initial conditions (2.13) – (2.15), we obtain problem (3.1) – (3.4) for  $v(t, R)$  in which

$$\mu_0(t) = - \left[ U'_R(t, R) + H(t)U(t, R) \right] \Big|_{R=R_d(t)} + \mu(t). \quad (3.18)$$

The solution of the latter problem is similar to the one discussed in Section 3.2.

The expression for  $\mu_0(t)$  contains

$$U'_R(t, R) \Big|_{R=R_d(t)} = \int_0^{R_{\text{eff}}} (\zeta T_{d0}(\zeta)) \frac{\partial G_1(t, R, \zeta)}{\partial R} \Big|_{R=R_d(t)} d\zeta, \quad (3.19)$$

where

$$\begin{aligned} \frac{\partial G_1(t, R, \zeta)}{\partial R} \Big|_{R=R_d(t)} &= \frac{1}{\kappa} \left[ \frac{\partial}{\partial R} (G_0(t, R - \zeta) - G_0(t, R + \zeta)) \right] \Big|_{R=R_d(t)} \\ &= \frac{1}{\kappa} \left[ \frac{\partial}{\partial \zeta} (-G_0(t, R - \zeta) - G_0(t, R + \zeta)) \right] \Big|_{R=R_d(t)}, \end{aligned} \quad (3.20)$$

$G_0$  is the same as in Equation (3.5). Remembering the latter equation we can rewrite the expression for  $\frac{\partial G_1(t, R, \zeta)}{\partial R} \Big|_{R=R_d(t)}$  in a more explicit form:

$$\begin{aligned} \frac{\partial G_1(t, R, \zeta)}{\partial R} \Big|_{R=R_d(t)} &= -\frac{1}{4\sqrt{\pi}(\kappa t)^{3/2}} \left\{ (R - \zeta) \exp \left[ -\frac{(R - \zeta)^2}{4\kappa t} \right] \right. \\ &\quad \left. - (R + \zeta) \exp \left[ -\frac{(R + \zeta)^2}{4\kappa t} \right] \right\} \Big|_{R=R_d(t)}. \end{aligned}$$

Hence, we obtain an explicit expression for  $\mu_0(t)$  in the form:

$$\begin{aligned} \mu_0(t) = & \frac{1}{4\sqrt{\pi}(\kappa t)^{3/2}} \int_0^{R_{\text{eff}}} (\zeta T_{d0}(\zeta)) \left\{ (R_d(t) - \zeta) \exp \left[ -\frac{(R_d(t) - \zeta)^2}{4\kappa t} \right] \right. \\ & \left. - (R_d(t) + \zeta) \exp \left[ -\frac{(R_d(t) + \zeta)^2}{4\kappa t} \right] \right\} d\zeta \\ & - \frac{H(t)}{2\sqrt{\pi\kappa t}} \int_0^{R_{\text{eff}}} (\zeta T_{d0}(\zeta)) \left\{ \exp \left[ -\frac{(R_d(t) - \zeta)^2}{4\kappa t} \right] - \exp \left[ -\frac{(R_d(t) + \zeta)^2}{4\kappa t} \right] \right\} d\zeta \\ & + M(t)R_d(t). \end{aligned} \quad (3.21)$$

In the limit  $t \rightarrow 0+$  the expression for  $\mu_0(t)$  is simplified to (see Appendix 5):

$$\mu_0(0) = - \left[ (\zeta T_{d0}(\zeta))'_{\zeta} \Big|_{\zeta=R_{d0}} + H(0)R_{d0}T_{d0}(R_{d0}) \right] + \mu(0). \quad (3.22)$$

Combining Equations (3.5) and (3.17) we can present the final solution to our problem in the form:

$$\begin{aligned} T(t, R) = & \frac{1}{R} \left[ U(t, R) + \frac{\sqrt{\kappa}}{2\sqrt{\pi}} \int_0^t \frac{\nu(\tau)}{\sqrt{t-\tau}} \left\{ \exp \left[ -\frac{(R - R_d(\tau))^2}{4\kappa(t-\tau)} \right] \right. \right. \\ & \left. \left. - \exp \left[ -\frac{(R + R_d(\tau))^2}{4\kappa(t-\tau)} \right] \right\} d\tau \right], \end{aligned} \quad (3.23)$$

where  $\nu(\tau)$  is the solution to Equation (3.10) with  $\mu_0(t)$  given by Equation (3.21),  $U(t, R)$  is given by Equation (3.13).

Note that taking into account the initial distribution of temperature along  $R$  is absolutely essential when the solution is applied to individual time steps. In the solution described in the last two sections, however, the same formulae describe the time evolution of droplet temperatures during the whole period of their evaporation. It is anticipated that in this case the effect of the initial distribution of droplet temperatures is not important in most practical applications. Hence, the solution described in Section 3.2 is expected to be more practically important than the solution described in this section.

Note that although the analysis presented so far refers to stationary droplets, it can be generalised in a straightforward way to the case of moving droplets, based on the effective thermal conductivity model [1, 44].

## 3.4 Implementation of the new solutions into a numerical code

In the solutions presented in the last two sections it was assumed that  $R_d(t)$  is known. From the point of view of the physical background to the problem, however,  $R_d(t)$  depends on the time evolution of the droplet temperature  $T(R, t)$ , which is the solution to the problem. Hence, an iterative process is required. Firstly, the time evolution of droplet radius  $R_d(t)$  is obtained using the conventional approach, when it remains constant during the time step, but changes from one time step to another due to the evaporation process. Then these values of  $R_d(t)$  are used in the new solutions to obtain updated values of the time evolution of the distribution of temperatures inside the droplet and on its surface  $T(R, t)$ . These new values of droplet temperature are used to update the function  $R_d(t)$ . This process is continued until convergence is achieved, which typically takes place after about 15 iterations.

## 3.5 Results

In Figs. 3.1-3.7 we compared the results of calculations of droplet surface temperatures and radii, taking into account the effects of evaporation, using the new integral solution for arbitrary  $R_d(t)$  but constant  $T_{d0}$  (Equation (3.11)), the previously reported solution, based on the linear approximation of  $R_d(t)$  (Equation (2.45)), and the conventional approach based on the assumption that droplet radius does not change during the time step. Droplets are assumed to be those of n-dodecane ( $M_f = 170$  kg/kmole), and ambient air is assumed to be at the pressure of  $p = 30$  atm = 3000 kPa (typical values for Diesel engine-like conditions).

The results of calculations for  $R_{d0} = 5$   $\mu\text{m}$ , and ambient air temperature 1000 K are shown in Fig. 3.1. One thousand time steps were used in the conventional approach and the approach based on Solution (2.45). In the integral solution based on Equation (3.11) the integral (A41) was approximated as the sum of 100 terms, and up to 15 iterations were used. At the first iteration the time evolution of the droplet radius was assumed to be the same as predicted by the conventional model.

As follows from Fig. 3.1, the results predicted by the integral solution (3.11)

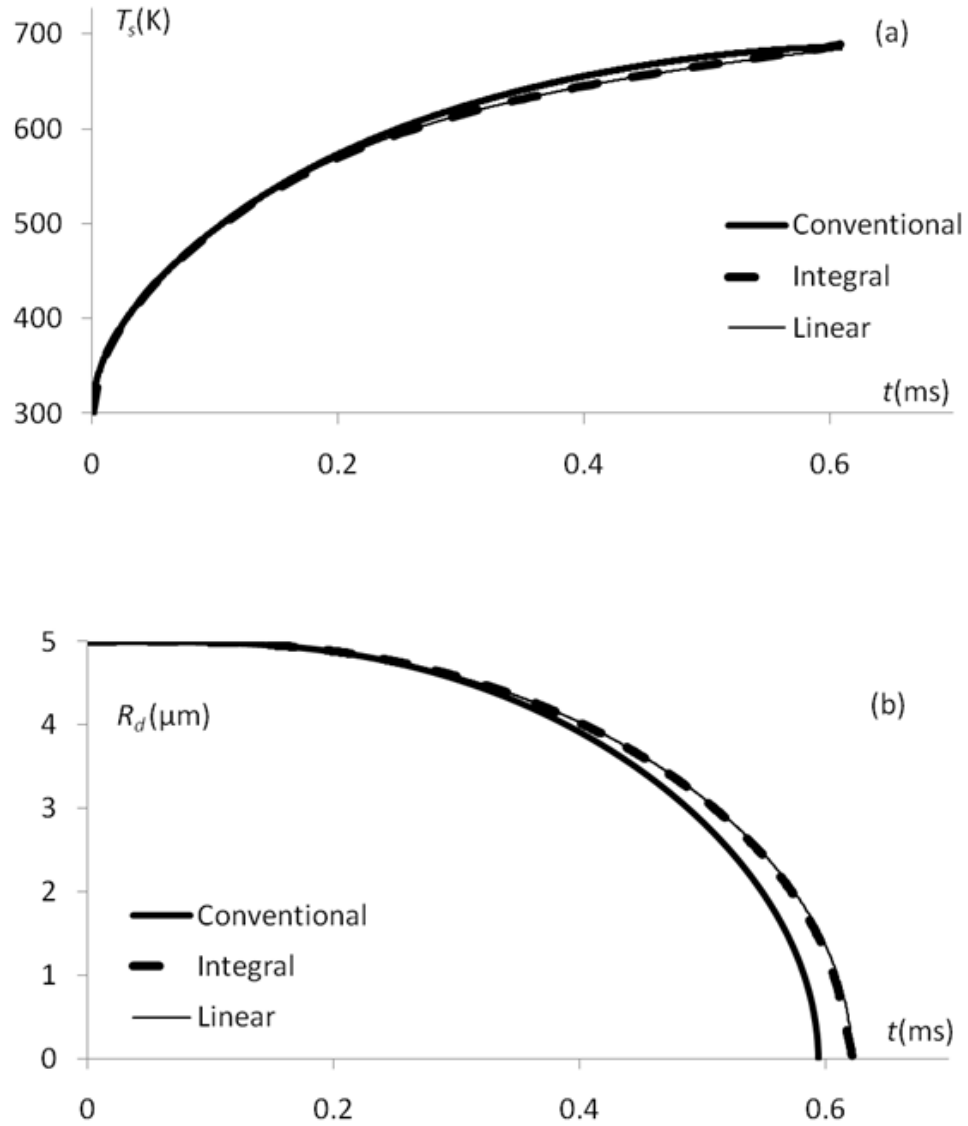


Figure 3.1: The plots of  $T_s$  versus time (a) and  $R_d$  versus time (b) using the conventional model (thick solid), integral model based on Equation (3.11) (dashed) and linear model (thin solid) for a stationary n-dodecane ( $M_f = 170$  kg/kmole) droplet with an initial radius  $5 \mu\text{m}$ , evaporating in ambient air at a pressure of  $p = 30 \text{ atm} = 3000 \text{ kPa}$  and temperature  $1000 \text{ K}$ .

and linear solution (2.45) practically coincide, which suggests that both approaches are correct and valid. Both these solutions predict lower droplet temperatures and longer evaporation times in agreement with the results reported in previous Chapter. Note that deviations between the predictions of the integral and linear solutions were observed in the immediate vicinity of the time when the droplet completely evaporates.

There were obvious numerical problems when we approached this time due to the fact that the time derivative of  $R_d$  becomes infinitely large. In practice the extrapolation, based on the assumption that the second derivative of  $R_d(t)$  is constant, was used for these times. This leads to small deviations between the predicted evaporation times. In the case shown in Fig. 3.1, the evaporation times predicted by the conventional model, linear solution, and integral solution were 0.595 ms, 0.622 ms and 0.628 ms respectively. That means that the difference between the evaporation times predicted by the linear and integral solutions was less than 1% and can be safely ignored in most practical applications (this error can be reduced further if required). The same comment applies to other cases considered below.

The effect of the choice of the number of iterations on the prediction of the integral solution is illustrated in Fig. 3.2 for the same case as shown in Fig. 3.1. This effect is shown only for the times when the deviation between the results predicted by the linear and integral solutions is maximal. For the first iteration, the time evolution of droplet radius is the same as predicted by the conventional model. The deviation of the corresponding droplet temperatures predicted by the integral and linear solutions appears to be quite noticeable. For the fifth iteration the droplet surface temperatures predicted by the integral and linear solutions practically coincide up to  $t \approx 0.45$  ms. The corresponding plots of  $R_d(t)$ , predicted by the integral solution, turned out to be closer to those predicted by the linear solution than those predicted by the conventional model. The closeness between the plots predicted by the linear and integral solutions improved as the number of iterations increased. However, even for the 15th iteration the deviation between the results remains visible, although it is not important for practical applications (cf. Fig. 3.1). For higher iterations the results are practically indistinguishable from those predicted by the 15th iteration. Interestingly, odd iterations predicted smaller  $R_d(t)$  and even iterations

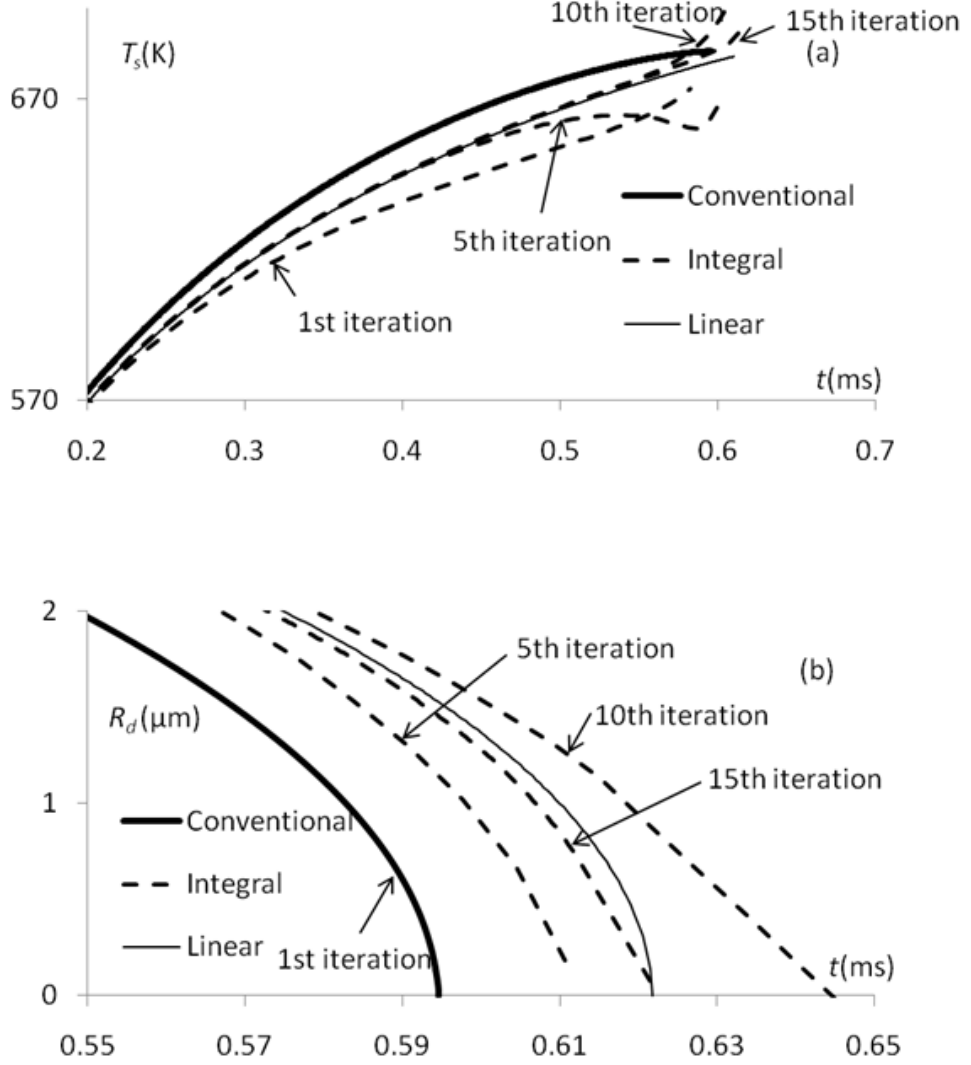


Figure 3.2: The same as Fig. 3.1 but for different numbers of iterations in the integral solution.

predicted larger  $R_d(t)$  compared with those predicted by the linear solution. At the qualitative level this could be related to the fact that a faster evaporation rate, assumed for the first iteration (conventional model), leads to a lower droplet surface temperature. At the second iteration, this lower droplet surface temperature leads to a slower evaporation rate etc.

As to the computational efficiency of the new integral model, we note that for a PC Xeon 3 GHz (the calculations were processed on one kernel only) with 2 GB RAM, the conventional approach requires 3586 s to calculate 1191 steps. Once these calculations have been completed, the integral model requires 453 s to calculate 15 iterations. This makes this model potentially suitable for incorporation into

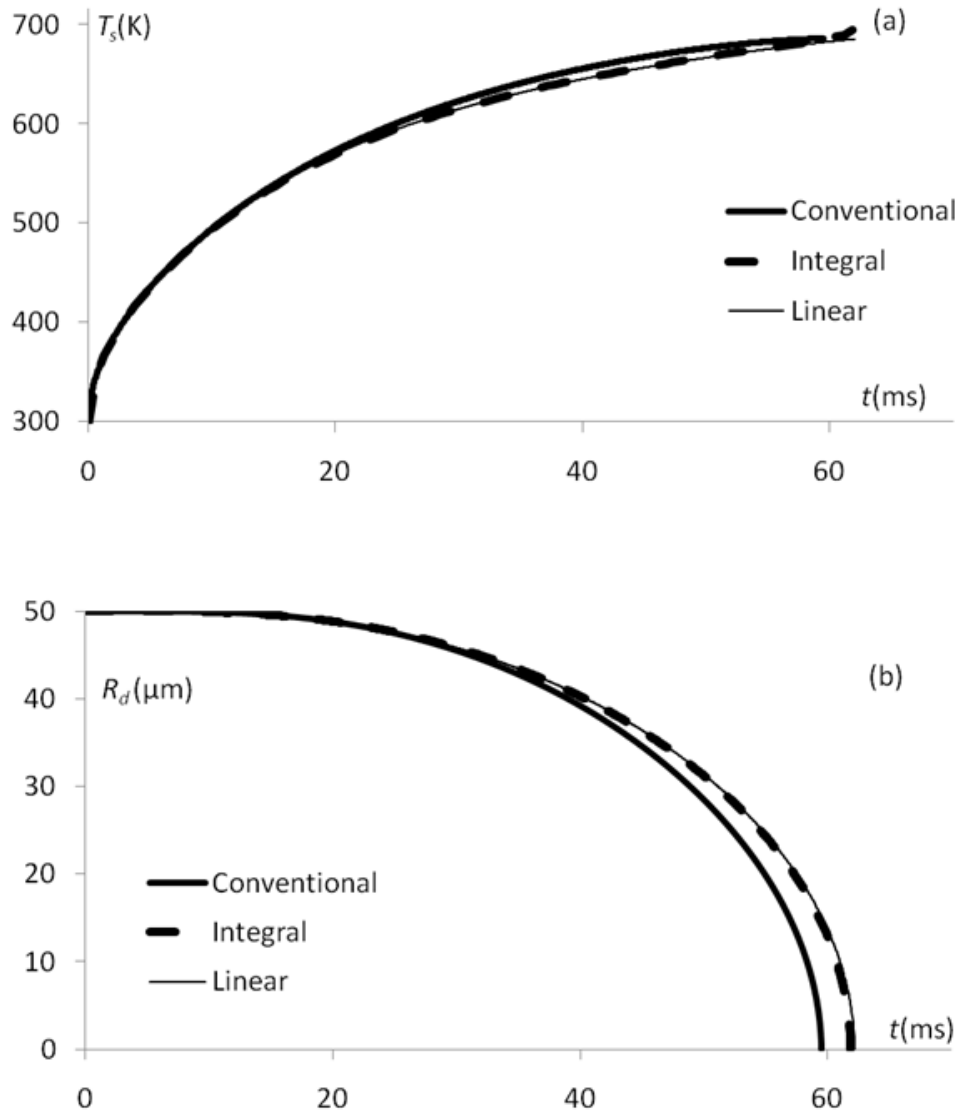


Figure 3.3: The same as Fig. 3.1 but for a droplet with initial radius  $50 \mu\text{m}$ .

computational fluid dynamics (CFD) codes.

The results, similar to those shown in Fig. 3.1, but for droplets with initial radii  $50$  and  $100 \mu\text{m}$  are shown in Figs. 3.3 and 3.4 respectively. As can be seen from these figures, the plots of droplet surface temperatures and radii are largely unaffected by the initial droplet radii. This agrees with similar results reported in Chapter 2 (see Figs. 2.4-2.6 ).

The results, similar to those shown in Fig. 3.1, but for the gas temperatures  $800$  and  $1000 \text{ K}$  are shown in Figs. 3.5 and 3.6 respectively. Comparing Figs. 3.1 and 3.5 one can see that a decrease in gas temperature by  $20\%$  leads to an increase in the evaporation time predicted by all models by more than  $50\%$ . The results predicted

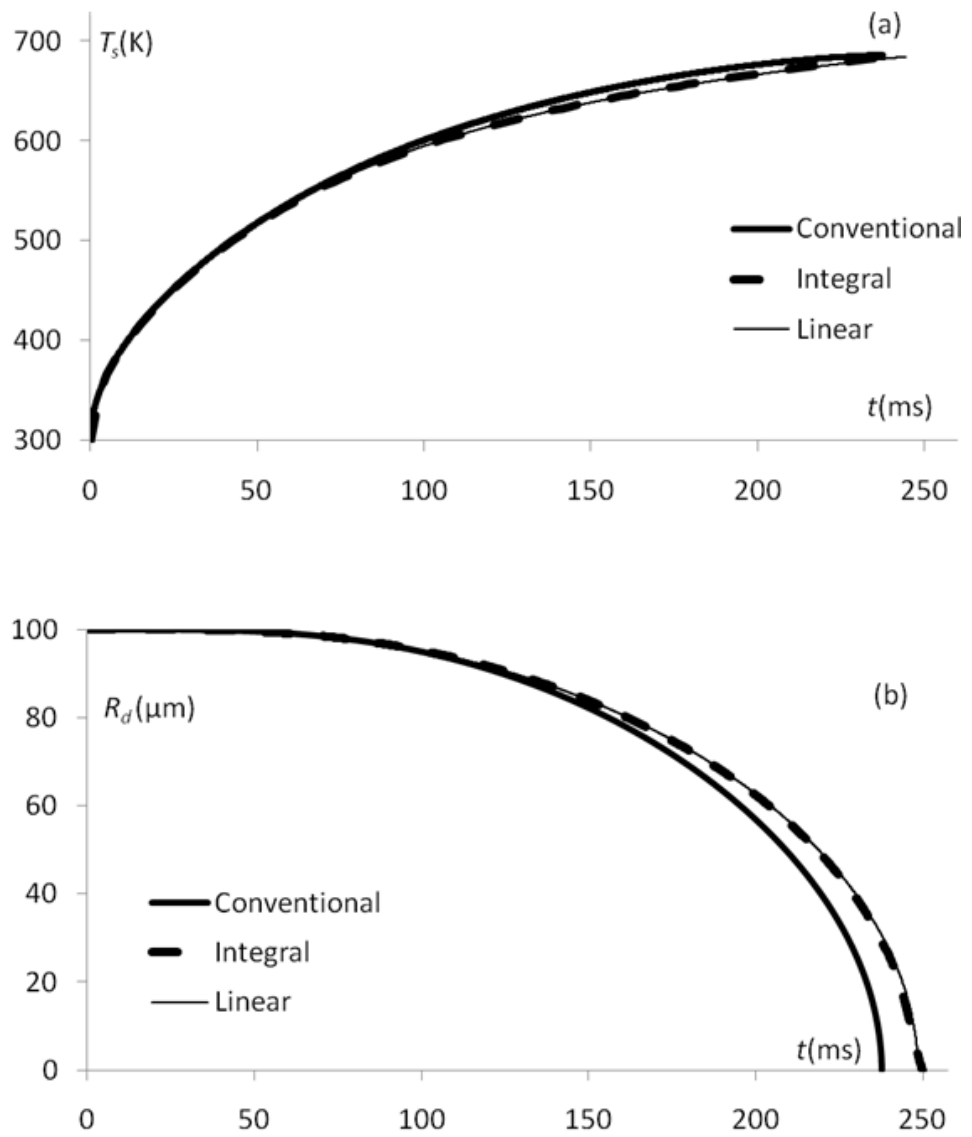


Figure 3.4: The same as Figs. 3.1 and 3.3 but for a droplet with initial radius 100  $\mu\text{m}$ .

by the integral and linear solutions for gas temperature equal to 800 K, are much closer to those predicted by the conventional model than is the case for gas temperature equal to 1200 K. In the case of droplet surface temperature, they are hardly distinguishable, and we had to use an insert figure to zoom the difference between them. As in the case shown in Fig. 3.1, the results predicted by the integral and linear models for gas temperatures 800 and 1200 K practically coincide. Comparing Figs. 3.1 and 3.6 one can see that an increase in gas temperature by 20% leads to a decrease in the evaporation time predicted by all models of more than 25%. The deviation between the results predicted by the integral and linear models and those predicted by the conventional model is noticeably larger in the case shown in Fig. 3.6 than in the case shown in Figs. 3.1 and 3.5, in agreement with similar results reported in Chapter 2 (see Fig. 2.7 ). Also, for the case shown in Fig. 3.6, the deviation between the results predicted by the integral and linear models is much more visible compared with the previous plots, especially at the final stage of droplet evaporation.

The plots of  $T$  versus  $\xi = R/R_d$  for  $T(R, t = 0) \equiv T_{d0}(R) = 300$  K,  $R_{d0} = 5$   $\mu\text{m}$ ,  $T_g = 1000$  K and various moments of time (indicated near the curves) are shown in Fig. 3.7. The calculations were performed based on Equation (3.11) (the case of constant  $T_{d0}(R)$ ) and Equation (3.23) (the general case of arbitrary  $T_{d0}(R)$ ). As can be seen from this figure, the predictions of Equations (3.11) and (3.23) coincide. This shows the correctness of both approaches to the problem. In agreement with the earlier models described in [1] and [19], Fig. 3.7 shows that the gradient of temperature inside droplets cannot be ignored at least at the initial stage of droplet heating and evaporation.

The effect of non-constant initial distribution of droplet temperature on the time and space evolution of this distribution is illustrated in Fig. 3.8. Two cases are compared in this figure. In both cases, the initial droplet radii are assumed to be equal to 5  $\mu\text{m}$ , and gas temperature is assumed to be constant and equal to  $T_g = 1000$  K. In the first case the initial distribution of temperature was assumed to be independent on  $R$  (or  $\xi$ ) and equal to 300 K, as in the case shown in Fig. 3.7. In this case the analysis was based on Equation (3.11). In the second case, the initial

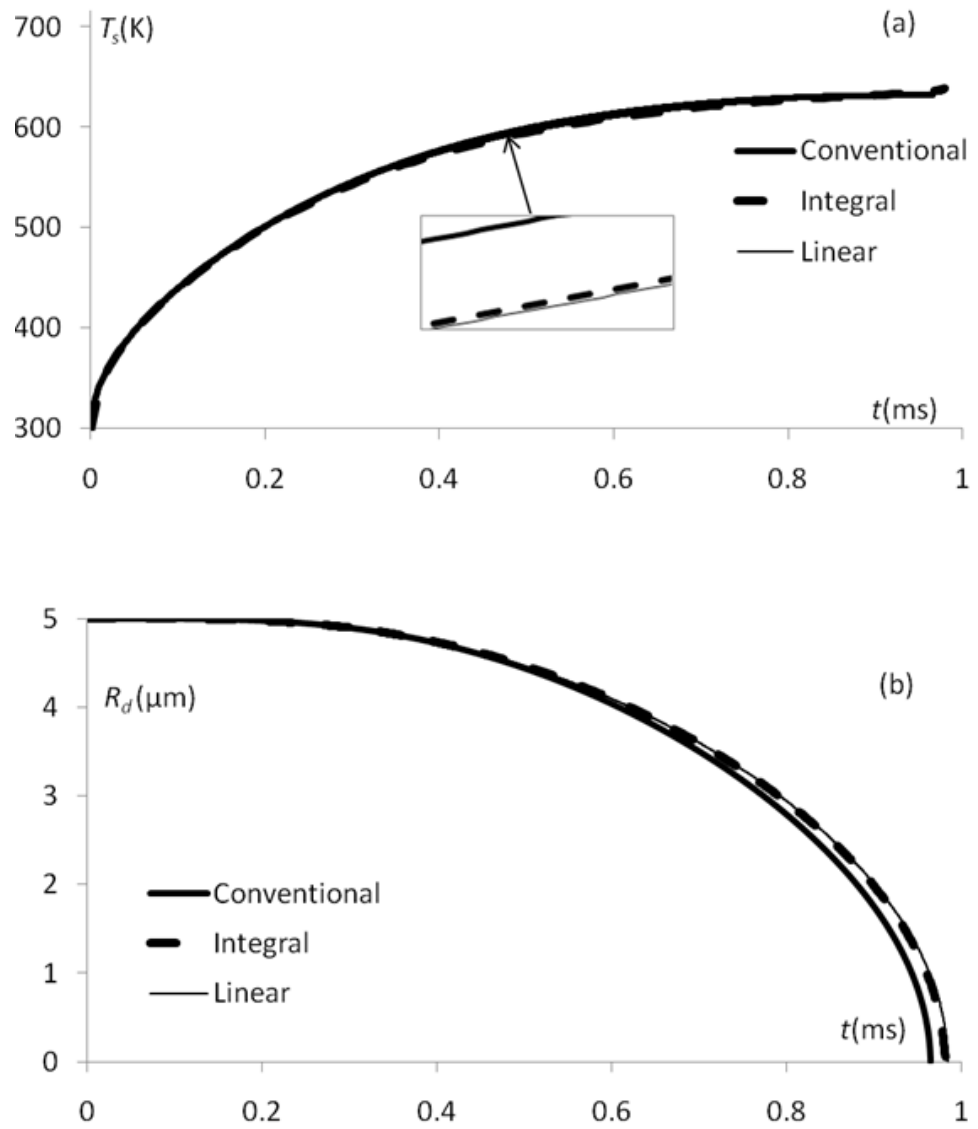


Figure 3.5: The same as Fig. 3.1 but for an ambient gas temperature equal to 800 K.

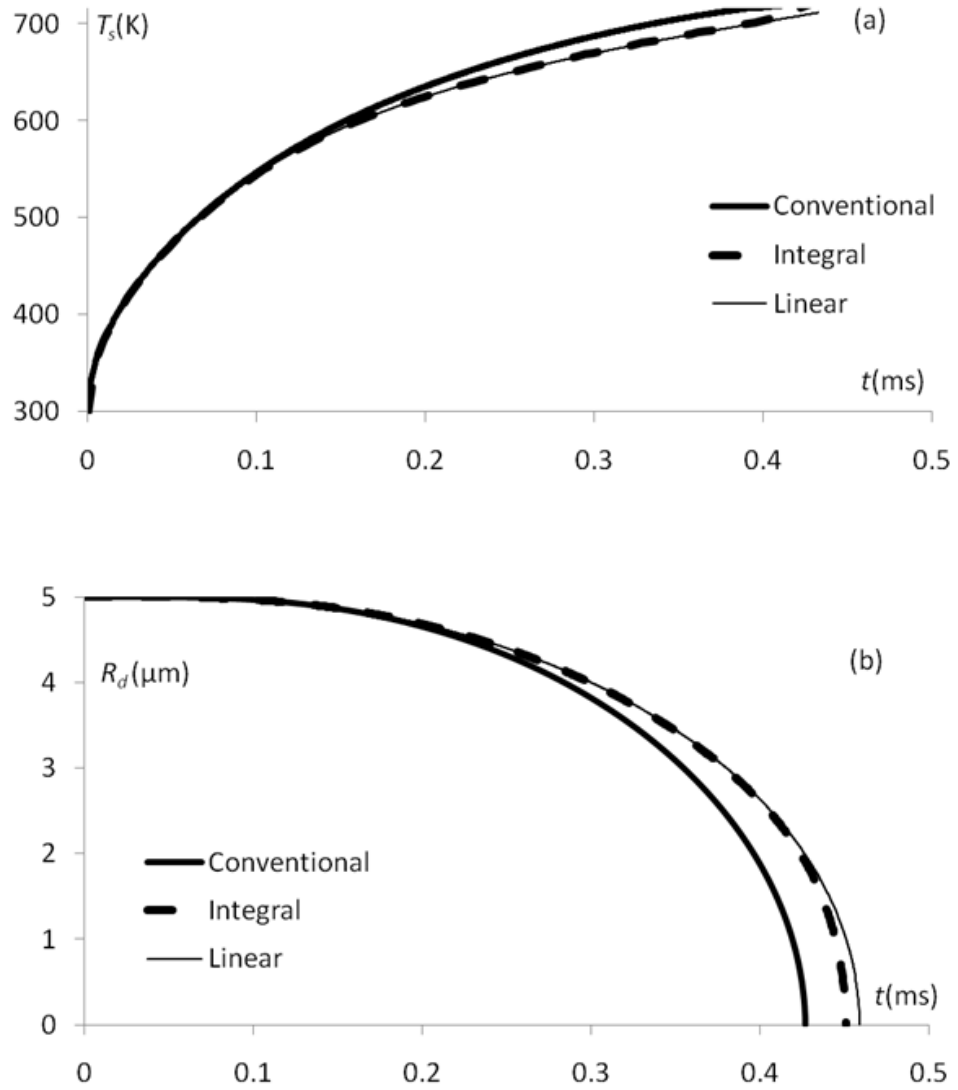


Figure 3.6: The same as Figs. 3.1 and 3.5 but for an ambient gas temperature equal to 1200 K.

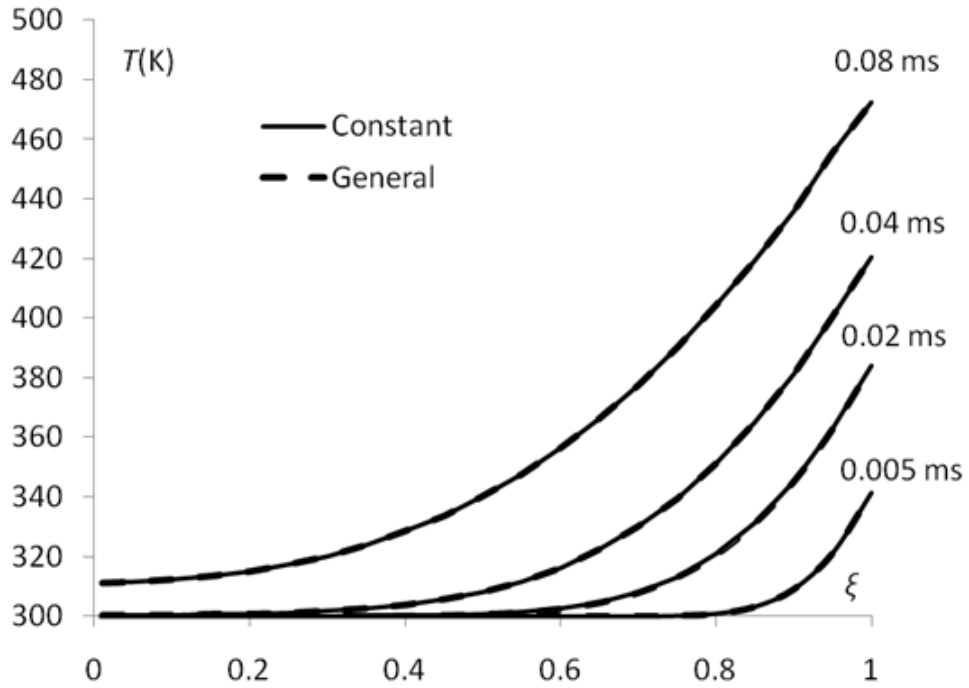


Figure 3.7: The plots of  $T$  versus  $\xi = R/R_d$  for a stationary n-dodecane ( $M_f = 170$  kg/kmole) droplet with initial radius  $5 \mu\text{m}$ , evaporating in ambient air at a pressure of  $p = 30 \text{ atm} = 3000 \text{ kPa}$  and temperature  $1000 \text{ K}$ . The moments of time are indicated near the curves. The calculations were performed based on Equations (3.11) (derived for constant initial distribution of temperatures inside droplets) and (3.23) (derived for the general case of the arbitrary distribution of the initial temperature inside the droplet).

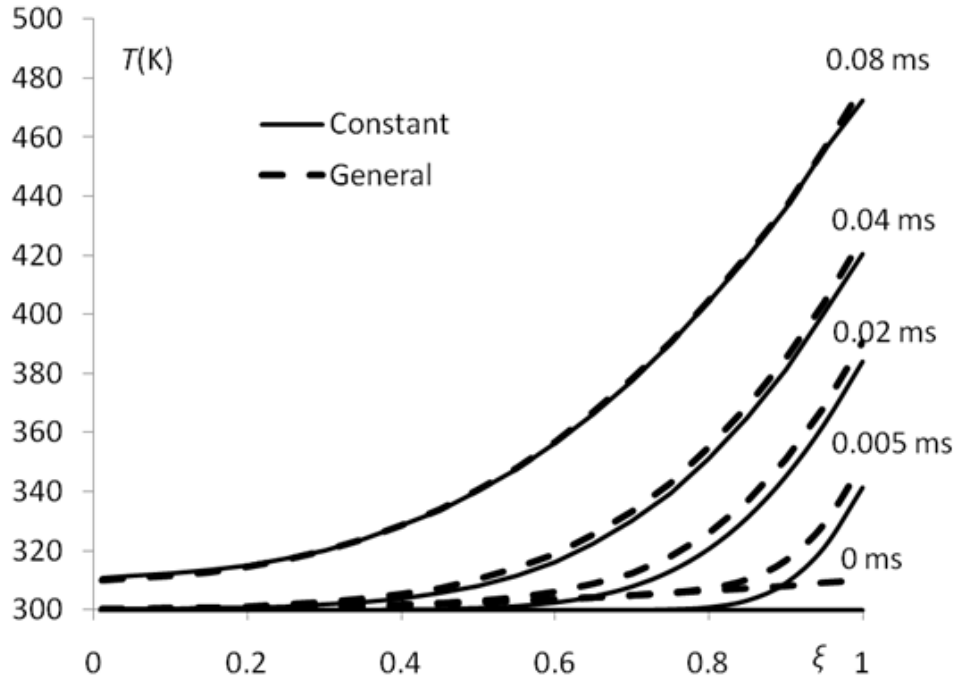


Figure 3.8: The same as Fig. 3.7 but for the general solution (Equation (3.23)) applied to the case when the initial distribution of temperature inside the droplet is given by Equation (3.24)).

distribution of droplet temperature was approximated as

$$T_{d0}(R) = 300 + 10(R/R_{d0})^2 = 300 + 10(\xi)^2, \quad (3.24)$$

and the analysis was based on Equation (3.23).

Comparing the plots referring to both cases, shown in Fig. 3.8, one can see that these plots visibly converge with time. This can be related to the fact that increased droplet surface temperature in the general case leads to decreased convective heating of droplets. Hence the droplet surface temperature increases more slowly in the general case than in the case of constant initial temperature inside droplets.

We appreciate that the errors associated with the conventional assumption that the droplet radii remain constant during the time step can be comparable with or even larger than those associated with other effects, including uncertainties in gas temperature measurements, convection heat transfer coefficient approximations and effect of interactions between droplets in realistic sprays. The importance of the latter effect is discussed in [14, 38], but its analysis lies beyond the scope of this Chapter.

## 3.6 Conclusions of Chapter 3

Two new solutions to the heat conduction equation, describing transient heating of an evaporating droplet, are suggested, assuming that the time evolution of droplet radius  $R_d(t)$  is known. The initial droplet temperature is assumed to be constant or allowed to change with the distance from the droplet centre. The results turned out to be the simplest in the first case and the main focus of our analysis is upon these. Since  $R_d(t)$  depends on the time evolution of the droplet temperature, an iterative process is required. Firstly, the time evolution of  $R_d(t)$  is obtained using the conventional approach, when it remains constant during the time step, but changes from one time step to another. The droplet surface temperature in this case is obtained from the analytical solution of the heat conduction equation inside the droplet. It is assumed that this droplet is heated by convection from the ambient gas, and its radius remains constant during the time step. Then these values of  $R_d(t)$  are used in the new solutions to obtain updated values of time evolution of the distribution of temperatures inside the droplet and on its surface. These new values of droplet temperature are used to update the function  $R_d(t)$ . This process continues until convergence is achieved, which typically takes place after about 15 iterations. The results of the calculations of droplet surface temperature, using this approach, are compared with the results obtained using the previously suggested approach when the droplet radius was assumed to be a linear function of time during individual time steps for typical Diesel engine-like conditions. For sufficiently small time steps the time evolutions of droplet surface temperatures and radii, predicted by both approaches coincide. This suggests that both approaches are correct and valid. Similarly to the case when droplet radius is assumed to be a linear function of time during the time step, the new solution predicts lower droplet temperatures and slower evaporation when the effects of the reduction of  $R_d$  are taken into account.

It is shown that in the case of constant droplet initial temperature, models both taking and not taking into account the changes in initial droplet temperature with the distance from the droplet centre, predict the same results. This suggests that both models are likely to be correct. It is shown that the temperatures predicted by the models based on the assumption of constant initial droplet temperature, and the one taking into account the increase in this temperature with the distance from

the droplet centre, tend to converge with time.

# Chapter 4

## New solutions to the species diffusion equation inside droplets in the presence of the moving boundary

### 4.1 Introduction of Chapter 4

The species diffusion equation, describing the dynamics of multi-component systems, its analysis and applications, has been widely discussed in the literature [53]. One of the most important applications of this equation is that to the analysis of evaporation of multi-component droplets [1, 54]. In realistic moving droplets, species diffusion takes place alongside species convection when Hill-type vortices are formed inside droplets [55]. In most practically relevant cases, however, the details of species distribution inside droplets are not important and the effects of species diffusion and convection can be described in terms of the spherically symmetric effective diffusivity model [1]. In [38] this model was applied to the analysis of heating and evaporation of bi-component ethanol/acetone droplets. In contrast to the previous studies of these processes, the authors of [38] based their analysis on the analytical solution to the species diffusion equation, which was incorporated into the numerical code, rather than on the numerical solution of this equation. This approach is expected to be more CPU efficient and accurate compared with the one based on the conventional

approach [16]. The model described in [38] has been generalised in [50] to take into account coupling between droplets and gas. As shown in Chapters 2, 3 and [23], in the case of the thermal conduction equation inside droplets the approximation that the droplet radius is constant during a time step leads to noticeable overestimation of droplet surface temperature and underestimation of its evaporation time, compared with the approach in which the change in droplet radius during the time step is ignored. Paired with the approach in which the change in droplet radius during the time step is ignored.

The main purpose of this chapter is to generalise the analytical solution to the species diffusion equation, reported in [38, 50], to the case when the changes in droplet radius during the time steps are taken into account. This new solution will be applied to the analysis of bi-component droplet evaporation. The importance of taking into account the changes in droplet radius during the time step will be investigated.

Basic equations and approximations for multi-component droplets used in our analysis are presented and discussed in Section 4.2. The details of the new analytical solution of the species diffusion equation are given in Section 4.3. In Section 4.4 this solution is applied to the analysis of bi-component droplet evaporation. Some results of calculation, taking into account the effects of the moving boundary on heat conduction and species diffusion equation inside droplets are presented in Section 4.5. The main results of the Chapter are summarised in Section 4.5.

## 4.2 Basic equations for multi-component droplets

Assuming that all processes inside droplets are spherically symmetric (droplets are stationary), the equations for mass fractions of liquid species  $Y_{li} \equiv Y_{li}(t, R)$  inside multi-component droplets can be presented in the following form [1]:

$$\frac{\partial Y_{li}}{\partial t} = D_l \left( \frac{\partial^2 Y_{li}}{\partial R^2} + \frac{2}{R} \frac{\partial Y_{li}}{\partial R} \right), \quad (4.1)$$

where  $i > 1$  and  $D_l$  is the liquid mass diffusivity.  $Y_{li}(t, R)$  is a twice continuously differentiable function. Equation (4.1) needs to be solved with the following boundary condition [1]:

$$\alpha_m(\epsilon_i - Y_{lis}) = -D_l \left. \frac{\partial Y_{li}}{\partial R} \right|_{R=R_d(t)-0}, \quad (4.2)$$

and the initial condition  $Y_{li}(t = 0) = Y_{li0}(R)$ , where  $Y_{lis} = Y_{lis}(t)$  are liquid components' mass fractions at the droplet's surface,

$$\alpha_m = \frac{|\dot{m}_d|}{4\pi\rho_l R_d^2}, \quad (4.3)$$

$\epsilon_i$  is the evaporation rate of species.

Note that  $0 \leq Y_{li} \leq 1$  due to the physical nature of this parameter.

We assume that  $R_d(t)$  is the linear function of  $t$  during each time step, described by Equation (2.8) in which  $\alpha = -\alpha_m/R_{d0}$ .

Although  $\alpha_m$  and  $\alpha$  are linked by a simple relation, it is important for us to retain the difference between these two parameters in this Chapter.  $\alpha_m$  describes the rate of removal of species from the surface of the droplet, while  $\alpha$  describes the rate of change in droplet radius during time steps. The latter effect was ignored in most previous analysis of this phenomenon, including [38, 50], where it was assumed that  $\alpha = 0$ , but  $\alpha_m \neq 0$  was still defined by Equation (4.3). In our analysis both these effects are taken into account.

Assuming that species concentrations in the ambient gas are equal to zero ( $Y_{vi\infty} = 0$ ), the values of  $\epsilon_i$  can be found from the following relation [38]:

$$\epsilon_i(t) = \frac{Y_{vis}}{\sum_j Y_{vjs}}, \quad (4.4)$$

where the subscript  $_v$  indicates the vapour phase. We assume that  $\epsilon_i$  are still defined by Equation (4.4) even in the case when these concentrations are not equal to zero. Equation (4.1) can be generalised to take into account the effect of moving droplets with the help of the effective diffusivity model [1] in which  $D_l$  in Equation (4.1) is replaced with

$$D_{\text{eff}} = \chi_Y D_l, \quad (4.5)$$

where the coefficient  $\chi_Y$  varies from 1 to 2.72 and can be approximated as:

$$\chi_Y = 1.86 + 0.86 \tanh [2.245 \log_{10} (\text{Re}_l \text{Sc}_l / 30)], \quad (4.6)$$

$\text{Sc}_l$  is the liquid Schmidt number defined as:

$$\text{Sc}_l = \frac{\nu_l}{D_l}, \quad (4.7)$$

$\nu_l$  is the liquid kinematic viscosity,  $\text{Re}_l$  is the Reynolds number based on droplet radius, liquid transport properties and the maximum surface velocity inside droplets.

The latter velocity was calculated as [44]:

$$U_s = \frac{1}{32} \Delta U \left( \frac{\mu_g}{\mu_l} \right) \text{Re}_d C_F, \quad (4.8)$$

where  $\Delta U \equiv U_g - U_d$  is the relative velocity between ambient gas and droplets,  $\mu_{g(l)}$  is the dynamic viscosity of gas (liquid),  $\text{Re}_d$  is the droplet Reynolds number based on the droplet diameter (denoted as  $\text{Re}_\infty$  in [44]),  $C_F$  is the friction drag coefficient estimated as [44]:

$$C_F = \frac{12.69}{\text{Re}_d^{2/3} (1 + B_M)}. \quad (4.9)$$

The value of  $U_s$ , predicted by Equation (4.8), is about 1.7 times less than predicted in [11], using an approach which differs slightly from the one suggested in [44]. Remembering that the result predicted by Equation (4.8) is closer to the earlier obtained numerical results (see [44] for the details), we decided to use (4.8) rather than the corresponding equation, given in [11] (see his Equation (2.74g)). Also, following [44] we used the coefficient 2.245, instead of 2.225, used in [11]. Note that for the values of parameters for which the new solution will be tested,  $\chi_Y \approx 2.72$  most of the time, and the results remain practically unchanged when  $U_s$  in the expression for  $\text{Re}_l$  is replaced with  $\Delta U$ .

In the case of isolated moving mono-component droplets, their evaporation rate is given by the following equation [1]:

$$\dot{m}_d = -2\pi R_d D_v \rho_{\text{total}} B_M \text{Sh}_{\text{iso}}, \quad (4.10)$$

where  $D_v$  is the binary diffusion coefficient of vapour in air,  $B_M$  is the Spalding mass transfer number, introduced in Equation (2.5),  $\text{Sh}_{\text{iso}}$  is the Sherwood number approximated for isolated droplets by the following expression:

$$\text{Sh}_{\text{iso}} = 2 \frac{\ln(1 + B_M)}{B_M} \left( 1 + \frac{(1 + \text{Re}_d \text{Sc}_a)^{1/3} \max[1, \text{Re}_d^{0.077}] - 1}{2F(B_M)} \right), \quad (4.11)$$

$$\text{Sc}_a = \frac{\nu_a}{D_v}$$

is the Schmidt number for the ambient gas,

$$F(B_M) = (1 + B_M)^{0.7} \frac{\ln(1 + B_M)}{B_M}.$$

It is assumed that this equation is valid for multi-component droplets by replacing  $Y_v$  with  $\sum_i Y_{vi}$  in Equation (2.5). The effects of interactions between droplets could

be accounted for by correcting the expression for  $\text{Sh}_{\text{iso}}$  (see [38, 49] for details). This effect is not taken into account in our analysis.

Note that Equation (4.10) is valid for arbitrary Lewis numbers, while the equation for  $\dot{m}_d$  used in Chapters 2 and 3 is valid only for Lewis numbers equal to 1.

To calculate the species mass evaporation rate  $\dot{m}_i$  and the values of the evaporation rate of species  $\epsilon_i$ , based on Equation (4.4), we need to calculate first the values of  $Y_{vis}$ . The latter depends on the partial pressure of species  $i$  in the vapour state in the immediate vicinity of the droplet surface [38]:

$$p_{vis} = X_{lis}\gamma_i p_{vis}^*, \quad (4.12)$$

where  $X_{lis}$  is the molar fraction of the  $i$ th species in the liquid near the droplet surface,  $p_{vis}^*$  is the partial vapour pressure of the  $i$ th species in the case when  $X_{lis} = 1$ ,  $\gamma_i$  is the activity coefficient. In our analysis we assume that  $\gamma_i = 1$  (the Raoult law is valid).

Remembering the Clausius-Clapeyron equation, Equation (4.12) for  $\gamma_i = 1$  can be rewritten as [38]:

$$p_{vis} = X_{lis}p_{\text{amb}} \exp \left[ \frac{L_i M_i}{R_u} \left( \frac{1}{T_{bi}} - \frac{1}{T_s} \right) \right], \quad (4.13)$$

where  $M_i$  is the molar mass and  $T_{bi}$  is the boiling temperature of the  $i$ th species,  $p_{\text{amb}}$  is the ambient pressure and  $R_u$  is the universal gas constant. When deriving Equation (4.13) it was taken into account that  $p_{vis}^*$  is equal to the ambient pressure when  $T_s = T_{bi}$ ,  $L_i$  is the latent heat of evaporation of species  $i$ .

Equation (4.13) is the generalisation of Equation (2.7).

### 4.3 Analytical solution of Equation (4.1)

Based on [19, 105], we introduce the following parameters and functions:

$$\begin{aligned} \xi &= R/R_d(t), \quad (0 \leq \xi \leq 1), \quad F(t, \xi) = RY_{li}(t, \xi R_{d0}), \\ F(t, \xi) &= \frac{1}{\sqrt{R_d(t)}} \exp \left[ -\frac{R'_d(t)R_d(t)}{4D_l} \xi^2 \right] W(t, \xi). \end{aligned} \quad (4.14)$$

These allow us to rewrite Equation (4.1), the corresponding initial condition and boundary condition (4.2) as:

$$R_d^2(t)W'_t(t, \xi) = D_l W''_{\xi\xi}(t, \xi), \quad (4.15)$$

where  $t \geq 0$ ,

$$W(t, \xi)|_{t=0} = W_0(\xi) \equiv R_{d0}^{3/2} \xi Y_{li0}(\xi R_{d0}) \exp \left[ \frac{R'_d(0) R_{d0}}{4D_l} \xi^2 \right], \quad (4.16)$$

$$W(t, \xi)|_{\xi=0} = 0, \quad (4.17)$$

$$\begin{aligned} & \left[ W'_\xi(t, \xi) + H_0(t) W(t, \xi) \right] \Big|_{\xi=1} \\ &= \mu_0(t) \equiv -\frac{\alpha_m \epsilon_i (R_d(t))^{5/2}}{D_l} \exp \left[ \frac{R'_d(t) R_d(t)}{4D_l} \right], \end{aligned} \quad (4.18)$$

where:

$$H_0(t) = -\frac{\alpha_m}{D_l} R_d(t) - 1 - \frac{R'_d(t) R_d(t)}{2D_l}.$$

Condition (4.17) is an additional boundary condition, which follows from the requirement that  $Y_{li}(t, R)$  is a twice continuously differentiable function. When deriving (4.15) we took into account that  $d^2 R_d/dt^2 = 0$ .

Further simplification of Equation (4.15) and the corresponding initial and boundary conditions is possible when we apply this equation to a short time step. In this case we can ignore the time dependence of  $H_0(t)$  and assume that  $H_0(t) \equiv h_0 = \text{const}$ .

Remembering Equation (2.8) we can write

$$h_0 = -\frac{\alpha_m}{D_l} R_d(t) - \frac{\alpha R_{d0}}{2D_l} R_d(t) - 1 \approx -\frac{\alpha_m}{D_l} R_{d0} - \frac{\alpha R_{d0}}{2D_l} R_{d0} - 1 < -1. \quad (4.19)$$

It is essential for us to retain both  $\alpha_m$  and  $\alpha$  in the expression for  $h_0$  if we intend to compare our results with the results of the conventional analysis when  $\alpha = 0$ , but  $\alpha_m \neq 0$ .

Our next goal is to find a change of variables such that the inhomogeneous boundary condition (4.18) is replaced by the homogeneous one. This is achieved by the introduction of the new function  $V(t, \xi)$  via the relation:

$$W(t, \xi) = V(t, \xi) + \frac{\mu_0(t)}{1 + h_0} \xi. \quad (4.20)$$

Formula (4.20) allows us to rearrange Equation (4.15) to:

$$R_d^2(t) V'_t(t, \xi) = D_l V''_{\xi\xi}(t, \xi) - \frac{\mu'_0(t)}{1 + h_0} R_d^2(t) \xi, \quad (4.21)$$

The initial and boundary conditions for Equation (4.21) can be presented as:

$$V(t, \xi)|_{t=0} = W_0(\xi) - \frac{\mu_0(0)}{1 + h_0} \xi,$$

$$V(t, \xi)|_{\xi=0} = 0, \quad \left[ V'_\xi(t, \xi) + h_0 V(t, \xi) \right] \Big|_{\xi=1} = 0.$$

As in Chapter 2, we look for the solution of Equation (4.21) in the form:

$$V(t, \xi) = \sum_{n=0}^{\infty} \Theta_n(t) v_n(\xi), \quad (4.22)$$

where functions  $v_n(\xi)$  form the full set of non-trivial solutions to the equation:

$$\frac{d^2 v}{d\xi^2} + p v = 0, \quad 0 \leq \xi \leq 1, \quad (4.23)$$

subject to boundary conditions:

$$v|_{\xi=0} = \left( \frac{dv}{d\xi} + h_0 v \right) \Big|_{\xi=1} = 0. \quad (4.24)$$

For  $p = 0$ , Equation (4.23) has no non-trivial solutions, satisfying the boundary conditions (4.24). For  $p \equiv -\lambda^2 < 0$ , this equation has the solution:

$$v_0(\xi) = \sinh(\lambda_0 \xi), \quad (4.25)$$

where  $\lambda_0$  is the solution to the equation

$$\tanh \lambda = -\frac{\lambda}{h_0}. \quad (4.26)$$

The latter equation has three solutions (positive, negative and zero) remembering that  $h_0 < -1$ . We are interested in the positive solution to this equation only [19].

Note that this solution does not exist in the case of the heat conduction equation, when  $h_0$  is greater than  $-1$  (see Chapter 2).

For  $p \equiv \lambda^2 > 0$ , Equation (4.23) has the solutions:

$$v_n(\xi) = \sin(\lambda_n \xi) \quad (4.27)$$

for  $n \geq 1$ , where  $\lambda_n$  are the solutions to the equation

$$\tan \lambda = -\frac{\lambda}{h_0}. \quad (4.28)$$

As in the case  $p < 0$  we disregard the solutions to this equation corresponding to zero and negative  $\lambda$ . A countable set of positive solutions to this equation (positive eigenvalues)  $\lambda_n$  are arranged in ascending order:

$$0 < \lambda_1 < \lambda_2 < \lambda_3 < \dots$$

It can be shown that functions  $v_n(\xi)$ ,  $n \geq 0$  are orthogonal for  $0 \leq \xi \leq 1$  (see Chapter 2).

The completeness of the set of functions  $v_n(\xi)$  for  $n \geq 0$  has been tested. Namely, we considered different functions not belonging to this set, and found that Fourier expansions of these functions on the set of  $\{v_n(\xi)\}_{n=0}^{\infty}$  coincide with the functions themselves. If the set of functions is not complete, then a Fourier expansion of an arbitrary function, constructed based on this set, does not coincide with this function.

The norms of functions  $v_n(\xi)$  for  $n \geq 0$  are given by the following expression

$$\|v_n\|^2 = \int_0^1 v_n^2(\xi) d\xi = \frac{(-1)^{\delta_{n,0}}}{2} \left[ 1 + \frac{h_0}{h_0^2 + (-1)^{\delta_{n,0}} \lambda_n^2} \right]. \quad (4.29)$$

where  $\delta_{n,0}$  is Kronecker's delta symbol.

Remembering that functions  $v_n(\xi)$  for  $n \geq 0$  are orthogonal and assuming that the set of these functions is complete, we can write:

$$f(\xi) \equiv -\xi/(1+h_0) = \sum_{n=0}^{\infty} f_n v_n(\xi), \quad (4.30)$$

$$W_0(\xi) = \sum_{n=0}^{\infty} q_n v_n(\xi), \quad (4.31)$$

where:

$$f_n = \frac{1}{\|v_n\|^2} \int_0^1 f(\xi) v_n(\xi) d\xi = \begin{cases} \frac{1}{\|v_0\|^2 \lambda_0^2} \sinh \lambda_0 & \text{when } n = 0 \\ -\frac{1}{\|v_n\|^2 \lambda_n^2} \sin \lambda_n & \text{when } n \geq 1 \end{cases},$$

$$q_n = \frac{1}{\|v_n\|^2} \int_0^1 W_0(\xi) v_n(\xi) d\xi.$$

Remembering Equations (4.22) and (4.30), Equation (4.21) can be rewritten as:

$$\sum_{n=0}^{\infty} \left( R_d^2(t) \frac{d\Theta_n(t)}{dt} + (-1)^{\delta_{n,0}} \Theta_n(t) D_l \lambda_n^2 \right) v_n(\xi) = \sum_{n=0}^{\infty} \left( f_n R_d^2(t) \frac{d\mu_0(t)}{dt} \right) v_n(\xi). \quad (4.32)$$

Both sides of Equation (4.32) are Fourier series with respect to functions  $v_n(\xi)$ . Two Fourier series are equal if, and only if, their coefficients are equal. This implies that:

$$R_d^2(t) \frac{d\Theta_n(t)}{dt} + (-1)^{\delta_{n,0}} \Theta_n(t) D_l \lambda_n^2 = f_n R_d^2(t) \frac{d\mu_0(t)}{dt}. \quad (4.33)$$

Equation (4.33) is to be solved subject to the initial condition:

$$\Theta_n(0) = q_n + \mu_0(0) f_n. \quad (4.34)$$

The general solution to the homogeneous equation:

$$R_d^2(t) \frac{d\Theta_n(t)}{dt} + (-1)^{\delta_{n,0}} \Theta_n(t) D_l \lambda_n^2 = 0 \quad (4.35)$$

can be presented as:

$$\ln(\Theta_n(t)/\Theta_n(0)) = -(-1)^{\delta_{n,0}} D_l \lambda_n^2 \int_0^t \frac{dt}{R_d^2(t)}. \quad (4.36)$$

Assuming that  $R_d(t)$  is a linear function of  $t$  given by Equation (2.8), Solution (4.36) can be presented in a more explicit form:

$$\Theta_n(t) = \Theta_n(0) \exp \left[ \frac{(-1)^{\delta_{n,0}} D_l \lambda_n^2}{\alpha R_{d0}^2} \left( \frac{1}{1 + \alpha t} - 1 \right) \right]. \quad (4.37)$$

One can see that the following function:

$$\Theta_{n \text{ (part)}}(t) = f_n \int_0^t \frac{d\mu_0(\tau)}{d\tau} \exp \left[ (-1)^{\delta_{n,0}} \frac{D_l \lambda_n^2}{\alpha R_{d0}^2} \left( \frac{1}{1 + \alpha t} - \frac{1}{1 + \alpha \tau} \right) \right] d\tau \quad (4.38)$$

satisfies Equation (4.33). Hence, this function can be considered as a particular solution of Equation (4.33). Integration by parts in (4.38) allows us to present  $\Theta_{n \text{ (part)}}(t)$  as:

$$\begin{aligned} \Theta_{n \text{ (part)}}(t) = f_n \left\{ \mu_0(t) - \mu_0(0) \exp \left[ -(-1)^{\delta_{n,0}} \frac{D_l \lambda_n^2 t}{R_{d0} R_d(t)} \right] \right. \\ \left. - \exp \left[ (-1)^{\delta_{n,0}} \frac{D_l \lambda_n^2}{\alpha R_{d0} R_d(t)} \right] \int_0^t (-1)^{\delta_{n,0}} \frac{\mu_0(\tau) D_l \lambda_n^2}{R_d^2(\tau)} \exp \left[ -(-1)^{\delta_{n,0}} \frac{D_l \lambda_n^2}{\alpha R_{d0} R_d(\tau)} \right] d\tau \right\}. \end{aligned} \quad (4.39)$$

Remembering Equations (4.37) and (4.38), the solution to Equation (4.33) can be presented as:

$$\begin{aligned} \Theta_n(t) = \Theta_n(0) \exp \left[ (-1)^{\delta_{n,0}} \frac{D_l \lambda_n^2}{\alpha R_{d0}^2} \left( \frac{1}{1 + \alpha t} - 1 \right) \right] \\ + f_n \int_0^t \frac{d\mu_0(\tau)}{d\tau} \exp \left[ (-1)^{\delta_{n,0}} \frac{D_l \lambda_n^2}{\alpha R_{d0}^2} \left( \frac{1}{1 + \alpha t} - \frac{1}{1 + \alpha \tau} \right) \right] d\tau. \end{aligned} \quad (4.40)$$

Remembering (4.39) and (4.34) we can write an alternative formula for  $\Theta_n(t)$ :

$$\begin{aligned} \Theta_n(t) = q_n \exp \left[ -(-1)^{\delta_{n,0}} \frac{D_l \lambda_n^2 t}{R_{d0} R_d(t)} \right] + f_n \mu_0(t) \\ - f_n (-1)^{\delta_{n,0}} D_l \lambda_n^2 \int_0^t \frac{\mu_0(\tau)}{R_d^2(\tau)} \exp \left[ (-1)^{\delta_{n,0}} \frac{D_l \lambda_n^2}{\alpha R_{d0}} \left( \frac{1}{R_d(t)} - \frac{1}{R_d(\tau)} \right) \right] d\tau. \end{aligned} \quad (4.41)$$

Remembering that Solution (4.41) is applied to a very short time step, changes of  $\mu_0(\tau)$  in the integrand before the exponential term can be ignored. This allows us to simplify (4.41) to (see Appendix 6):

$$\Theta_n(t) = [q_n + f_n\mu_0(0)] \exp \left[ -(-1)^{\delta_{n,0}} \frac{D_l \lambda_n^2 t}{R_{d0} R_d(t)} \right] + f_n\mu_0(t) - f_n\mu_0(0). \quad (4.42)$$

Note that  $\Theta_n(t)$  in the form (4.40) satisfies Equation (4.33), while  $\Theta_n(t)$  in the form (4.42) does not satisfy it. This is related to the fact that Equation (4.33) was derived under the assumption that Series (4.22), after being substituted into Equation (4.21), can be differentiated term by term (derivative of the series is equal to the series of derivatives). This assumption is valid when  $\Theta_n(t)$  is taken in the form (4.40), but it is not valid when  $\Theta_n(t)$  is taken in the form (4.42), as:

$$\mu_0(t) \frac{d^2}{d\xi^2} \left( \sum_{n=0}^{\infty} f_n v_n \right) \neq \mu_0(t) \sum_{n=0}^{\infty} f_n \frac{d^2 v_n}{d\xi^2}$$

(the series on the right hand side of this formula diverges). Note that Series (4.22) satisfies Equation (4.21) regardless of whether  $\Theta_n(t)$  is taken in the form (4.40) or in the form (4.42).

Remembering (4.30) and (4.42), Equation (4.22) can be rewritten as:

$$V(t, \xi) = \sum_{n=0}^{\infty} \check{\Theta}_n(t) v_n(\xi) - \frac{\mu_0(t)}{1+h_0} \frac{R}{R_d(t)} + \frac{\mu_0(0)}{1+h_0} \frac{R}{R_d(t)}, \quad (4.43)$$

where

$$\check{\Theta}_n(t) = [q_n + f_n\mu_0(0)] \exp \left[ -(-1)^{\delta_{n,0}} \frac{D_l \lambda_n^2 t}{R_{d0} R_d(t)} \right]. \quad (4.44)$$

The final equation for mass fraction inside the droplet can be presented as:

$$Y_{li}(R) = \frac{1}{R\sqrt{R_d(t)}} \exp \left[ -\frac{\alpha R_{d0} R^2}{4D_l R_d(t)} \right] \left[ \sum_{n=1}^{\infty} \check{\Theta}_n(t) \sin \left( \lambda_n \frac{R}{R_d(t)} \right) + \check{\Theta}_0(t) \sinh \left( \lambda_0 \frac{R}{R_d(t)} \right) + \frac{\mu_0(0)}{1+h_0} \frac{R}{R_d(t)} \right], \quad (4.45)$$

where  $\check{\Theta}_n$  is given by Equation (4.44).

Having substituted (4.44) into (4.45) we can rearrange the latter equation for the short time step to

$$Y_{li}(R) = \frac{\alpha_m \epsilon_i \exp \left[ \frac{\alpha R_{d0}}{4D_l} \left( \frac{R_{d0} R_d(t) - R^2}{R_d(t)} \right) \right]}{\alpha_m + \frac{\alpha R_{d0}}{2}} \frac{R_{d0}^{5/2}}{R_d^{5/2}(t)} + \frac{1}{R\sqrt{R_d(t)}} \exp \left[ -\frac{\alpha R_{d0} R^2}{4D_l R_d(t)} \right] \times \left[ \sum_{n=1}^{\infty} [q_n + f_n\mu_0(0)] \exp \left[ -\frac{D_l \lambda_n^2 t}{R_{d0} R_d(t)} \right] \sin \left( \lambda_n \frac{R}{R_d(t)} \right) + \right.$$

$$[q_0 + f_0\mu_0(0)] \exp \left[ \frac{D_l \lambda_0^2 t}{R_{d0} R_d(t)} \right] \sinh \left( \lambda_0 \frac{R}{R_d(t)} \right). \quad (4.46)$$

When  $\alpha = 0$  but  $\alpha_m \neq 0$  during the time step, Equation (4.46) can be further simplified to

$$Y_{li}(R) = \epsilon_i + \frac{1}{R\sqrt{R_d(t)}} \left[ \sum_{n=1}^{\infty} [q_n + f_n\mu_0(0)] \exp \left[ -\frac{D_l \lambda_n^2 t}{R_{d0} R_d(t)} \right] \sin \left( \lambda_n \frac{R}{R_d(t)} \right) + [q_0 + f_0\mu_0(0)] \exp \left[ \frac{D_l \lambda_0^2 t}{R_{d0} R_d(t)} \right] \sinh \left( \lambda_0 \frac{R}{R_d(t)} \right) \right]. \quad (4.47)$$

This equation is identical to Equation (13) of [38]. Note that in [38] and [50] the norm of  $v_n$  ( $\|v_n\|^2$ ) is dimensional. The ratio of  $\|v_n\|^2$  used in [38, 50] and in this Chapter is equal to  $R_{d0}$ .

Let us now relax our assumption that  $H_0(t) \equiv h_0 = \text{const}$  and assume that:

$$H_0(t) = h_0 + h_1(t), \quad (4.48)$$

where  $h_0 = \text{const} < -1$ . In view of (4.48) we can rewrite the boundary condition at  $\xi = 1$  for Equation (4.15) in the form:

$$\left[ W'_\xi(t, \xi) + h_0 W(t, \xi) \right] \Big|_{\xi=1} = \mu_0(t) - h_1(t) W(t, 1) \equiv \hat{\mu}_0(t). \quad (4.49)$$

Assuming that  $\hat{\mu}_0(t)$  is known, we can formally use the previously obtained solutions (4.20) and (4.22) to present the solution to Problem (4.15)–(4.18) in the form:

$$W(t, \xi) = \frac{\hat{\mu}_0(t)}{1 + h_0} \xi + V(t, \xi) = \sum_{n=0}^{\infty} v_n(\xi) q_n \exp \left[ -(-1)^{\delta_{n,0}} \frac{D_l \lambda_n^2 t}{R_{d0} R_d(t)} \right] - \sum_{n=0}^{\infty} v_n(\xi) (-1)^{\delta_{n,0}} f_n D_l \lambda_n^2 \times \int_0^t \frac{\hat{\mu}_0(\tau)}{R_d^2(\tau)} \exp \left[ (-1)^{\delta_{n,0}} \frac{D_l \lambda_n^2}{\alpha R_{d0}} \left( \frac{1}{R_d(t)} - \frac{1}{R_d(\tau)} \right) \right] d\tau, \quad (4.50)$$

where Expression (4.41) for  $\Theta_n(t)$  has been used.

In contrast to the previous case of  $H_0(t) = \text{const}$ , Equation (4.50) does not give us an explicit solution for  $W(t, \xi)$  since  $\hat{\mu}_0(t)$  depends on  $W(t, 1)$ .

Equation (4.50) can be presented in a more compact form:

$$W(t, \xi) = \mathcal{V}(t, \xi) - \int_0^t \hat{\mu}_0(\tau) G(t, \tau, \xi) d\tau, \quad (4.51)$$

where

$$\begin{aligned}\mathcal{V}(t, \xi) &= \sum_{n=0}^{\infty} v_n(\xi) q_n \exp \left[ -(-1)^{\delta_{n,0}} \frac{D_l \lambda_n^2 t}{R_{d0} R_d(t)} \right] \\ G(t, \tau, \xi) &= - \sum_{n=0}^{\infty} v_n(\xi) \\ &\times \frac{D_l v_n(1)}{R_d^2(\tau) \|v_n\|^2} \exp \left[ (-1)^{\delta_{n,0}} \frac{D_l \lambda_n^2}{\alpha R_{d0}} \left( \frac{1}{R_d(t)} - \frac{1}{R_d(\tau)} \right) \right].\end{aligned}$$

Explicit expressions for  $f_n$  have been used in these formulae. Both functions  $\mathcal{V}(t, \xi)$  and  $G(t, \tau, \xi)$  are assumed to be known.

Remembering (4.49), we can rewrite Equation (4.51) as:

$$W(t, \xi) = \mathcal{V}(t, \xi) - \int_0^t [\mu_0(\tau) - h_1(\tau)W(\tau, 1)] G(t, \tau, \xi) d\tau. \quad (4.52)$$

This is an integral representation for a solution to Problem (4.15)–(4.18) for time dependent  $H_0(t)$  given by Equation (4.48). For  $\xi = 1$ , integral representation (4.52) reduces to the Volterra integral equation of the second kind for function  $W(t, 1)$ :

$$W(t, 1) = \mathcal{V}(t, 1) - \int_0^t [\mu_0(\tau) - h_1(\tau)W(\tau, 1)] G(t, \tau, 1) d\tau. \quad (4.53)$$

One can show that:

$$\frac{v_n^2(\xi = 1)}{\|v_n\|^2} = \frac{2(-1)^{\delta_{n,0}} \lambda_n^2}{(-1)^{\delta_{n,0}} \lambda_n^2 + h_0^2 + h_0}. \quad (4.54)$$

Remembering (4.54) we obtain:

$$\begin{aligned}G(t, \tau, 1) &= - \frac{2D_l}{R_d^2(\tau)} \sum_{n=0}^{\infty} \frac{(-1)^{\delta_{n,0}} \lambda_n^2}{h_0^2 + h_0 + (-1)^{\delta_{n,0}} \lambda_n^2} \\ &\times \exp \left[ (-1)^{\delta_{n,0}} \frac{D_l \lambda_n^2}{\alpha R_{d0}} \left( \frac{1}{R_d(t)} - \frac{1}{R_d(\tau)} \right) \right].\end{aligned} \quad (4.55)$$

Equation (4.53) has a unique solution, although this solution cannot be found in an explicit form. The numerical solution can be found as described in Appendix 2. Once the solution to this equation has been found we can substitute it into integral representation (4.52) and find the required solution to the initial and boundary value Problem (4.15) – (4.18). The required distribution of  $Y_{li}$  is found to be:

$$Y_{li}(t, R) = \frac{1}{R\sqrt{R_d(t)}} \exp \left[ - \frac{R'_d(t)R^2}{4D_l R_d(t)} \right] W(t, R/R_d(t)). \quad (4.56)$$

The numerical algorithm, in which the above solution is used for the analysis of droplet heating and evaporation is essentially the same as described in Section 4 of

[50]. Since the main focus of this Chapter is on the analysis of the new physical effects produced by the droplet moving boundary, the optimisation of the algorithm is beyond its scope (cf. the analysis of accuracy and CPU efficiency of the related algorithm, not taking into account the effects of the moving boundary, described in Section 7 of [50]). Note that the speed of convergence of the algorithm turned out to be very high. Even calculations based on 100 time steps led to almost the same results as those based on  $10^5$  time steps. In the case of 100 time steps the CPU time was less than 5 sec. Calculations were performed on a 3 GHz CPU, 2 GB RAM work station.

## 4.4 Application to bi-component droplets

### 4.4.1 Effect of species diffusion

In this section, Solution (4.47) is applied to the analysis of bi-component droplet heating and evaporation in an environment close to the one described in [38]. We will consider only the case of an initial 50% ethanol – 50% acetone mixture and droplets with initial diameter equal to  $142.7 \mu\text{m}$ . In contrast to [38] we ignore the interaction between droplets and the time evolution of droplet velocity and assume that this velocity is equal to  $12.71 \text{ m/s}$  (the initial droplet velocity described in [38]). The mixture is assumed to be ideal (the Raoult law is valid). The effects of droplets on gas have been ignored at this stage.

To separate the effect of the moving boundary on the species diffusion equation from a similar effect on the heat conduction equation inside droplets, described in previous Chapters, we make a rather artificial assumption that the droplet temperature is homogeneous and fixed. We assume that this temperature is equal to  $37.5 \text{ }^\circ\text{C}$  (the initial temperature considered in [38]). This approach allowed us to study the effect of the moving boundary on species diffusion alone, and not the effects of the moving boundary on both species diffusion and heat conduction simultaneously. In the latter case we would not be able to separate these two effects.

The plots of mass fraction of ethanol,  $Y_{\text{eth}}$ , versus normalised radius  $\xi$  for three moments of time (0.001 s, 0.01 s and 0.03 s), predicted by the conventional model, and the new model, taking into account the effects of the moving boundary, are

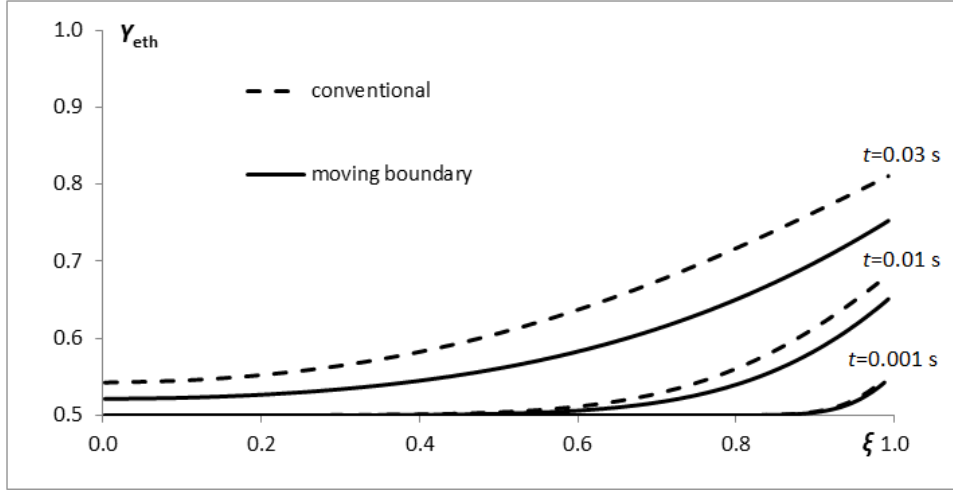


Figure 4.1: The plots of ethanol mass fraction  $Y_{\text{eth}}$  versus  $\xi = R/R_d$ , as predicted by the conventional model (dashed) and the new model, taking into account the effect of the moving boundary (solid), for times 0.001 s, 0.01 s and 0.03 s. We consider an initial 50% ethanol – 50% acetone mixture and droplets with initial diameter equal to  $142.7 \mu\text{m}$ .

shown in Fig. 4.1. As expected, both models predict the increase of  $Y_{\text{eth}}$  with increasing  $\xi$  and time. This is related to higher volatility of acetone in the ethanol/acetone mixture. As one can see from Fig. 4.1, at times less than 0.001 s the predictions of the conventional and the new models are practically indistinguishable. At later times, however, the new model always predicts lower values of  $Y_{\text{eth}}$  compared with the conventional model. In fact the effect of the moving boundary on the distribution of species looks stronger than a similar effect on the distribution of temperature inside droplets as reported in Chapter 2.

The plots of  $Y_{\text{eth}}$  at the droplet surface ( $Y_{\text{eth}}(\xi = 1)$ ) versus time, predicted by the conventional model, and the new model, taking into account the effect of the moving boundary, are shown in Fig. 4.2. As one can see from this figure, both models predict the increase of  $Y_{\text{eth}}(\xi = 1)$  with increasing time until  $Y_{\text{eth}}(\xi = 1)$  approaches 1 (all acetone from the droplet's surface has evaporated). This agrees with the results shown in Fig. 4.1. As in the case shown in Fig. 4.1, the new model always predicts lower values of  $Y_{\text{eth}}(\xi = 1)$  compared with the conventional model, except at short times and the times when  $Y_{\text{eth}}(\xi = 1)$  approaches unity.

The plots of the droplet radius  $R_d$  versus time, predicted by the conventional

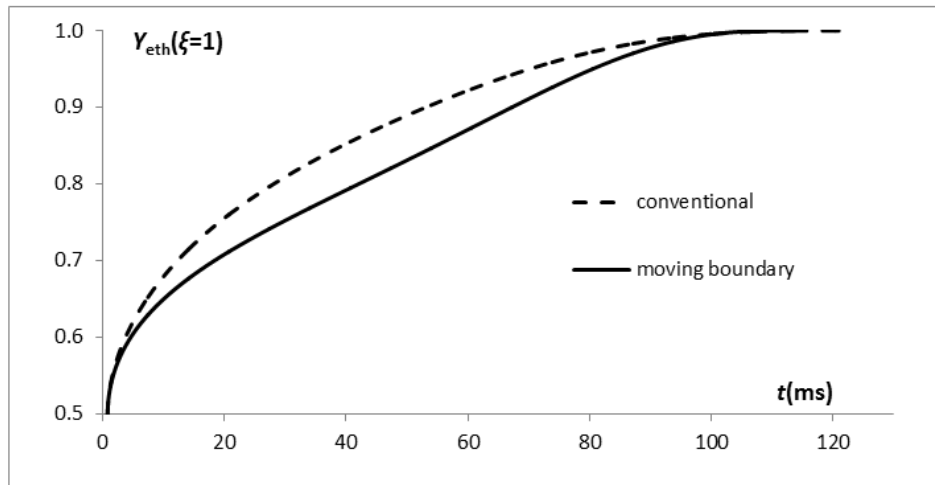


Figure 4.2: The plots of  $Y_{\text{eth}}(\xi = 1)$  versus time, as predicted by the conventional model (dashed) and the new model, taking into account the effect of the moving boundary (solid).

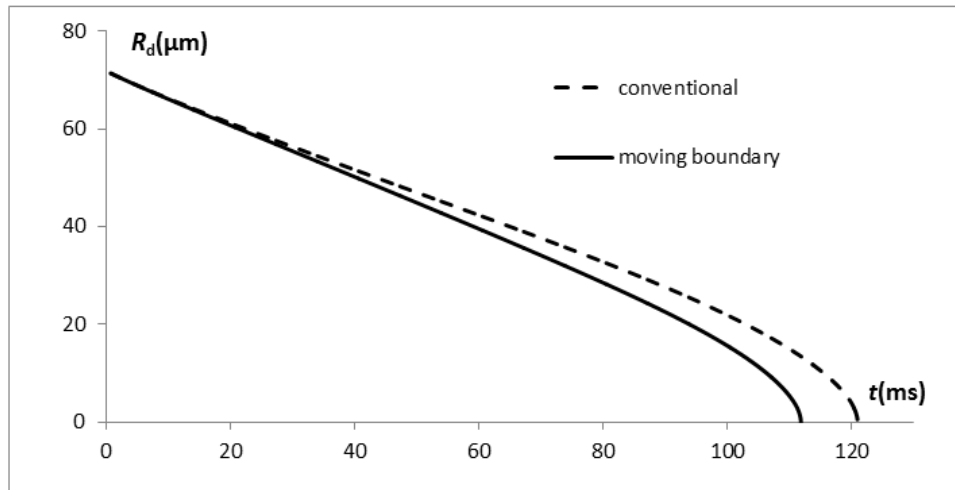


Figure 4.3: The plots of droplet radius  $R_d$  versus time, as predicted by the conventional model (dashed) and the new model, taking into account the effect of the moving boundary (solid).

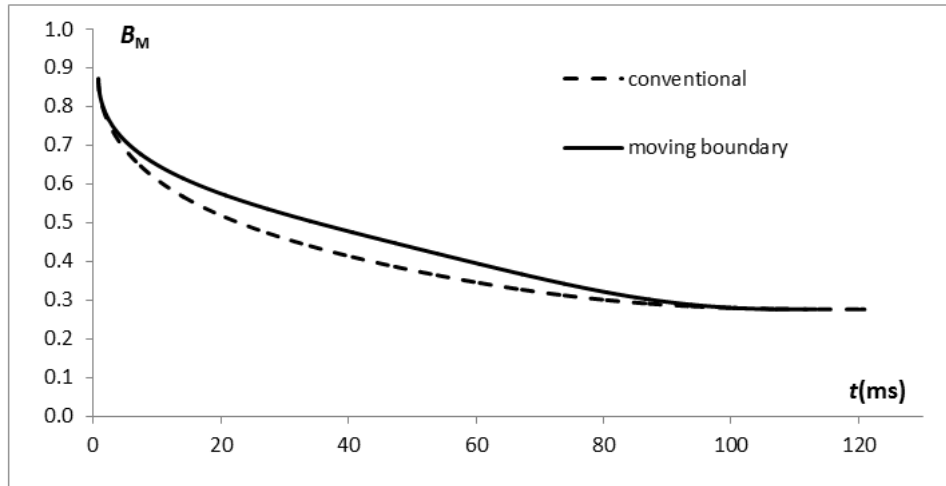


Figure 4.4: The plots of Spalding mass transfer number  $B_M$  versus time, as predicted by the conventional model (dashed) and the new model, taking into account the effect of the moving boundary (solid).

model, and the new model, taking into account the effects of the moving boundary, are shown in Fig. 4.3. As one can see from this figure, taking into account the effect of the moving boundary leads to the acceleration of droplet evaporation compared with the prediction of the conventional model. This effect is opposite to the one reported earlier for the effect of the moving boundary on the thermal conductivity inside droplets. In the latter case, the effect of the moving boundary led to slowing down of droplet evaporation. The physical background to the effect shown in Fig. 4.3 is that the new model predicts higher mass fraction of acetone at the surface of the droplet, as shown in Fig. 4.2, which evaporates faster than ethanol.

Note that for mono-component droplets at fixed temperature we would expect that the  $d^2$ -law should be valid. This is obviously not the case shown in Fig. 4.3. The reason for this is that the evaporation of multi-component droplets leads to changes in the Spalding mass transfer number  $B_M$  due to the changes in vapour composition near the droplet's surface. The plots of  $B_M$  versus time, predicted by the conventional model, and the new model, taking into account the effects of the moving boundary, are shown in Fig. 4.4. As can be seen from this figure, both models predict the decrease in  $B_M$  with time except at the final stage of droplet evaporation, when the droplet becomes mono-component, consisting only of ethanol. The new model predicts larger  $B_M$  compared with the conventional model. Note that except

at the final stage of droplet evaporation  $B_M$  is approximately proportional to droplet radius  $R_d$ . In this case, remembering that  $B_M < 1$ , we can expect that  $dR_d/dt$  is close to being constant, in agreement with Fig. 4.3.

#### 4.4.2 Combined effects of species and thermal diffusion

In this section the effect of the moving boundary on both heat transfer and species diffusion equations is discussed. The model is based on the model from Chapter 2 and model discussed in this chapter earlier.

The experimental set-up used for validation of the model is the same as described in [38, 49, 55]. In what follows this setup and input parameters are briefly summarised. A monodisperse droplet stream was generated by a Rayleigh-type disintegrating liquid jet. The initial fuel temperature was measured near the nozzle by a thermocouple. Downstream distance from the injector was converted into time with the help of the space evolution of the droplet velocity. Droplets were injected into a quiescent atmosphere at room temperature. Droplet temperatures were measured using the technique described in [49, 55]. The input parameters for the models were the initial droplet temperature (assuming that this temperature is homogeneous), ambient gas temperature (assuming that this temperature remains constant during the experiment), the distance parameter (ratio of the distances between droplets and their diameters) and the droplet velocities. Our analysis is focused on pure acetone, ethanol and various mixtures of acetone and ethanol droplets.

Substance	Approximation of $U_{\text{drop}}$ in m/s ( $t$ is in ms)
100% acetone	$12.81 - 0.316 t$
100% ethanol	$12.30 - 0.344 t$
25% ethanol + 75% acetone	$12.75 - 0.370 t$
50% ethanol + 50% acetone	$12.71 - 0.448 t$
75% ethanol + 25% acetone	$12.28 - 0.306 t$

Table 4.1: Approximations of acetone, ethanol and their mixtures' droplet velocities.

The measured time evolution of the droplet velocities in the axial direction was

shown to be close to a linear function. The relevant approximations of the experimental results are summarised in Table 4.1 (reproduced from [38]).

Substance	Droplet temp.	Diameter	Gas temp.	Dist. parameter
100% acetone	35.1°C	143.4 $\mu\text{m}$	21.5°C	7.7
100% ethanol	38.0°C	140.8 $\mu\text{m}$	22.0°C	7.1
25% ethanol + 75% acetone	32.5°C	133.8 $\mu\text{m}$	21.1°C	8.7
50% ethanol + 50% acetone	37.5°C	142.7 $\mu\text{m}$	20.8°C	7.53
75% ethanol + 25% acetone	38.6°C	137.1 $\mu\text{m}$	21.6°C	7.53

Table 4.2: The measured initial values of droplet temperature, diameter, ambient gas temperature and distance parameter for the same cases as in Table 4.1.

The measured initial values of droplet temperature, diameter, ambient gas temperature and distance parameter  $C$  (ratio of the distance between droplets to their diameters) for the same cases as in Table 4.1 are shown in Table 4.2. Gas temperature was constant during the measurements. The changes in  $C$  from the previous to the current time step were taken into account based on the following equation:

$$C_{\text{new}} = C_{\text{old}} \frac{U_{\text{drop,new}}}{U_{\text{drop,old}}} \frac{R_{d,\text{old}}}{R_{d,\text{new}}}, \quad (4.57)$$

where subscripts <sub>new</sub> and <sub>old</sub> refer to the values of variables at the previous time step and one time step behind respectively. In this case the values of  $R_{d,\text{old}}$  and  $R_{d,\text{new}}$  are known at the current time step.

The plots of time evolutions of the temperatures at the centre and the surface of the droplets and the average droplet temperatures, predicted by the models not taking into account the effect of the moving boundary and taking into account this effect for both temperature and species diffusion for the 25% ethanol – 75% acetone and 50% ethanol – 50% acetone mixture droplets, are shown in Fig. 4.5. As can be seen from this figure, the effect of the moving boundary on the predicted temperatures can be safely ignored in the analysis of experimental data described earlier. The same conclusion can be drawn for the case of the 75% ethanol – 25% acetone mixture droplets (figure is not shown).

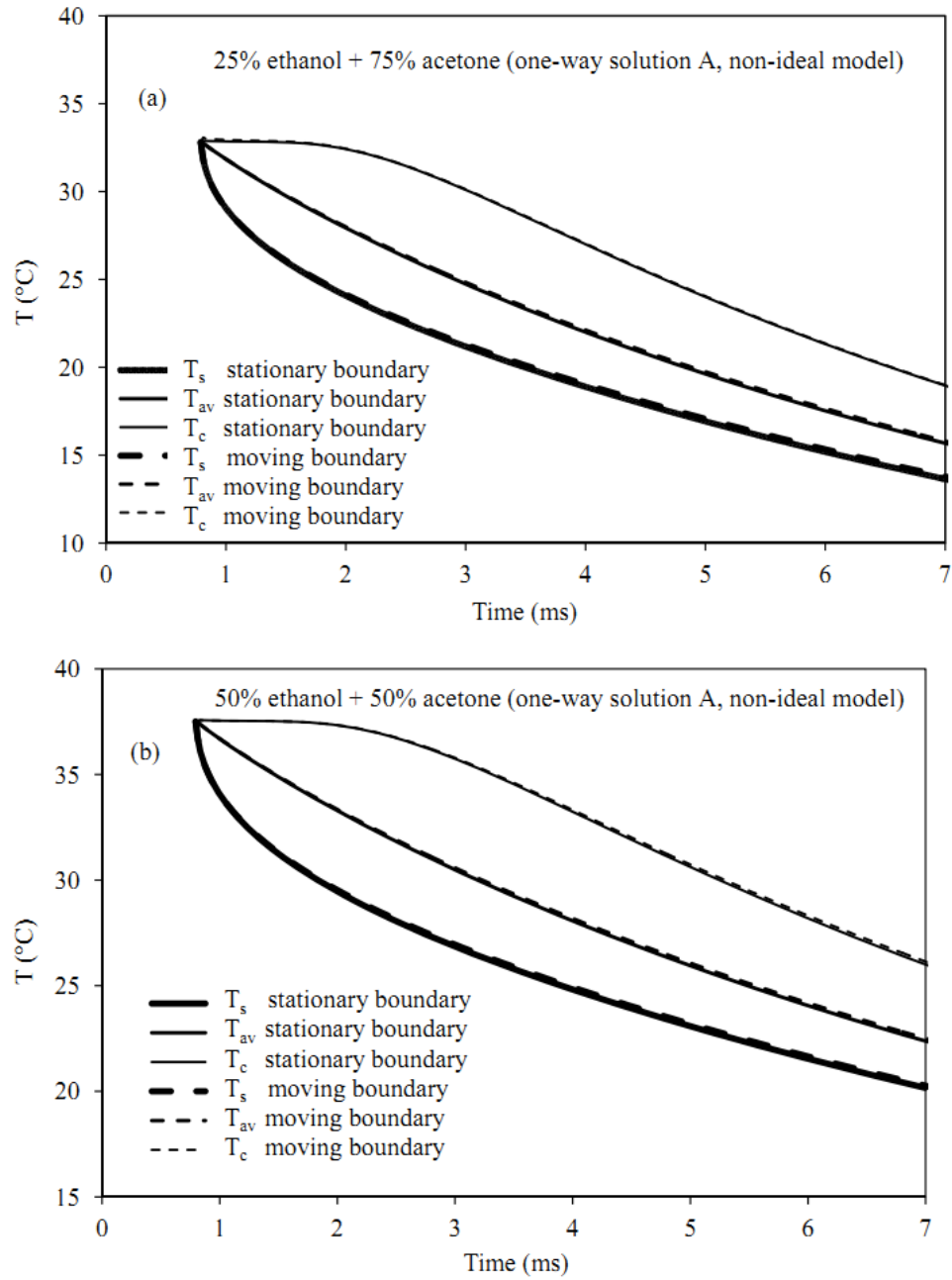


Figure 4.5: The time evolution of droplet surface, average and centre temperatures ( $T_s$ ,  $T_{av}$  and  $T_c$ ), predicted by the one-way Solution A for the non-ideal model, taking and not taking into account the effects of the moving boundary during individual time steps (moving and stationary boundaries) on the solutions to both heat transfer and species diffusion equations for the 25% ethanol – 75% acetone mixture droplets with the values of the initial parameters, droplet velocity and gas temperature given in Tables 4.1 and 4.2 (a); the same as (a) but for the 50% ethanol – 50% acetone mixture droplets (b).

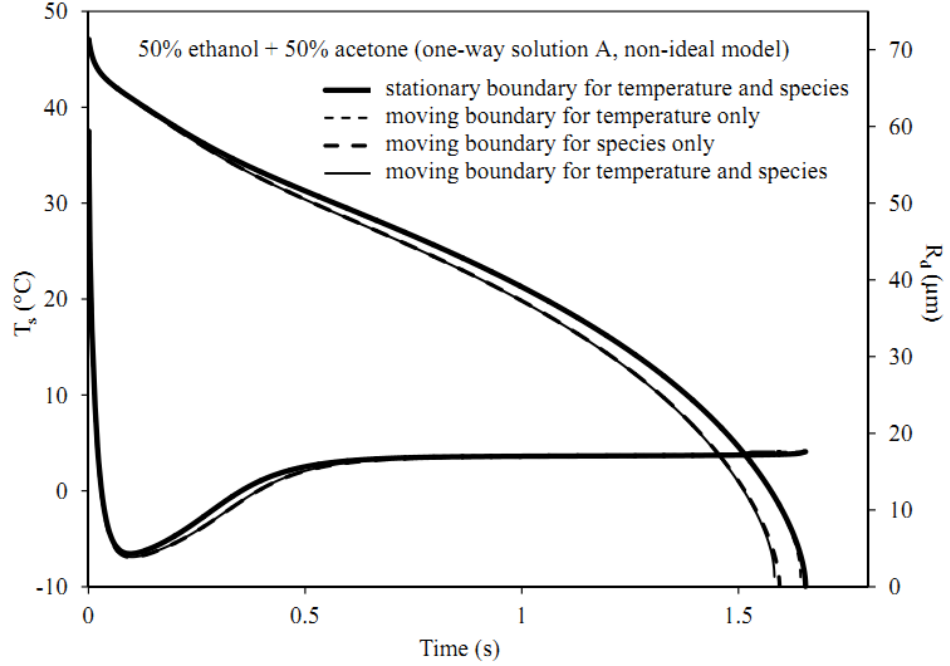


Figure 4.6: The time evolution of droplet surface temperatures ( $T_s$ ) and radius ( $R_d$ ), predicted by the one-way Solution A for the non-ideal model, taking and not taking into account the effects of the moving boundary during individual time steps on the solutions to the heat transfer equation only, species diffusion equation only and both heat transfer and species diffusion equations for the 50% ethanol – 50% acetone mixture droplets with the values of the initial parameters, and gas temperature given in Table 4.2, assuming that the droplet velocity is constant and equal to 12.71 m/s.

In Fig. 4.5 a hypothetical case is shown when the 50% ethanol – 50% acetone mixture droplets are cooled down or heated and evaporated until complete evaporation takes place. Both plots for the droplet surface temperature and droplet radius are shown. The same values as shown in Table 4.2 for the initial droplet temperature, diameter, distance parameter and gas temperature are used, but in contrast to the case shown in Table 4.1, it is assumed that the droplet velocity remains constant and equal to 12.71 m/s. The cases of the stationary boundary during individual time steps, the cases when the effects of the moving boundary are taken into account for the heat transfer and species diffusion equations separately during individual time steps, and the case when these effects are taken into account simultaneously for heat transfer and species diffusion are shown.

As can be seen from this figure, the plots taking into account the effects of

the moving boundary on the heat transfer equation only, and ignoring this effect altogether practically coincide. That means that this effect can be safely ignored for this case. Also, the plots taking into account the effects of the moving boundary on the solution to the species diffusion equation, and taking it into account for both solutions to the heat transfer and species diffusion equations practically coincide, but the difference between both these curves and the ones ignoring this effect altogether can be clearly seen after about 0.1 s. The effect of the moving boundary is a reduction of the predicted droplet surface temperature between about 0.1 to 0.6 s. During this period the droplet surface temperature is below the ambient gas temperature. Hence the reduction of the droplet surface temperature is expected to increase the heat flux from the ambient gas to the droplets, leading to the acceleration of droplet evaporation. This agrees with the predicted time evolution of the droplet radius, taking and not taking into account the effect of the moving boundary, shown in Fig. 4.6.

In Fig. 4.7 the case similar to the one shown in Fig. 4.6, but for gas temperature equal to 1000 K, is shown. In this case, droplet surface temperature increases during the whole period of droplet heating and evaporation, in contrast to the case shown in Fig. 4.6. As one can see from Fig. 4.7, the plots taking into account the effects of the moving boundary on the solution to the heat transfer equation, and ignoring this effect altogether practically coincide, as in the case shown in Fig. 4.7. Also, similarly to the case shown in Fig. 4.6, the plots taking into account the effects of the moving boundary on the solution to the species diffusion equations, and taking it into account for both heat transfer and species diffusion equations practically coincide, but the difference between both these curves and the ones ignoring this effect altogether can be clearly seen after about 5 ms. This difference between the plots is much more visible than in the case shown in Fig. 4.6. As in the case shown in Fig. 4.6, the effect of the moving boundary is to reduce the predicted droplet surface temperature leading to the increase of the heat flux from the ambient gas to the droplets and acceleration of droplet evaporation. This agrees with the predicted time evolution of droplet radius, taking and not taking into account the effect of the moving boundary, shown in Fig. 4.7.

The plots of time evolution of the surface mass fraction of ethanol  $Y_{1,s,\text{eth}}$  for the

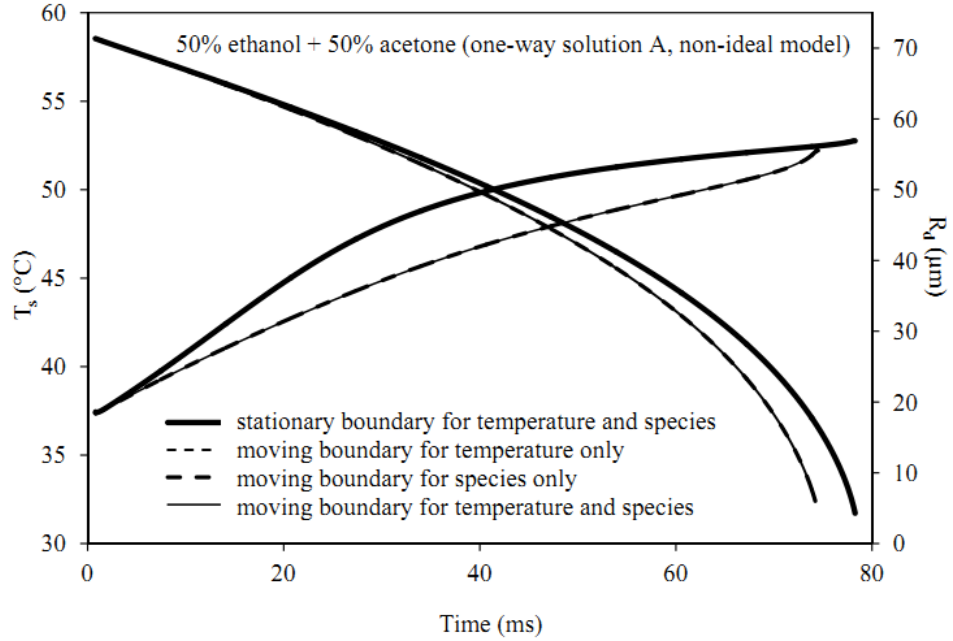


Figure 4.7: The same as Fig. 4.6 but for the gas temperature equal to 1000 K.

same case as shown in Fig. 4.7, are shown in Fig. 4.8. Similarly to the case shown in Fig. 4.7, the main effect of the moving boundary on the solution to the species diffusion equation is its influence on the values of  $Y_{1,s,\text{eth}}$ . This effect leads to visible reductions of the values of  $Y_{1,s,\text{eth}}$  until the complete evaporation of the droplet takes place.

## 4.5 Conclusions of Chapter 4

Two new solutions to the equation, describing the diffusion of species during multi-component droplet evaporation, are suggested. The first solution is the explicit analytical solution to this equation, while the second one reduces the solution of the differential transient species diffusion equation to the solution of the Volterra integral equation of the second kind. Both solutions take into account the effect of the reduction of the droplet radius due to evaporation, assuming that this radius is a linear function of time. These solutions can be considered as the generalisations of the solutions earlier reported in [38, 50]. The analytical solution is presented in the case when parameter  $h_0$  can be assumed to be constant (less than  $-1$ ) during the time step. These solutions are complementary to the ones suggested earlier in

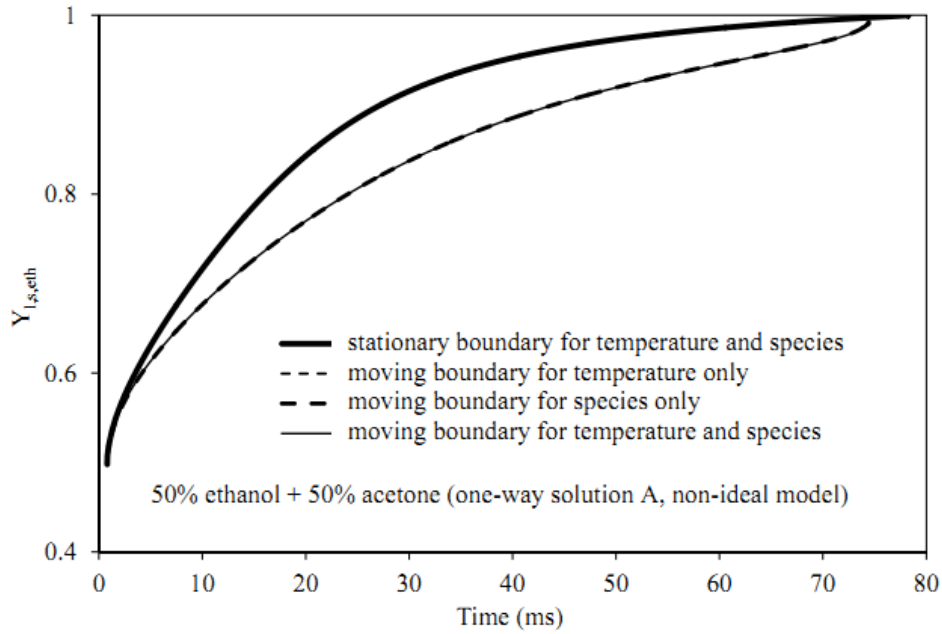


Figure 4.8: The same as Fig. 4.7 but for the mass fraction of ethanol at the surface of the droplet.

Chapter 2, which took into account the effect of the moving boundary due to droplet evaporation on the distribution of temperature inside the droplet.

The analytical solution has been incorporated into a zero dimensional CFD code and applied to the analysis of bi-component droplet heating and evaporation. The case of initial 50% ethanol – 50% acetone mixture and droplets with initial diameter equal to  $142.7 \mu\text{m}$ , as in our earlier paper [38], has been considered. Effects of droplets on gas have been ignored at this stage and droplet velocity has been assumed to be constant and equal to  $12.71 \text{ m/s}$ . To separate the effect of the moving boundary on the species diffusion equation from similar effects on the heat conduction equation inside droplets, described in previous two Chapters, a rather artificial assumption that the droplet temperature is homogeneous and fixed has been made.

It has been pointed out that the moving boundary slows down the increase in the mass fraction of ethanol (the less volatile substance in the mixture) during the evaporation process and leads to the acceleration of droplet evaporation.

It is pointed out that for the conditions of the experiment described briefly earlier, the predictions of the models, taking and not taking into account the effects of the moving boundary during the time step on the solutions to the heat transfer and

species diffusion equations, are very close. The deviation between the predictions of these models can be ignored in this case. At the same time, the difference in the predictions of these models needs to be taken into account when the whole period of droplet evaporation up to the complete evaporation of droplets is considered. The effect of the moving boundary is shown to be much stronger for the solution to the species diffusion equation than for the solution to the heat conduction equation inside droplets.

# Chapter 5

## Transient heating of a semitransparent spherical body immersed into a gas with inhomogeneous temperature distribution

### 5.1 Introduction of Chapter 5

The main objective of this Chapter is to generalise the model described in [52] to the case when the initial gas temperature is not homogeneous in the vicinity of droplets. This new generalised model can be applied to any problem of body heating/cooling when this body is immersed into an ambient gas with temperature varying with time (but constant during the time step).

Basic equations and approximations of the model are described in Section 5.2. The new analytical solution to the heat conduction equation in the body and surrounding gas is presented in Section 5.3. This solution is analysed in Section 5.4, and the main results of the Chapter are summarised in Section 5.5.

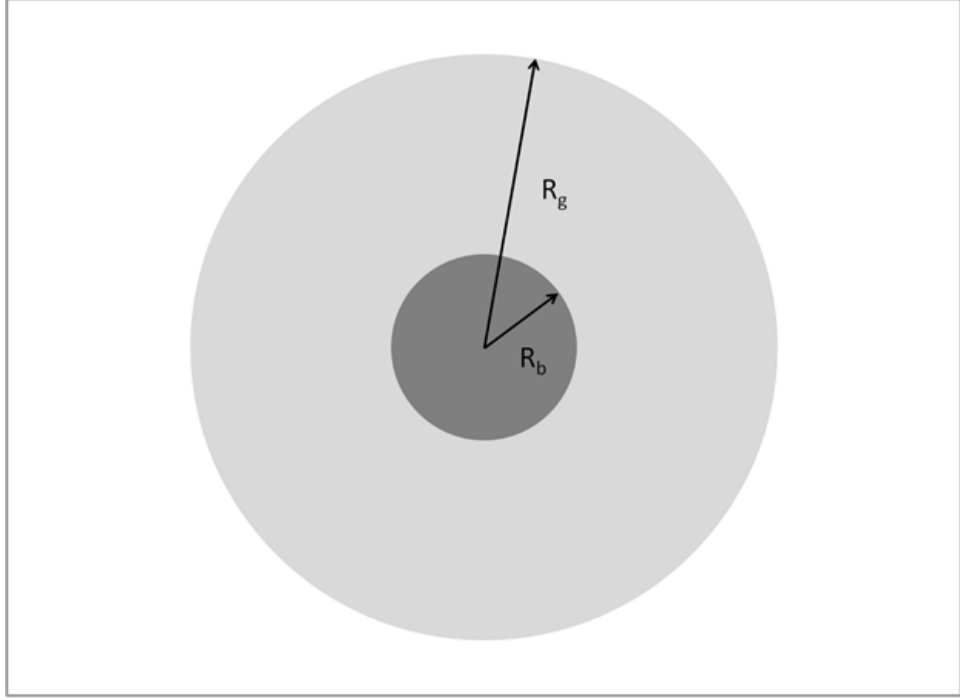


Figure 5.1: A schematic presentation of a spherical body of radius  $R_b$  immersed in the center of a gaseous sphere of radius  $R_g$ .

## 5.2 Basic equations and assumptions

As in [52], let us assume that a spherical body of radius  $R_b$  and initial temperature  $T_{b0}(R)$  is immersed in the center of a gaseous sphere of radius  $R_g$  at temperature  $T_{g0}(R)$ , as schematically shown in Fig. 5.1. The outer surface temperature of the gaseous sphere remains constant and equal to  $T_{g0}(R_g)$ .  $R_g$  is greater than  $R_b$  but finite.

The variation of the temperatures in the gas-body domain is described by the heat conduction equation in the form [105, 106]:

$$\frac{\partial T}{\partial t} = \kappa \left( \frac{\partial^2 T}{\partial R^2} + \frac{2}{R} \frac{\partial T}{\partial R} \right) + P(t, R), \quad (5.1)$$

where

$$\kappa = \begin{cases} \kappa_b = k_b / (c_b \rho_b) & \text{when } R \leq R_b \\ \kappa_g = k_g / (c_{pg} \rho_g) & \text{when } R_b < R \leq R_g, \end{cases} \quad (5.2)$$

$$T(R_g) = T_{g0}(R_g) = \text{const.}$$

Equation (5.1) is identical to Equation (2.1). In contrast to Equation (2.1), however,  $\kappa$  in Equation (5.1) is not constant and the latter Equation refers to both

liquid and gas. Equation (5.1) is the same as used in [52] except that  $T_{g0}$  is not constant but depends on  $R$  in the range  $R_b < R \leq R_g$ . The model for the radiation term  $P(t, R)$  is the same as used in [52].

As in [52], Equation (5.1) needs to be solved subject to initial and boundary conditions:

$$T|_{t=0} = \begin{cases} T_{b0}(R) & \text{when } R \leq R_b \\ T_{g0}(R) & \text{when } R_b < R \leq R_g, \end{cases} \quad (5.3)$$

$$T|_{R=R_b^-} = T|_{R=R_b^+}, \quad k_b \frac{\partial T}{\partial R} \Big|_{R=R_b^-} = k_g \frac{\partial T}{\partial R} \Big|_{R=R_b^+}, \quad T|_{R=R_g} = T_{g0}(R_g). \quad (5.4)$$

The physical meaning of the value of  $R_g - R_b$  can be interpreted in terms of the so called ‘film’ theory [44]. The key concept of this theory is thermal film thickness  $\delta_T$ , the expression for which is derived from the requirement that the rate of a purely molecular transport by thermal conduction through the film must be equal to the actual intensity of the convective heat transfer between the body surface and the external flow. For the case of heat conduction at the surface of a sphere this requirement can be written as [131]:

$$q_s'' = \frac{k_g \Delta T}{R_b - \frac{R_b^2}{R_b + \delta_{T0}}} = h \Delta T, \quad (5.5)$$

where  $q_s'' = |\dot{q}_s|/(4\pi R_b^2)$  is the value of the heat flux at the surface of the droplet,  $\Delta T = T_g - T_s$ , index  $_0$  here indicates that the effects of the Stefan flow are not taken into account (no evaporation) and  $h$  is the convection heat transfer coefficient. From Equation (5.5) it follows that

$$\delta_{T0} = \frac{2R_b}{\text{Nu}_0 - 2}, \quad (5.6)$$

where  $\text{Nu}_0$  is the Nusselt number of the non-evaporating body.

The value of  $R_g - R_b$  in our model is identified with  $\delta_{T0}$ . Following [44],  $\text{Nu}_0$  is estimated as

$$\text{Nu}_0 = 1 + (1 + \text{RePr})^{1/3} \max [1, \text{Re}^{0.077}], \quad (5.7)$$

where  $\text{Re}$  and  $\text{Pr}$  are Reynolds and Prandtl numbers respectively.

If we impose an additional requirement that the initial heat rate inside the ‘film’ does not depend on  $R$ , we get the following equation for  $T_{g0}(R)$

$$\frac{4\pi k_g (T_{g0}(R_g) - T_{b0})}{\frac{1}{R_b} - \frac{1}{R_g}} = \frac{4\pi k_g (T_{g0}(R) - T_{b0})}{\frac{1}{R_b} - \frac{1}{R}}. \quad (5.8)$$

The introduction of non-zero  $Re$  affects our earlier assumption about the spherical symmetry of the problem and  $h = k_g/R_b$ . This can be overcome if we replace  $k_g$  by

$$k_{g,\text{eff}} = k_g \text{Nu}_0/2$$

to satisfy Equation (5.5). If the body is liquid then  $k_b$  would need to be replaced by the effective liquid thermal conductivity, following the effective thermal conductivity model [44]. These effects are not considered in this Chapter.

Note that the ‘film theory’ based on Equations (5.5)-(5.8) was developed under the assumption that droplet heating is quasi-steady. This obviously contradicts the unsteady formulation of the problem (5.1)-(5.4). This contradiction, however, seems to be unavoidable, as the value of  $R_g - R_b$  in our model needs to be imposed ‘externally’ as an input parameter. In our previous paper [52], we considered a range of values of  $R_g - R_b$  without any attempt to link them with the underlying physics of the phenomenon.

### 5.3 The analytical solution

The solution to Equation (5.1) subject to initial and boundary conditions (5.3)-(5.4) in the limiting case of  $R_g \rightarrow \infty$ ,  $T_{b0} = \text{const}$ ,  $T_{g0}(R) = \text{const}$  and in the absence of radiation was reported in [67]. In [52] an alternative form of this solution was found, based on the assumptions that  $R_g$  is finite,  $T_{b0}$  depends on  $R$  and taking into account the contribution of thermal radiation. In this Chapter the model is further generalised to take into account the dependence of  $T_{g0}$  on  $R$  in the range  $R_b < R \leq R_g$ . This leads us to the following expression for  $T(R, t)$  (see Appendix 7):

$$T(R, t) = T_{g0}(R_g) + \frac{1}{R} \sum_{n=1}^{\infty} \left[ \exp(-\lambda_n^2 t) \frac{1}{\|v_n\|^2} \left( \int_0^{R_b} (-(T_{g0}(R_g) - T_{b0}(R)) R v_n(R) c_b \rho_b dR \right. \right. \\ \left. \left. + \int_{R_b}^{R_g} (-(T_{g0}(R_g) - T_{g0}(R)) R v_n(R) c_{pg} \rho_g dR) + \int_0^t \exp(-\lambda_n^2 (t - \tau)) p_n(\tau) d\tau \right) \right] v_n(R), \quad (5.9)$$

where

$$v_n(R) = \begin{cases} \frac{\sin(\lambda_n a_b R)}{\sin(\lambda_n a_b R_b)} & \text{when } R < R_b \\ \frac{\sin(\lambda_n a_g (R - R_g))}{\sin(\lambda_n a_g (R_b - R_g))} & \text{when } R_b \leq R \leq R_g, \end{cases} \quad (5.10)$$

$$\|v_n\|^2 = \frac{c_b \rho_b R_b}{2 \sin^2(\lambda_n a_b R_b)} + \frac{c_{pg} \rho_g (R_g - R_b)}{2 \sin^2(\lambda_n a_g (R_b - R_g))} - \frac{k_b - k_g}{2 R_b \lambda_n^2},$$

$$p_n(t) = \frac{c_b \rho_b}{\|v_n\|^2} \int_0^{R_b} R P(t, R) v_n(R) dR.$$

A countable set of positive eigenvalues  $\lambda_n$  is found from the solution to the equation:

$$\sqrt{k_b c_b \rho_b} \cot(\lambda a_b R_b) - \sqrt{k_g c_{pg} \rho_g} \cot(\lambda a_g (R_b - R_g)) = \frac{k_b - k_g}{R_b \lambda}. \quad (5.11)$$

These are arranged in ascending order  $0 < \lambda_1 < \lambda_2 < \dots$ .  $a_b = \sqrt{\frac{c_b \rho_b}{k_b}}$ ,  $a_g = \sqrt{\frac{c_{pg} \rho_g}{k_g}}$ .

Having introduced new dimensionless variables:

$$\tilde{T} = \frac{T(R, t)}{T_{g0}(R_g)}, \quad \tilde{T}_b = \frac{T_{b0}(R)}{T_{g0}(R_g)}, \quad \tilde{T}_g = \frac{T_{g0}(R)}{T_{g0}(R_g)}, \quad r = \frac{R}{R_b}, \quad r_g = \frac{R_g}{R_b},$$

and ignoring the contribution of thermal radiation, Equation (5.9) can be simplified to

$$\tilde{T} = 1 + \frac{R_b}{r} \sum_{n=1}^{\infty} \left[ \exp(-\lambda_n^2 t) \frac{1}{\|v_n\|^2} \left( \int_0^1 (-(1 - \tilde{T}_b) r v_n(R_b r) c_b \rho_b dr \right. \right. \\ \left. \left. + \int_1^{r_g} (-(1 - \tilde{T}_g) r v_n(R_b r) c_{pg} \rho_g dr) \right) \right] v_n(R_b r), \quad (5.12)$$

If  $T_{g0}(R) = T_{g0}(R_g) = \text{const}$  and  $T_{b0}$  does not depend on  $R$  then Equation (5.9) can be simplified to

$$T(R, t) = T_{g0} + \frac{1}{R} \sum_{n=1}^{\infty} \left[ \exp(-\lambda_n^2 t) \frac{(T_{g0} - T_{b0}) \sqrt{k_b c_b \rho_b}}{\lambda_n \|v_n\|^2} \left[ R_b \cot(\lambda_n a_b R_b) - \frac{1}{\lambda_n a_b} \right] \right. \\ \left. + \int_0^t \exp(-\lambda_n^2 (t - \tau)) p_n(\tau) d\tau \right] v_n(R). \quad (5.13)$$

This solution was studied in detail in the previous paper [52].

## 5.4 Analysis

Let us consider typical values of parameters for the case when Diesel fuel droplets with an initial temperature of 300 K are injected into a gas at temperature 900 K and pressure 30 atm (situation typical for Diesel engines [42]):

$$\rho_b = 600 \text{ kg/m}^3 \quad k_b = 0.145 \text{ W/(mK)} \quad c_b = 2830 \text{ J/(kgK)}$$

$$\rho_g = 23.8 \text{ kg/m}^3 \quad k_g = 0.061 \text{ W/(mK)} \quad c_{pg} = 1120 \text{ J/(kgK)}.$$

This leads us to the following estimates of thermal diffusivities of the body and gas as defined by Equation (5.2):

$$\kappa_b = 8.54 \times 10^{-8} \text{ m}^2/\text{s}; \quad \kappa_g = 2.29 \times 10^{-6} \text{ m}^2/\text{s}.$$

Note that we took gas temperature slightly higher than the one used in [52], where it was assumed that  $T_{g0}(R_g) = 800$  K. The values of transport coefficients for gas were taken to be the same as in [42, 52]. The difference of the values of these coefficients for these two temperatures were ignored as in [52].

We assume that the droplets can be treated as a body the temperature of which is initially homogeneous, while  $T_{g0}(R_g) = 900$  K and  $R_b = 10 \text{ }\mu\text{m}$ . Pr is assumed to be equal to 0.7 and two values of Re are considered: 1 and 5. Remembering (5.6), this leads to the following values of  $R_g$ :

$$R_{g1} = 3.301 R_b \quad \text{and} \quad R_{g2} = 11.337 R_b.$$

Two cases of the initial distribution of gas temperature in the range  $R_b < R \leq R_g$  are considered. Firstly, we assume that  $T_{g0}(R)$  satisfies Equation (5.8), which leads to the following expression:

$$T_{g0}(R) = T_{b0} + [T_{g0}(R_g) - T_{b0}] \frac{\frac{1}{R_b} - \frac{1}{R}}{\frac{1}{R_b} - \frac{1}{R_g}}. \quad (5.14)$$

Secondly we assume that

$$T_{g0}(R) = T_{g0}(R_g). \quad (5.15)$$

The latter case is identical to the one considered in [52].

The analysis of the effects of thermal radiation would lead to the results identical to the ones reported in [52]. This will not be considered in this work.

The analysis will be focused on the dimensionless time (Fourier number), distance and temperature defined as:

$$\text{Fo} = t\kappa_g/R_b^2, \quad r = R/R_b, \quad \hat{T}_{(s)} = (T_{g0}(R_g) - T_{(s)}(R, t))/(T_{g0}(R_g) - T_{b0}).$$

The calculations were performed using the package Wolfram Mathematica v 6.0 on a one 3.0 GHz Kernel. 100 terms of the series were taken.

Plots of  $\hat{T}$  versus  $r$  for  $R_g = 3.301 R_b$  and four Fo are shown in Fig. 5.2. The plots are shown for both initial distributions of gas temperature in  $R_b < R \leq R_g$ , defined

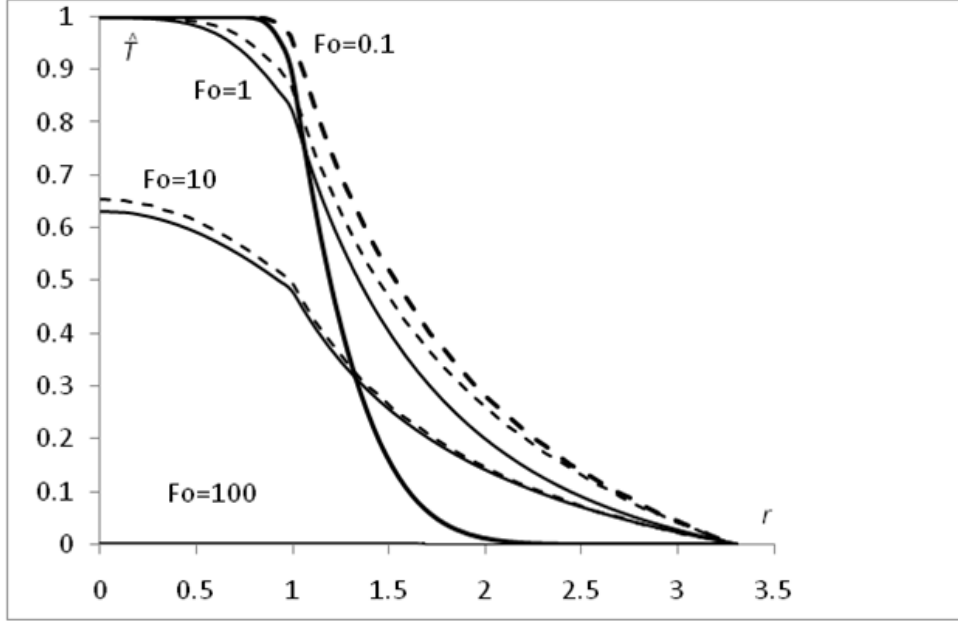


Figure 5.2: The plots of  $\hat{T} \equiv (T_{g0}(R_g) - T(R, t))/(T_{g0}(R_g) - T_{b0})$  versus  $r = R/R_b$  for  $r_g \equiv R_g/R_b = 3.301$  and four Fo (indicated near the curves). Solid curves refer to the initial distribution (5.15), while dashed curves refer to the initial distribution (5.14). The thickness of the curves is inversely proportionate to Fo.

by Expressions (5.14) and (5.15). As follows from this figure, for  $Fo = 0.1$  most of the interior of the body is not affected by high gas temperature for both initial distributions of  $T_{g0}(R)$ , but the body temperatures near the surface are affected stronger by gas for distribution (5.15), compared with distribution (5.14). The difference in gas temperatures ( $r > 1$ ) for these initial distributions of  $T_{g0}(R)$  is clearly visible as expected. For  $Fo = 1$  and  $Fo = 10$  a more rapid heating of the body for distribution (5.15), compared with distribution (5.14), is seen much more clearly compared with the case  $Fo = 0.1$ . Gas temperatures, predicted by both distributions, in these cases are much closer compared with the case  $Fo = 0.1$ . For  $Fo = 100$ , for both initial temperature distributions, both body and gas temperatures become very close to  $T_{g0}(R_g)$ .

The plots, similar to those shown in Fig. 5.2 but for  $R_g = 11.337 R_b$ , are presented in Fig. 5.3. Comparing Figs. 5.2 and 5.3 one can see that the trends of the curves in both figures are essentially the same, although the difference in the body heat-up for  $Fo = 1$  and  $Fo = 10$ , predicted for distributions (5.14) and (5.15), is more clearly visible in Fig. 5.3 than in Fig. 5.2.

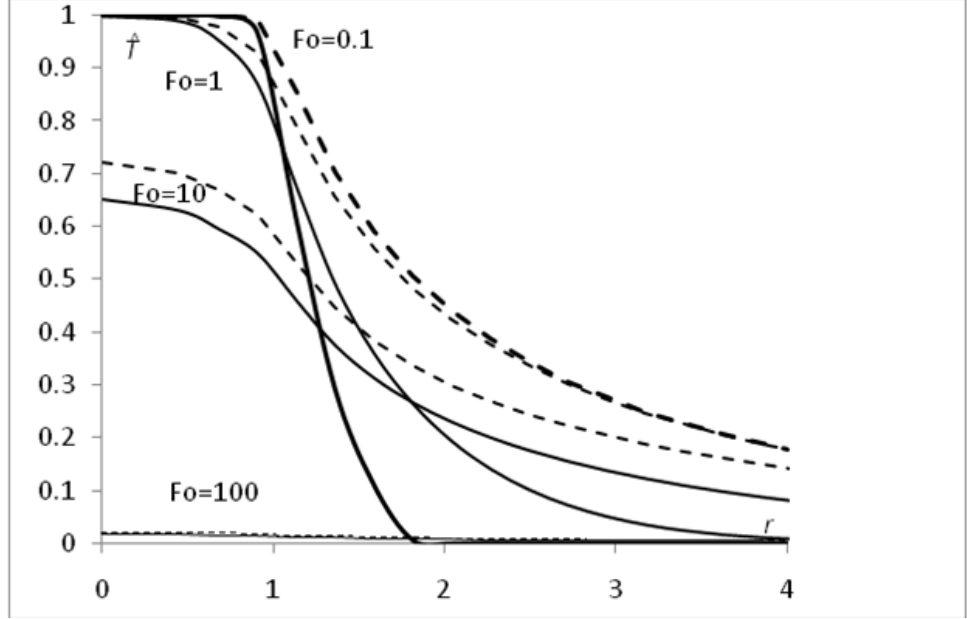


Figure 5.3: The same as Fig. 5.2 but for  $r_g = 11.337$ .

The plots of  $\hat{T}_s$  versus Fo for  $R_g = 3.301 R_b$ ,  $R_g = 11.337 R_b$  and both initial distributions of  $T_{g0}(R)$  are shown in Fig. 5.4. As follows from this figure, the body surface is always heated quicker for distribution (5.15) compared with distribution (5.14) as expected. Also, the body is heated quicker for  $R_g = 3.301 R_b$  than for  $R_g = 11.337 R_b$ . All these results are consistent with those shown in Figs. 5.2 and 5.3.

Ignoring the effects of the body movement, we can estimate the heat flux arriving at its surface as

$$q'' = k_g \left. \frac{\partial T}{\partial R} \right|_{R=R_b+0} = k_b \left. \frac{\partial T}{\partial R} \right|_{R=R_b-0}. \quad (5.16)$$

On the other hand, from the Newton's law follows that

$$q''_N = h (T_{g0}(R_g) - T_s), \quad (5.17)$$

where  $h = \frac{k_g}{R_b}$  for a spherically symmetric process. In the steady state limit,  $q'' = q''_N$ . However, in the general transient case, they are linked by the equation

$$q'' = \chi q''_N, \quad (5.18)$$

where

$$\chi = \frac{k_g \left. \frac{\partial T}{\partial R} \right|_{R=R_b+0}}{\frac{k_g}{R_b} (T_{g0}(R_g) - T_s)} = \frac{R_b \left. \frac{\partial T}{\partial R} \right|_{R=R_b+0}}{T_{g0}(R_g) - T_s}. \quad (5.19)$$

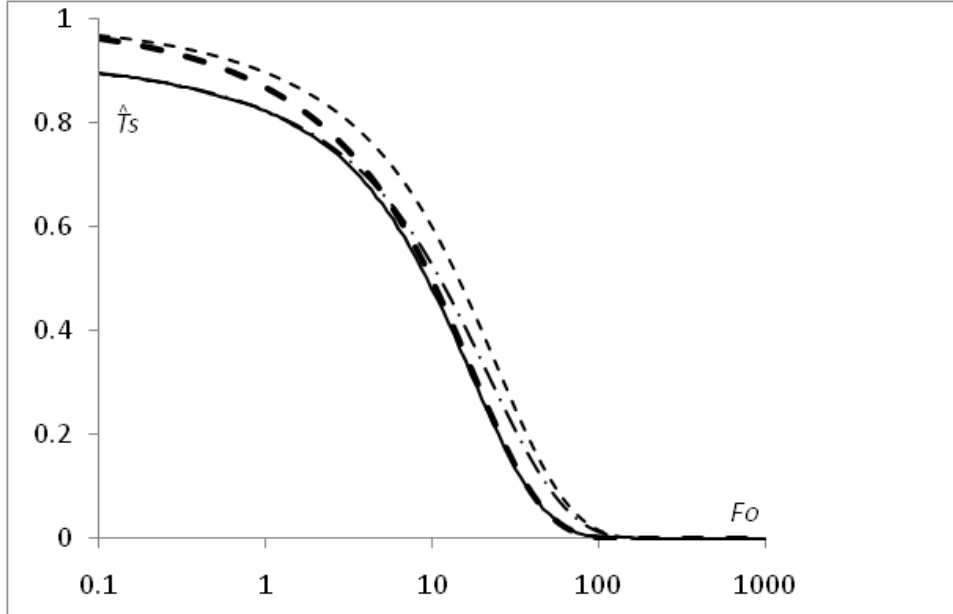


Figure 5.4: The plots of  $\hat{T}_s \equiv (T_{g0}(R_g) - T_s(R, t))/(T_{g0}(R_g) - T_{b0})$  versus  $Fo$  for  $r_g = 3.301$  and distribution (5.15) (solid),  $r_g = 11.337$  and distribution (5.15) (dashed-dotted),  $r_g = 3.301$  and distribution (5.14) (thick dashed),  $r_g = 11.337$  and distribution (5.14) (thin dashed).

If the Newton's law is valid then  $\chi = 1$ . As shown in [52] for the special case of a body immersed into a homogeneous gas, this is not valid in the general transient case.

The plots of  $\chi$  versus  $Fo$  for various  $r_g \equiv R_g/R_b$ , and both initial distributions of  $T_{g0}(R)$  are shown in Fig. 5.5. The solid plots referring to distribution (5.15) are identical to those presented in [52]. The solid plot referring to  $R_g = 50R_b$  is practically indistinguishable from the one which follows from the analysis by Cooper [67], obtained in the limit  $R_g = \infty$  using the approach totally different from ours. This coincidence confirms the validity of both approaches.

The dashed curves, obtained for the initial distribution (5.15), coincide with the solid curves referring to distribution (5.14) in the limit of large  $Fo$ . For small  $Fo$  the deviations between the curves corresponding to distributions (5.14) and (5.15) is clearly seen. For distribution (5.15),  $\chi$  rapidly increases with decreasing  $Fo$  ( $\chi \rightarrow \infty$  when  $Fo \rightarrow 0$ ). For distribution (5.14),  $\chi$  approaches the finite values when  $Fo \rightarrow 0$ , being always less than predicted for distribution (5.15). The values of  $\chi$  in the limit

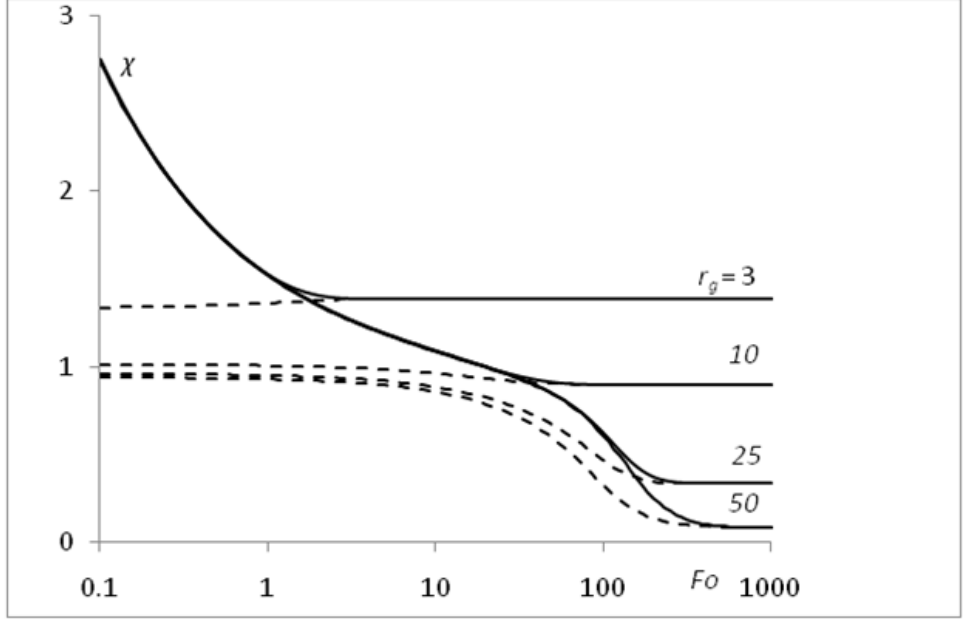


Figure 5.5: The plots of  $\chi$  versus  $Fo$  for four  $r_g$  (indicated near the curves). Solid curves refer to the initial distribution (5.15), while dashed curves refer to the initial distribution (5.14).

$Fo \rightarrow 0$  can be estimated analytically from (5.15) and (5.18) as

$$\chi = \frac{\tilde{R}_g}{\tilde{R}_g - 1}. \quad (5.20)$$

Note that the values of  $\chi$  for  $Fo = 0.1$ , can differ by up to about 8% from those predicted by (5.20) (although the values of temperature were calculated with errors less than about 0.5%). This is related to very slow convergence of the corresponding series in (5.9) for the derivative of the temperature in the vicinity of the droplet surface (up to 3000 terms in this series were taken).

## 5.5 Conclusions of Chapter 5

The problem of heating of a body immersed into gas with inhomogeneous temperature distribution is solved analytically assuming that at a certain distance  $R_g - R_b$  from the body gas temperature remains constant. This problem is the generalisation of the problem solved earlier when gas, into which the body is immersed, is assumed to be initially homogeneous. This solution is applied to the case when the distribution of gas temperature is chosen such that heat flux in gas initially does not depend

on the distance from the body surface, if this distance is less than  $R_g - R_b$ . The solution is applied to modelling body heating in conditions close to those observed in Diesel engines.

It is pointed out that inhomogeneous gas temperature distribution leads to slowing down of body heating compared with the case when the body is immersed into a homogeneous gas. In the long time limit, the distribution of temperature in the body and gas practically does not depend on the initial distribution of gas temperature.

The study of the correction of the convective heat transfer coefficient for the case of body immersion in gas with homogeneous temperature distribution confirmed the results earlier reported in [52]. For small  $Fo$ , this correction does not depend on the size of the gas domain, and reaches about 2.8 at  $Fo = 0.1$ . For  $Fo > 1$  this correction becomes sensitive to the size of the domain. For large domains it has been shown to be the same as follows from the earlier model suggested in [67] for an infinitely large domain occupied by the gas. The values of this correction to Newton's law vary from about 0.1 (large domain occupied by gas and  $Fo = 500$ ) to 2.8 at  $Fo = 0.1$ . In the case of body immersion into an inhomogeneous gas, for large times this correction is essentially the same as predicted by the model described in [52]. For short times, this correction approaches finite values, well below those predicted in [52]. For large gas domains these values are close to 1. These results essentially confirm the main conclusion of [52] that ignoring these corrections is expected to lead to unacceptably large errors in computations.

# Chapter 6

## Conclusions

New solutions to the heat conduction equation, describing transient heating of an evaporating droplet, are suggested. These solutions take into account the effect of the reduction of the droplet radius due to evaporation, assuming that this radius is a linear function of time. The latter assumption does not allow us to apply these solutions to describe the whole process, from the start of evaporation, until the moment in time when the droplet completely evaporates. However, these solutions are expected to be used to describe droplet heating and evaporation over a small time step when other parameters, except droplet radius and temperature, can be assumed constant. In this case they can be considered as generalisations of the approach currently used in all research and commercial computational fluid dynamics (CFD) codes known to us (KIVA, FLUENT, PHOENICS etc.), in which it is assumed that droplet radius is constant during the time step.

The analytical solution has been incorporated into the zero dimensional CFD code and applied to the analysis of Diesel fuel droplet heating and evaporation in typical engine conditions. Effects of droplets on gas have been ignored at this stage. The results have been compared with those which follow from the conventional (traditional) approach to modelling droplet heating and evaporation, based on the assumption that the droplet radius is constant over the time step (but changes from one time step to another). It has been pointed out that the new approach leads to the prediction of lower droplet temperatures and longer evaporation times than the traditional method.

Larger time steps can be used in the case of the new approach compared with

the conventional one to achieve the same accuracy of calculation.

The boundary immobilization method was considered, in tandem with the Keller box finite-difference scheme, for the accurate numerical solution of the transient heat conduction equation inside droplets. This numerical solution was found to agree well with that obtained based on the above mentioned approach. This suggests that both approaches are likely to be correct.

Two new solutions to the heat conduction equation are suggested, assuming that the time evolution of droplet radius is known. The initial droplet temperature is assumed to be constant or allowed to change with the distance from the droplet centre. The results turned out to be the simplest in the first case and the main focus of our analysis has been upon these. Since  $R_d(t)$  depends on the time evolution of the droplet temperature, an iterative process is required. Firstly, the time evolution of  $R_d(t)$  is obtained using the conventional approach, when it remains constant during the time step, but changes from one time step to another. The droplet surface temperature in this case is obtained from the analytical solution to the heat conduction equation inside the droplet. It is assumed that this droplet is heated by convection from the ambient gas, and its radius remains constant during the time step. Then these values of  $R_d(t)$  are used in the new solutions to obtain updated values of time evolution of the distribution of temperatures inside the droplet and on its surface. These new values of droplet temperature are used to update the function  $R_d(t)$ . This process continues until convergence is achieved, which typically takes place after about 15 iterations. The results of the calculations of droplet surface temperature, using this approach, are compared with the results obtained using the previously suggested approach when the droplet radius was assumed to be a linear function of time during individual time steps for typical Diesel engine-like conditions. For sufficiently small time steps the time evolutions of droplet surface temperatures and radii, predicted by both approaches coincide as expected. Similarly to the case when droplet radius is assumed to be a linear function of time during the time step, the new solution predicts lower droplet temperatures and slower evaporation when the effects of the reduction of  $R_d$  are taken into account.

It is shown that in the case of constant droplet initial temperature, models both taking and not taking into account the changes in initial droplet temperature with

the distance from the droplet centre, predict the same results. This suggests that both models are likely to be correct. It is shown that the temperatures predicted by the models based on the assumption of constant initial droplet temperature, and the one taking into account the increase in this temperature with the distance from the droplet centre, tend to converge with time.

Two new solutions to the equation, describing the diffusion of species during multi-component droplet evaporation, are suggested. Both solutions take into account the effect of the reduction of the droplet radius due to evaporation, assuming that this radius is a linear function of time. The first solution is the explicit analytical solution to this equation, while the second one reduces the solution of the differential transient species diffusion equation to the solution of the Volterra integral equation of the second kind. These solutions can be considered as the generalisations of the solutions earlier reported in [38, 50]. These solutions are complementary to the ones suggested earlier, which took into account the effect of the moving boundary due to droplet evaporation on the distribution of temperature inside the droplet.

The analytical solution has been incorporated into a zero dimensional CFD code and applied to the analysis of bi-component droplet heating and evaporation. To separate the effect of the moving boundary on the species diffusion equation from similar effects on the heat conduction equation inside droplets, described in previous two chapters, a rather artificial assumption that the droplet temperature is homogeneous and fixed has been made. It has been pointed out that the moving boundary slows down the increase in the mass fraction of ethanol (the less volatile substance in the mixture) during the evaporation process and leads to the acceleration of droplet evaporation.

It is pointed out that for the conditions of the experiment described in [38], the predictions of the models, taking and not taking into account the effects of the moving boundary during the time step on the solutions to the heat transfer and species diffusion equations, are very close. The deviation between the predictions of these models can be ignored in this case. At the same time, the difference in the predictions of these models needs to be taken into account when the whole period of droplet evaporation up to the complete evaporation of droplets is considered. The effect of the moving boundary is shown to be much stronger for the solution to

the species diffusion equation than for the solution to the heat conduction equation inside droplets.

The problem of heating of a body immersed into gas with inhomogeneous temperature distribution is solved analytically assuming that at a certain distance  $R_g - R_b$  from the body gas temperature remains constant. This problem is the generalisation of the problem solved earlier when gas, into which the body is immersed, is assumed to be initially homogeneous. This solution is applied to the case when the distribution of gas temperature is chosen such that heat flux in gas initially does not depend on the distance from the body surface, if this distance is less than  $R_g - R_b$ . The solution is applied to modelling body heating in conditions close to those observed in Diesel engines.

It is pointed out that inhomogeneous gas temperature distribution leads to slowing down of body heating compared with the case when the body is immersed into a homogeneous gas. In the long time limit, the distribution of temperature in the body and gas practically does not depend on the initial distribution of gas temperature. The study of the correction of the convective heat transfer coefficient for the case of body immersion in gas with homogeneous temperature distribution confirmed the results earlier reported in [52]. For small Fo, this correction does not depend on the size of the gas domain, and reaches about 2.8 at Fo= 0.1. For Fo> 1 this correction becomes sensitive to the size of the domain. For large domains it has been shown to be the same as follows from the earlier model suggested in [67] for an infinitely large domain occupied by the gas. The values of this correction to Newton's law vary from about 0.1 (large domain occupied by gas and Fo= 500) to 2.8 at Fo= 0.1. In the case of body immersion into an inhomogeneous gas, for large times this correction is essentially the same as predicted by the model described in [52]. For short times, this correction approaches finite values, well below those predicted in [52]. For large gas domains these values are close to 1. These results essentially confirm the main conclusion of [52] that ignoring these corrections is expected to lead to unacceptably large errors in computations.

# References

- [1] S.S. Sazhin. Advanced models of fuel droplet heating and evaporation. *Progress in Energy and Combustion Science*, 32(2):162–214, 2006.
- [2] S.S. Sazhin, I.N. Shishkova, and M.R. Heikal. Kinetic modelling of fuel droplet heating and evaporation: calculations and approximations. *International Journal of Engineering Systems Modelling and Simulation*, 2(3):169–176, 2010.
- [3] B.Y. Cao, J.F. Xie, and S.S. Sazhin. Molecular dynamics study on evaporation and condensation of n-dodecane at liquid–vapor phase equilibria. *The Journal of Chemical Physics*, 134:164309, 2011.
- [4] J.F. Xie, S.S. Sazhin, and B.Y. Cao. Molecular dynamics study of the processes in the vicinity of the n-dodecane vapour/liquid interface. *Physics of Fluids*, 23:112104, 2011.
- [5] I.N. Shishkova and S.S. Sazhin. A numerical algorithm for kinetic modelling of evaporation processes. *Journal of Computational Physics*, 218(2):635–653, 2006.
- [6] S.S. Sazhin, I.N. Shishkova, A.P. Kryukov, V.Y. Levashov, and M.R. Heikal. Evaporation of droplets into a background gas: Kinetic modelling. *International Journal of Heat and Mass Transfer*, 50:2675–2691, 2007.
- [7] S.S. Sazhin, I.N. Shishkova, T. Kristyadi, S.P. Martynov, and M.R. Heikal. Droplet heating and evaporation: hydrodynamic and kinetic models. *Heat Transfer Research*, 39(4):293–303, 2008.
- [8] S.S. Sazhin and I.N. Shishkova. A kinetic algorithm for modelling the droplet

- evaporation process in the presence of heat flux and background gas. *Atomization and Sprays*, 19:473–489, 2009.
- [9] R.D. Reitz and C.J. Rutland. Development and testing of diesel engine cfd models. *Progress in Energy and Combustion Science*, 21(2):173–196, 1995.
- [10] J.B. Heywood. *Internal Combustion Engines Fundamentals*. McGraw-Hill Book Company;, New York, 1988.
- [11] W.A. Sirignano. *Fluid Dynamics and Transport of Droplets and Sprays*. Cambridge University Press (Cambridge, UK), 1999.
- [12] S.K. Aggarwal and H.C. Mongia. Multicomponent and high-pressure effects on droplet vaporization. *Journal of Engineering for Gas Turbines and Power*, 124(2):248–255, 2002.
- [13] Y. Ra and R.D. Reitz. A vaporization model for discrete multi-component fuel sprays. *International Journal of Multiphase Flow*, 35(2):101–117, 2009.
- [14] T. Kristyadi, V. Deprédurand, G. Castanet, F. Lemoine, S.S. Sazhin, A. Elwardany, E.M. Sazhina, and M.R. Heikal. Monodisperse monocomponent fuel droplet heating and evaporation. *Fuel*, 89(12):3995–4001, 2010.
- [15] S.S. Sazhin, P.A. Krutitskii, W.A. Abdelghaffar, E.M. Sazhina, S.V. Mikhailovsky, S.T. Meikle, and M.R. Heikal. Transient heating of diesel fuel droplets. *International Journal of Heat and Mass Transfer*, 47(14-16):3327–3340, 2004.
- [16] S.S. Sazhin, W.A. Abdelghaffar, P.A. Krutitskii, E.M. Sazhina, and M.R. Heikal. New approaches to numerical modelling of droplet transient heating and evaporation. *International Journal of Heat and Mass Transfer*, 48(19):4215–4228, 2005.
- [17] S.S. Sazhin, W.A. Abdelghaffar, E.M. Sazhina, and M.R. Heikal. Models for droplet transient heating: effects on droplet evaporation, ignition, and break-up. *International Journal of Thermal Sciences*, 44(7):610–622, 2005.
- [18] S.S. Sazhin, T. Kristyadi, W.A. Abdelghaffar, and M.R. Heikal. Models for fuel droplet heating and evaporation: Comparative analysis. *Fuel*, 85:1613–1630, 2006.

- [19] S.S. Sazhin, P.A. Krutitskii, I.G. Gusev, and M.R. Heikal. Transient heating of an evaporating droplet. *International Journal of Heat and Mass Transfer*, 53:2826–2836, 2010.
- [20] S.S. Sazhin, P.A. Krutitskii, I.G. Gusev, and M.R. Heikal. Transient heating of an evaporating droplet with presumed time evolution of its radius. *International Journal of Heat and Mass Transfer*, 54(5-6):1278–1288, 2011.
- [21] I.G. Gusev, P.A. Krutitskii, S.S. Sazhin, and A.E. Elwardany. New solutions to the species diffusion equation inside droplets in the presence of the moving boundary. *International Journal of Heat and Mass Transfer*, 2011 (in press).
- [22] S.S. Sazhin, I.G. Gusev, P.A. Krutitskii, and M.R. Heikal. Transient heating of a semitransparent spherical body immersed into a gas with inhomogeneous temperature distribution. *International Journal of Thermal Sciences*, 50(7):1215–1222, 2011.
- [23] S.L. Mitchell, M. Vynnycky, I.G. Gusev, and S.S. Sazhin. An accurate numerical solution for the transient heating of an evaporating spherical droplet. *Applied Mathematics and Computation*, 217:9219–9233, 2011.
- [24] A.E. Elwardany, I.G. Gusev, G. Castanet, F. Lemoine, and S.S. Sazhin. Mono- and multi-component droplet cooling/heating and evaporation: comparative analysis of numerical models. *Atomization and Sprays*, 2011(almost accepted).
- [25] S.S. Sazhin, I.N. Shishkova, A. Elwardany, I.G. Gusev, and M. Heikal. Modelling of droplet heating and evaporation: recent results and unsolved problems. In *Journal of Physics, Conference Series, 268, 012026. International Workshop on Multi-Rate Processes & Hysteresis in Mathematics*, University of Pecs, Hungary, May 31 – June 3 2010. Physics and Information Sciences.
- [26] S.S. Sazhin, I.G. Gusev, A. Elwardany, A.Yu.Snegirev, and M. Heikal. New approaches to modelling droplet heating and evaporation. In *Proceedings of DIPSI Workshop 2011 on Droplet Impact Phenomena & Spray Investigation*, pages 59–65, Bergamo, Italy, May 27 2011. Dip. di Ingegneria industriale, Universita degli studi di Bergamo. (CD).

- [27] S.S. Sazhin, A. Elwardany, I.G. Gusev, I.N. Shishkova, and M. Heikal. Modelling of fuel droplet heating and evaporation: recent results and unsolved problems. In *Engineering Research Anniversary volume honouring Amalia and Miklos Ivanyi*, pages pp. B:197–B:209, University of Pecs, Hungary, October 25-26 2010. Pollack Mihaly Faculty of Engineering, University of Pecs.
- [28] I.G. Gusev, P.A. Krutitskii, and S.S. Sazhin. Droplet heating and evaporation in the presence of a moving boundary: numerical analysis based on analytical solutions. In *Book of Abstracts*, page 42, University of Brighton (UK), 12-14th July 2010. 11th International Conference on Integral Methods in Science and Engineering.
- [29] S.S. Sazhin, I.N. Shishkova, I.G. Gusev, A. Elwardany, P.A. Krutitskii, and M. Heikal. Fuel droplet heating and evaporation: new hydrodynamic and kinetic models. In *Book of Abstracts*, page 26, Washington, 8-13 August 2010. 11th International Conference on Integral Methods in Science and Engineering.
- [30] S.S. Sazhin, I.N. Shishkova, I.G. Gusev, and M. Heikal. Hydrodynamic and kinetic models for monocomponent droplet heating and evaporation: recent developments. In *Book of Abstracts*, page 183, Kaohsiung City, Taiwan, 2-5 November 2010. 21st International Symposium on Transport Phenomena.
- [31] S.S. Sazhin, A. Elwardany, I.G. Gusev, J.-F. Xie., B.-Y Cao, I.N. Shishkova, A.Yu. Snegirev, and M. Heikal. Modelling of complex hydrocarbon droplet heating and evaporation: hydrodynamic, kinetic and molecular dynamics approaches. In *Book of Abstracts*, Saint Petersburg, Russia, June 24-27 2011. 25th European Symposium on Applied Thermodynamics.
- [32] I.G. Gusev, S.S. Sazhin, and M. Heikal. The effects of the moving boundary on the heating of evaporating droplets. In *Proceedings of ILASS Europe 2011*, page 119, Estoril, Portugal, 5-7 September 2011. 24th European Conference on Liquid Atomization and Spray Systems.
- [33] S.S. Sazhin, I.G. Gusev, M. Heikal, and P.A. Krutitskii. Modelling of liquid droplet heating and evaporation taking into account the effects of the moving boundary. In *Program and Book of Abstracts*, page 75, Kyoto, 22–26 September

2011. The Asian Symposium on Computational Heat Transfer and Fluid Flow - 2011 (ASCH2011).
- [34] G. Miliauskas. Regularities of unsteady radiative-convective heat transfer in evaporating semitransparent liquid droplets. *International Journal of Heat and Mass Transfer*, 44:785–798, 2001.
- [35] A.D. Polyinin, A.M. Kutepov, A.V. Vyazmin, and D.A. Kazenin. *Hydrodynamics, Mass and Heat Transfer in Chemical Engineering*. Taylor & Francis, 2002.
- [36] A. Faghri and Y. Zhang. *Transport Phenomena in Multiphase Systems*. Academic Press, 2006.
- [37] S. Sazhin. Modelling of sprays using computational fluid dynamics codes. *Pollack Periodica*, 4(1):5–16, 2009.
- [38] S.S. Sazhin, A. Elwardany, P.A. Krutitskii, G. Castanet, F. Lemoine, E.M. Sazhina, and M.R. Heikal. A simplified model for bi-component droplet heating and evaporation. *International Journal of Heat and Mass Transfer*, 53(21-22):4495–4505, 2010.
- [39] I. Goldfarb, V. Goldshtein, G. Kuzmenko, and J.B. Greenberg. On thermal explosion of a cool spray in a hot gas. In *Symposium (International) on Combustion*, volume 27, pages 2367–2374. Elsevier, 1998.
- [40] A.C. McIntosh, V. Gol'dshtein, I. Goldfarb, and A. Zinoviev. Thermal explosion in a combustible gas containing fuel droplets. *Combustion Theory and Modelling*, 2(2):153–165, 1998.
- [41] I. Goldfarb, V. Gol'dshtein, G. Kuzmenko, and S. Sazhin. Thermal radiation effect on thermal explosion in gas containing fuel droplets. *Combustion Theory and Modelling*, 3(4):769–787, 1999.
- [42] S.S. Sazhin, G. Feng, M.R. Heikal, I. Goldfarb, V. Gol'dshtein, and G. Kuzmenko. Thermal ignition analysis of a monodisperse spray with radiation. *Combustion and Flame*, 124(4):684–701, 2001.

- [43] V. Bykov, I. Goldfarb, V. Goldshtein, and J.B. Greenberg. Thermal explosion in a hot gas mixture with fuel droplets: a two reactant model. *Combustion Theory and Modelling*, 6(2):339–359, 2002.
- [44] B. Abramzon and W.A. Sirignano. Droplet vaporization model for spray combustion calculations. *International Journal of Heat and Mass Transfer*, 32(9):1605–1618, 1989.
- [45] R.J. Haywood, R. Nafziger, and M. Renksizbulut. A detailed examination of gas and liquid transient processes in convection and evaporation. *ASME Journal Heat Transfer*, 111:495–502, 1989.
- [46] C.H. Chiang, M.S. Raju, and W.A. Sirignano. Numerical analysis of convecting, vaporizing fuel droplet with variable properties. *International Journal of Heat and Mass Transfer*, 35(5):1307–1324, 1992.
- [47] E.M. Sazhina, S.S. Sazhin, M.R. Heikal, V.I. Babushok, and R.J.R. Johns. A detailed modelling of the spray ignition process in diesel engines. *Combustion Science and Technology*, 160(1):317–344, 2000.
- [48] G. Castanet, M. Lebouché, and F. Lemoine. Heat and mass transfer of combusting monodisperse droplets in a linear stream. *International Journal of Heat and Mass Transfer*, 48:3261–3275, 2005.
- [49] C. Maqua, G. Castanet, F. Grisch, F. Lemoine, T. Kristyadi, and S.S. Sazhin. Monodisperse droplet heating and evaporation: experimental study and modelling. *International Journal of Heat and Mass Transfer*, 51(15-16):3932–3945, 2008.
- [50] S.S. Sazhin, A.E. Elwardany, P.A. Krutitskii, V. Depredurand, G. Castanet, F. Lemoine, E.M. Sazhina, and M.R. Heikal. Multi-component droplet heating and evaporation: Numerical simulation versus experimental data. *International Journal of Thermal Sciences*, 50(7):1164–1180, 2011.
- [51] C. Bertoli and M. Migliaccio. Finite conductivity model for diesel spray evaporation computations. *International Journal of Heat and Fluid Flow*, 20(5):552–561, 1999.

- [52] S.S. Sazhin, P.A. Krutitskii, S.B. Martynov, D. Mason, M.R. Heikal, and E.M. Sazhina. Transient heating of a semitransparent spherical body. *International Journal of Thermal Sciences*, 46(5):444–457, 2007.
- [53] R.B. Bird, W.E. Stewart, and E.N. Lightfoot. *Transport Phenomena*. John Wiley & Sons, Chichester, 2002.
- [54] G. Brenn. Concentration fields in evaporating droplets. *International Journal of Heat and Mass Transfer*, 48:395–402, 2005.
- [55] C. Maqua, G. Castanet, and F. Lemoine. Bi-component droplets evaporation: temperature measurements and modelling. *Fuel*, 87:2932–2942, 2008.
- [56] G.M. Faeth. Evaporation and combustion of sprays. *Progress in Energy and Combustion Science*, 9(1-2):1–76, 1983.
- [57] A.Y. Tong and W.A. Sirignano. Multicomponent transient droplet vaporization with internal circulation: integral equation formulation and approximate solution. *Numerical Heat Transfer*, 10(3):253–278, 1986.
- [58] G. Continillo and W.A. Sirignano. Unsteady, spherically-symmetric flame propagation through multicomponent fuel spray clouds. In *Modern research topics in aerospace propulsion- In honor of Corrado Casci(A 91-45656 19-31)*, volume 1, pages 173–198. New York, Springer-Verlag, 1991.
- [59] M. Klingsporn and U. Renz. Vaporization of a binary unsteady spray at high temperature and high pressure. *International Journal of Heat and Mass Transfer*, 37:265–272, 1994.
- [60] P.L.C. Lage, C.M. Hackenberg, and R.H. Rangel. Nonideal vaporization of dilating binary droplets with radiation absorption. *Combustion and Flame*, 101:36–44, 1995.
- [61] D.J. Torres, P.J. O’Rourke, and A.A. Amsden. Efficient multicomponent fuel algorithm. *Combustion Theory and Modelling*, 7(1):67–86, 2003.
- [62] J. Tamim and W.L.H. Hallett. A continuous thermodynamics model for multicomponent droplet vaporization. *Chemical Engineering Science*, 50(18):2933–2942, 1995.

- [63] A.M. Lippert and R.D. Reitz. Modeling of Multicomponent Fuels Using Continuous Distributions With Application to Droplet Evaporation and Sprays. *SAE Technical Paper*, SP-1306:No. 972882, 1997.
- [64] G-S. Zhu, R.D. Reitz, and Aggarwal S.K. Gas-phase unsteadiness and its influence on droplet vaporization in sub- and super-critical environments. *International Journal of Heat and Mass Transfer*, 44:3081–93, 2001.
- [65] M. Burger, R. Schmehl, K. Prommersberger, O. Schfer, R. Koch, and S. Wittig. Droplet evaporation modelling by the distillation curve model: accounting for kerosene fuel and elevated pressures. *International Journal of Heat and Mass Transfer*, 46:4403–4412, 2003.
- [66] S.S. Sazhin, A. Elwardany, E.M. Sazhina, and M.R. Heikal. A quasi-discrete model for heating and evaporation of complex multicomponent hydrocarbon fuel droplets. *International Journal of Heat and Mass Transfer*, 54:4325–4332, (2011).
- [67] F. Cooper. Heat transfer from a sphere to an infinite medium. *International Journal of Heat and Mass Transfer*, 20(9):991–993, 1977.
- [68] J. Bellan. Supercritical (and subcritical) fluid behavior and modelling: drops, steams, shear and mixing layers, jets and sprays. *Progress in Energy and Combustion Science*, 26:329–66, 2000.
- [69] S.D. Givler and J. Abraham. Supercritical droplet vaporization and combustion studies. *Progress in Energy and Combustion Science*, 22:1–28, 1996.
- [70] F. Mashayek and R.V.R. Pandya. Analytical description of particle/droplet-laden turbulent flows. *Progress in Energy and Combustion Science*, 29(4):329–378, 2003.
- [71] E. Babinsky and P.E. Sojka. Modeling drop size distributions. *Progress in Energy and Combustion Science*, 28(4):303–329, 2002.
- [72] S.D. Sovani, P.E. Sojka, and A.H. Lefebvre. Effervescent atomization. *Progress in Energy and Combustion Science*, 27(4):483–521, 2001.

- [73] E. Loth. Numerical approaches for motion of dispersed particles, droplets and bubbles. *Progress in Energy and Combustion Science*, 26(3):161–223, 2000.
- [74] M. Orme. Experiments on droplet collisions, bounce, coalescence and disruption. *Progress in Energy and Combustion Science*, 23(1):65–79, 1997.
- [75] H.A. Dwyer, P. Stapf, and R. Maly. Unsteady vaporization and ignition of a three-dimensional droplet array. *Combustion and Flame*, 121(1-2):181–194, 2000.
- [76] K. Harstad and J. Bellan. Evaluation of commonly used assumptions for isolated and cluster heptane drops in nitrogen at all pressures. *Combustion and Flame*, 127(1-2):1861–1879, 2001.
- [77] F. Mashayek. Dynamics of evaporating drops. part ii: free oscillations. *International Journal of Heat and Mass Transfer*, 44(8):1527–1541, 2001.
- [78] F. Mashayek, N. Ashgriz, W.J. Minkowycz, and B. Shotorban. Coalescence collision of liquid drops. *International Journal of Heat and Mass Transfer*, 46(1):77–89, 2003.
- [79] C. Mihálykó, B.G. Lakatos, A. Matejdesz, and T. Blicke. Population balance model for particle-to-particle heat transfer in gas–solid systems. *International Journal of Heat and Mass Transfer*, 47(6):1325–1334, 2004.
- [80] M. Shusser and D. Weihs. Stability of rapidly evaporating droplets and liquid shells. *International Journal of Multiphase Flow*, 27(2):299–345, 2001.
- [81] K. Kamiuto and S. San Yee. Correlated radiative transfer through a packed bed of opaque spheres. *International Communications in Heat and Mass Transfer*, 32(1-2):133–139, 2005.
- [82] E.F. Crafton and W.Z. Black. Heat transfer and evaporation rates of small liquid droplets on heated horizontal surfaces. *International Journal of Heat and Mass Transfer*, 47(6):1187–1200, 2004.
- [83] Y. Meleán and L.D.G. Sigalotti. Coalescence of colliding van der waals liquid drops. *International Journal of Heat and Mass Transfer*, 48(19-20):4041–4061, 2005.

- [84] R.T. Imaoka and W.A. Sirignano. A generalized analysis for liquid-fuel vaporization and burning. *International Journal of Heat and Mass Transfer*, 48(21):4342–4353, 2005.
- [85] R.T. Imaoka and W.A. Sirignano. Transient vaporization and burning in dense droplet arrays. *International Journal of Heat and Mass Transfer*, 48(21):4354–4366, 2005.
- [86] S.G. Kandlikar and M.E. Steinke. Contact angles and interface behavior during rapid evaporation of liquid on a heated surface. *International Journal of Heat and Mass Transfer*, 45:3771–80, 2002.
- [87] S.C. Li. Spray stagnation flames. *Progress in Energy and Combustion Science*, 23(4):303–347, 1997.
- [88] C.H. Tsai, S.S. Hou, and T.H. Lin. Spray flames in a one-dimensional duct of varying cross-sectional area. *International Journal of Heat and Mass Transfer*, 48(11):2250–2259, 2005.
- [89] C. Crua, D.A. Kennaird, S.S. Sazhin, M.R. Heikal, and M.R. Gold. Diesel autoignition at elevated in-cylinder pressures. *International Journal of Engine Research*, 5(4):365–374, 2004.
- [90] S.S. Sazhin, E.M. Sazhina, and M.R. Heikal. Modelling of the gas to fuel droplets radiative exchange. *Fuel*, 79(14):1843–1852, 2000.
- [91] L.A. Dombrovsky, S.S. Sazhin, E.M. Sazhina, G. Feng, M.R. Heikal, M.E.A. Bardsley, and S.V. Mikhalovsky. Heating and evaporation of semi-transparent diesel fuel droplets in the presence of thermal radiation. *Fuel*, 80(11):1535–1544, 2001.
- [92] L.A. Dombrovsky, S.S. Sazhin, S.V. Mikhalovsky, R. Wood, and M.R. Heikal. Spectral properties of diesel fuel droplets. *Fuel*, 82(1):15–22, 2003.
- [93] L. Dombrovsky and S. Sazhin. Absorption of thermal radiation in a semi-transparent spherical droplet: a simplified model. *International Journal of Heat and Fluid Flow*, 24(6):919–927, 2003.

- [94] S.S. Sazhin, W.A. Abdelghaffar, E.M. Sazhina, SV Mikhailovsky, S.T. Meikle, and C. Bai. Radiative heating of semi-transparent diesel fuel droplets. *Journal of Heat Transfer*, 126:105, 2004.
- [95] L. Dombrovsky and S. Sazhin. Absorption of external thermal radiation in asymmetrically illuminated droplets. *Journal of Quantitative Spectroscopy and Radiative Transfer*, 87(2):119–135, 2004.
- [96] B. Abramzon and S. Sazhin. Convective vaporization of a fuel droplet with thermal radiation absorption. *Fuel*, 85(1):32–46, 2006.
- [97] S.S. Sazhin, T. Kristyadi, W.A. Abdelghaffar, S. Begg, M.R. Heikal, S.V. Mikhailovsky, S.T. Meikle, and O. Al-Hanbali. Approximate analysis of thermal radiation absorption in fuel droplets. *Journal of Heat Transfer*, 129:1246, 2007.
- [98] Ch Soret. Sur l'état d'équilibre que prend au point de vue de sa concentration une dissolution saline primitivement homogène dont deux parties sont portées à des températures différentes. *Archives des Sciences Physiques et Naturelles*, 2:48–61, 1879.
- [99] S.R. de Groot and P. Mazur. *Non-equilibrium Thermodynamics*. Amsterdam: North-Holland Publishing Company, 1962.
- [100] R.M.L. Coelho and A. Silva Telles. Extended graetz problem accompanied by dufour and soret effects. *International Journal of Heat and Mass Transfer*, 45(15):3101–3110, 2002.
- [101] A. Postelnicu. Influence of a magnetic field on heat and mass transfer by natural convection from vertical surfaces in porous media considering Soret and Dufour effects. *International Journal of Heat and Mass Transfer*, 47:1467–72, 2004.
- [102] V. Gopalakrishnan and J. Abraham. Effects of multicomponent diffusion on predicted ignition characteristics of an n-heptane diffusion flame. *Combustion and Flame*, 136:557–566, 2004.

- [103] A.P. Kryukov, V.Y. Levashov, and S.S. Sazhin. Evaporation of diesel fuel droplets: kinetic versus hydrodynamic models. *International Journal of Heat and Mass Transfer*, 47(12):2541–2549, 2004.
- [104] S.S. Sazhin, I.N. Shishkova, A.P. Kryukov, V.Y. Levashov, and M.R. Heikal. Evaporation of droplets into a background gas: Kinetic modelling. *International Journal of Heat and Mass Transfer*, 50(13-14):2675–2691, 2007.
- [105] E.M. Kartashov. *Analytical Methods in the Thermal Conductivity Theory of Solids*. Vyshaya Shkola, 2001 (in Russian).
- [106] H.S. Carslaw and J.C. Jaeger. *Conduction of Heat in Solids*. Clarendon Press, Oxford, 1986.
- [107] L.A. Dombrovsky. Absorption of thermal radiation in large semi-transparent particles at arbitrary illumination of a polydisperse system. *International Journal of Heat and Mass Transfer*, 47:5511–5522, 2004.
- [108] B. Abramzon and S. Sazhin. Droplet vaporization model in the presence of thermal radiation. *International Journal of Heat and Mass Transfer*, 48:1868–1873, 2005.
- [109] S. Savović and J. Caldwell. Finite difference solution of one-dimensional stefan problem with periodic boundary conditions. *International Journal of Heat and Mass Transfer*, 46:2911–2916, 2003.
- [110] J. Caldwell and Y.Y. Kwan. Numerical methods for one-dimensional stefan problems. *Communications in Numerical Methods in Engineering*, 20(7):535–545, 2004.
- [111] J. Caldwell and S. Savović. Numerical solution of Stefan problem by variable space grid and boundary immobilization method. *Journal of Mathematical Sciences*, 13:67–79, 2002.
- [112] J. Caldwell and Y.Y. Kwan. Starting solutions for the boundary immobilization method. *Communications in Numerical Methods in Engineering*, 21:289–295, 2005.

- [113] S. Savović and J. Caldwell. Finite-difference solution of one-dimensional Stefan problem with periodic boundary conditions. *International Journal of Heat and Mass Transfer*, 46:2911–2916, 2003.
- [114] S. Kutluay, A.R. Bahadir, A. Ozdes, S. Kutluay, AR Bahadir, and A. Özdeş. The numerical solution of one-phase classical stefan problem. *Journal of Computational and Applied Mathematics*, 81(1):135–144, 1997.
- [115] P.C. Meek and J. Norbury. Nonlinear moving boundary problems and a Keller box scheme. *SIAM Journal on Numerical Analysis*, 21:883–893, 1984.
- [116] S.L. Mitchell and M. Vynnycky. Finite-difference methods with increased accuracy and correct initialization for one-dimensional Stefan problems. *Applied Mathematics and Computation*, 215:1609–1621, 2009.
- [117] M. Vynnycky and S.L. Mitchell. On the solution of Stefan problems with delayed onset of phase change. Presented at HEFAT2010, 7th International Conference on Heat Transfer, Fluid Mechanics and Thermodynamics, 19-21 July 2010, Antalya, Turkey, 2010.
- [118] A. Esen and S. Kutluay. A numerical solution of the Stefan problem with a Neumann-type boundary condition by enthalpy method. *Applied Mathematics and Computation*, 148:321–329, 2004.
- [119] J. Caldwell and C.-C. Chan. Spherical solidification by the enthalpy method and the heat balance integral method. *Applied Mathematical Modelling*, 24:45–53, 2000.
- [120] F. Liu and D. L. S. McElwain. A computationally efficient solution technique for moving-boundary problems in finite media. *IMA Journal of Applied Mathematics*, 59(1):71–84, 1997.
- [121] Rizwan-uddin. A nodal method for phase change moving boundary problems. *International Journal of Computational Fluid Dynamics*, 11:211–221, 1999.
- [122] J. Caldwell and C.K. Chiu. Numerical solution of one-phase Stefan problems by the heat balance integral method, Part I - cylindrical and spherical geo-

- metries. *Communications in Numerical Methods in Engineering*, 16:569–583, 2000.
- [123] J. Caldwell and C.K. Chiu. Numerical solution of one-phase Stefan problems by the heat balance integral method, Part II - special small time starting procedure. *Communications in Numerical Methods in Engineering*, 16:585–593, 2000.
- [124] T.R. Goodman. The heat-balance integral and its application to problems involving a change of phase. *Transactions of the ASME Journal*, 80(2):335–342, 1958.
- [125] S.L. Mitchell and T.G. Myers. A heat balance integral method for one-dimensional finite ablation. *AIAA Journal Thermophysics and Heat Transfer*, 22(2): 508–514, 2008.
- [126] S.L. Mitchell and T.G. Myers. Approximate solution methods for one-dimensional solidification from an incoming fluid. *Applied Mathematics and Computation*, 202(1):311–326, 2008.
- [127] T.G. Myers, S.L. Mitchell, G. Muchatibaya, and M.Y. Myers. A cubic heat balance integral method for one-dimensional melting of a finite thickness layer. *International Journal of Heat and Mass Transfer*, 50: 5305–5317, 2007.
- [128] T.G. Myers. Optimizing the exponent in the heat balance and refined integral methods. Submitted to *Int. Comm. Heat & Mass Trans.*, 2008.
- [129] S.L. Mitchell and T.G. Myers. Application of standard and refined heat balance integral methods to one-dimensional Stefan problems. *SIAM Review*, 52(1): 57–86, 2010.
- [130] A.N. Tikhonov and A.A. Samarsky. *Equations of Mathematical Physics*. Nauka Publishing House, 1972 (in Russian).
- [131] F.P. Incropera and D.P. DeWitt. *Fundamentals of Heat and Mass Transfer*. John Wiley & Sons;, New York, 1996.
- [132] V. S. Vladimirov. *Equations of Mathematical Physics*. Marcel Dekker, N, 1971.

# Appendices

## Appendix 1

### Convergence of the Series in $G_1(t, \tau, \xi)$ and Estimate of $G_1(t, \tau, \xi)$ at $t - \tau \rightarrow 0$

Let us assume that

$$0 \leq \tau \leq t < t_e = -1/\alpha$$

and introduce the new function:

$$f(t, \tau) \equiv -\frac{1}{\alpha R_{d0}} \left( \frac{1}{R_d(t)} - \frac{1}{R_d(\tau)} \right) = \frac{t - \tau}{R_d(t)R_d(\tau)}. \quad (A11)$$

In the case of a time step,  $t_e$  needs to be replaced by  $\Delta t$ . As it was done earlier, to simplify the notation it is assumed that  $t_0$  (the start of the time step) is equal to zero. This comment and assumption apply to both Appendices 1 and 2. Note that

$$f(t, \tau) \geq \frac{t - \tau}{R_{d0}^2} \quad (A12)$$

since  $\alpha < 0$  and  $R_d(t) \leq R_{d0}$ .

It follows from (2.31) and the estimate  $\lambda_n > n$  for  $n > 1$  that  $\|v_n\|^2 > 1/4$  for  $n > 1$ . Therefore:

$$\|v_n\|^2 \geq c_0, \quad n \geq 1, \quad (A13)$$

where  $c_0 = \min\{\|v_1\|^2, 1/4\}$  is a positive constant.

Condition (A12) allows us to make the following estimate:

$$\exp[-\kappa \lambda_n^2 f(t, \tau)] \leq \exp\left[-\kappa n^2 \frac{t - \tau}{R_{d0}^2}\right], \quad n > 1, \quad (A14)$$

where we took into account that  $\lambda_n > n$  for  $n > 1$  (see Equation (17) in [15]). Using (A14) one can conclude that the series in  $G_1(t, \tau, \xi)$  converges absolutely and

uniformly to the continuous function for  $(t - \tau, \xi) \in [\delta, -1/\alpha) \times [0, 1]$  for any small  $\delta > 0$  since:

$$\exp\left[-\kappa n^2 \frac{t - \tau}{R_{d0}^2}\right] \leq \exp\left[-\kappa n^2 \frac{\delta}{R_{d0}^2}\right], \quad |\sin \lambda_n \xi| \leq 1. \quad (A15)$$

Indeed, each term with  $n > 1$  in the series in  $G_1(t, \tau, \xi)$  for  $(t - \tau, \xi) \in [\delta, -1/\alpha) \times [0, 1]$  can be majorized by the corresponding term of the convergent number series

$$\kappa c_0^{-1} \exp\left(-\kappa n^2 \frac{\delta}{R_{d0}^2}\right).$$

Now we estimate  $G_1(t, \tau, \xi)$  for small  $t - \tau > 0$ . Inequalities (A13) and (A14) allow us to write:

$$\begin{aligned} |G_1(t, \tau, \xi)| &\leq c_0^{-1} \kappa \left\{ 1 + \sum_{n=2}^{\infty} \exp\left[-\kappa n^2 f(t, \tau)\right] \right\} \\ &\leq c_0^{-1} \kappa \left\{ 1 + \sum_{n=2}^{\infty} \exp\left[-\kappa n^2 (t - \tau)/R_{d0}^2\right] \right\} \equiv \tilde{G}(t - \tau). \end{aligned} \quad (A16)$$

The sum  $\sum_{n=2}^{\infty} \exp[-\kappa n^2 (t - \tau)/R_{d0}^2]$  can be considered as a sum of areas of polygons of unit width placed under the curve  $\exp[-\kappa y^2 (t - \tau)/R_{d0}^2]$ . This sum is less than the area under this curve. Hence,

$$\begin{aligned} \sum_{n=2}^{\infty} \exp\left[-\kappa n^2 (t - \tau)/R_{d0}^2\right] &< \int_1^{\infty} \exp\left[-\kappa y^2 (t - \tau)/R_{d0}^2\right] dy \\ &< \int_0^{\infty} \exp\left[-\kappa y^2 (t - \tau)/R_{d0}^2\right] dy = \frac{R_{d0}}{\sqrt{\kappa(t - \tau)}} \int_0^{\infty} \exp\left[-z^2\right] dz \\ &= \frac{R_{d0} \sqrt{\pi}}{2\sqrt{\kappa(t - \tau)}} \end{aligned} \quad (A17)$$

Having substituted (A17) into (A16) we obtain:

$$|G_1(t, \tau, \xi)| \leq \tilde{G}(t - \tau) < c_0 \kappa \left[ 1 + \frac{R_{d0} \sqrt{\pi}}{2\sqrt{\kappa(t - \tau)}} \right] < \tilde{c} / \sqrt{t - \tau}, \quad (A18)$$

$$t - \tau \in (0, t_{00}],$$

for any small fixed  $t_{00} \in (0, -1/\alpha)$ . The new constant  $\tilde{c}$  depends on  $t_{00}$ . Inequality (A18) holds uniformly for  $\xi \in [0, 1]$ .

## Appendix 2

### Numerical solution of Equation (2.51)

Let  $\psi(t) \equiv W(t, 1)$  and rewrite Equation (2.51) as:

$$\psi(t) = \mathcal{V}(t, 1) - \int_0^t [\mu_0(\tau) - h_1(\tau)\psi(\tau)] G(t, \tau, 1) d\tau. \quad (\text{A21})$$

We look for the solution of Equation (A21) for  $t \in [0, \hat{t}]$ , where  $\hat{t}$  is a constant,  $\hat{t} < t_e$ . Let  $\Delta t = \hat{t}/N$  and  $t_n = n\Delta t$ , where  $N$  is the total number of time steps,  $n = 0, 1, \dots, N$  is the number of the current time step. Note that  $t_0 = 0$  and  $t_N = \hat{t}$ . Discretisation of Equation (A21) gives:

$$\psi(t_n) = \mathcal{V}(t_n, 1) - \sum_{j=1}^n \int_{t_{j-1}}^{t_j} [\mu_0(\tau) - h_1(\tau)\psi(\tau)] G(t_n, \tau, 1) d\tau, \quad (\text{A22})$$

where  $n = 1, \dots, N$ . Note that  $\psi(t_0) = \psi(0) = \mathcal{V}(0, 1) = W_0(1)$  is a known constant.

The first  $(n - 1)$  integrals in this sum can be approximated as:

$$\begin{aligned} & \int_{t_{j-1}}^{t_j} [\mu_0(\tau) - h_1(\tau)\psi(\tau)] G(t_n, \tau, 1) d\tau \\ & \approx \{ \mu_0(\tau_j) - h_1(\tau_j) [\psi(t_j) + \psi(t_{j-1})] / 2 \} G(t_n, \tau_j, 1) \Delta t, \end{aligned} \quad (\text{A23})$$

where  $j = 1, 2, \dots, n - 1$ ,  $\tau_j = t_j - \frac{1}{2}\Delta t$ . Approximation (A23) is valid since all functions in the integrand are continuous and we look for the solution in the class of continuous functions.

In Approximation (A23) the known functions are taken at  $\tau = \tau_j$  (middle of the range  $[t_{j-1}, t_j]$ ), while the unknown functions are taken as the average of the values at the end points  $t_{j-1}$  and  $t_j$ .

The last term in the sum in Equation (A22) requires special investigation since the kernel  $G(t_n, \tau, 1)$  in the integrand becomes singular when  $\tau \rightarrow t_n - 0$  (see Estimate (A18)). All other functions in this integrand, including the unknown function  $\psi(t)$ , are assumed continuous. Hence, we can write:

$$\begin{aligned} & \int_{t_{n-1}}^{t_n} [\mu_0(\tau) - h_1(\tau)\psi(\tau)] G(t_n, \tau, 1) d\tau \\ & \approx \left\{ \mu_0(\tau_n) - h_1(\tau_n) \frac{\psi(t_n) + \psi(t_{n-1})}{2} \right\} \int_{t_{n-1}}^{t_n} G(t_n, \tau, 1) d\tau. \end{aligned} \quad (\text{A24})$$

In view of Series (2.53) we can write:

$$\int_{t_{n-1}}^{t_n} G(t_n, \tau, 1) d\tau$$

$$\begin{aligned}
&= -2\kappa \sum_{m=1}^{\infty} \frac{\lambda_m^2}{h_0^2 + h_0 + \lambda_m^2} \int_{t_{n-1}}^{t_n} \frac{1}{R_d^2(\tau)} \exp \left[ \frac{\kappa \lambda_m^2}{\alpha R_{d0}} \left( \frac{1}{R_d(t_n)} - \frac{1}{R_d(\tau)} \right) \right] d\tau \\
&= -2\kappa \sum_{m=1}^{\infty} \frac{\lambda_m^2}{h_0^2 + h_0 + \lambda_m^2} \frac{1}{\kappa \lambda_m^2} \exp \left[ \frac{\kappa \lambda_m^2}{\alpha R_{d0}} \left( \frac{1}{R_d(t_n)} - \frac{1}{R_d(\tau)} \right) \right] \Big|_{\tau=t_{n-1}}^{\tau=t_n} \\
&= -2\kappa \sum_{m=1}^{\infty} \frac{\lambda_m^2}{h_0^2 + h_0 + \lambda_m^2} \frac{1}{\kappa \lambda_m^2} \left\{ 1 - \exp \left[ \frac{\kappa \lambda_m^2}{\alpha R_{d0}} \left( \frac{1}{R_d(t_n)} - \frac{1}{R_d(t_{n-1})} \right) \right] \right\} \\
&= -2 \sum_{m=1}^{\infty} \frac{1}{h_0^2 + h_0 + \lambda_m^2} \left\{ 1 - \exp \left[ \frac{-\kappa \lambda_m^2 \Delta t}{R_d(t_n) R_d(t_{n-1})} \right] \right\} \\
&= -\frac{1}{1 + h_0} + 2 \sum_{m=1}^{\infty} \frac{1}{h_0^2 + h_0 + \lambda_m^2} \exp \left[ \frac{-\kappa \lambda_m^2 \Delta t}{R_d(t_n) R_d(t_{n-1})} \right] \equiv g_n. \tag{A25}
\end{aligned}$$

If  $h_0 = 0$  then  $\lambda_m = \pi(m - (1/2))$  in series (A25). The combination of Formulae (A23) – (A25) allows us to present the discretised form of Equation (A21) (Equation (A22)) as follows:

$$\begin{aligned}
\psi(t_n) &= \mathcal{V}(t_n, 1) - \{\mu_0(\tau_n) - h_1(\tau_n) [\psi(t_n) + \psi(t_{n-1})] / 2\} g_n \\
&\quad - \sum_{j=1}^{n-1} \{\mu_0(\tau_j) - h_1(\tau_j) [\psi(t_j) + \psi(t_{j-1})] / 2\} G(t_n, \tau_j, 1) \Delta t, \tag{A26}
\end{aligned}$$

where  $n = 1, 2, \dots, N$ , and  $g_n$  is given by Series (A25).

Equation (A26) can be rearranged to the form particularly convenient for the numerical analysis:

$$\begin{aligned}
\psi(t_n) &= \frac{1}{1 - 0.5h_1(\tau_n)g_n} \left\{ \mathcal{V}(t_n, 1) - \left[ \mu_0(\tau_n) - \frac{h_1(\tau_n)\psi(t_{n-1})}{2} \right] g_n \right. \\
&\quad \left. - \sum_{j=1}^{n-1} \{\mu_0(\tau_j) - h_1(\tau_j) [\psi(t_j) + \psi(t_{j-1})] / 2\} G(t_n, \tau_j, 1) \Delta t \right\}. \tag{A27}
\end{aligned}$$

For  $n = 1$  the sum in Formula (A27) is equal to zero and  $\psi(t_0)$  is a known constant (see above). This allows us to calculate  $\psi(t_1)$  explicitly using Formula (A27). Once  $\psi(t_1)$  has been calculated we can use Formula (A27) for calculation of  $\psi(t_2)$  etc. At the  $n$ th step, Formula (A27) is used for calculation of  $\psi(t_n)$  using the values of  $\psi(t_0), \psi(t_1), \dots, \psi(t_{n-1})$  calculated at the previous steps. At this step all terms in the sum  $\sum_{j=1}^{n-1}$  are already known.

Once we have obtained the numerical solution to the integral equation (2.51) we are in a position to calculate numerically function  $W(t, \xi)$  using its integral representation (2.49), where:

$$\hat{\mu}_0(t) = \mu_0(t) - h_1(t)\psi(t).$$

Using the same discretisation by  $t$  and  $\tau$  as above, we can present the discretised form of this representation as:

$$\begin{aligned}
W(\hat{t}, \xi) &= \mathcal{V}(\hat{t}, \xi) - \sum_{j=1}^N \int_{t_{j-1}}^{t_j} \hat{\mu}_0(\tau) G(\hat{t}, \tau, \xi) d\tau \\
&= \mathcal{V}(\hat{t}, \xi) - \sum_{j=1}^{N-1} \frac{\hat{\mu}_0(t_{j-1}) + \hat{\mu}_0(t_j)}{2} G(\hat{t}, \tau_j, \xi) \Delta t - \frac{\hat{\mu}_0(t_{N-1}) + \hat{\mu}_0(t_N)}{2} \\
&\quad \times \int_{t_{N-1}}^{t_N} G(t_N, \tau, \xi) d\tau. \tag{A29}
\end{aligned}$$

Note that  $t_N = \hat{t}$ . If  $N = 1$  then the sum in Equation (A29) is equal to zero. The last integral in Equation (A29) is improper and needs to be calculated separately. Remembering the definition of  $G(t, \tau, \xi)$ , and almost repeating the derivation of Equation (A25), we can write:

$$\begin{aligned}
\int_{t_{N-1}}^{t_N} G(t_N, \tau, \xi) d\tau &= -2 \sum_{m=1}^{\infty} \frac{h_0^2 + \lambda_m^2}{h_0^2 + h_0 + \lambda_m^2} \frac{\sin \lambda_m \sin \lambda_m \xi}{\lambda_m^2} \\
&\quad \times \left\{ 1 - \exp \left[ \frac{-\kappa \lambda_m^2 \Delta t}{R_d(t_N) R_d(t_{N-1})} \right] \right\} \\
&= -\frac{\xi}{1 + h_0} + 2 \sum_{m=1}^{\infty} \frac{h_0^2 + \lambda_m^2}{h_0^2 + h_0 + \lambda_m^2} \frac{\sin \lambda_m \sin \lambda_m \xi}{\lambda_m^2} \exp \left[ \frac{-\kappa \lambda_m^2 \Delta t}{R_d(t_N) R_d(t_{N-1})} \right].
\end{aligned}$$

Having substituted the latter equation into (A29), and remembering the definition of  $\hat{\mu}_0(t_j)$ , we obtain the required value of  $W(\hat{t}, \xi)$ .

## Appendix 3

### Numerical solution of the integral Equation (3.10)

Remembering Equations (3.6) and (3.8) we can rewrite Equation (3.10) as:

$$\nu(t) + \int_0^t \nu(\tau) \left\{ \frac{1}{\sqrt{t-\tau}} \Omega(t, \tau) + \omega(t, \tau) \right\} d\tau = 2\mu_0(t), \tag{A31}$$

where:

$$\begin{aligned}
\Omega(t, \tau) &= \frac{1}{\sqrt{\pi}} \left\{ -\frac{1}{2\sqrt{\kappa}} \frac{R_d(t) - R_d(\tau)}{t - \tau} + \sqrt{\kappa} H(t) \right\} \\
&\quad \times \exp \left[ -\frac{(R_d(t) - (R_d(\tau)))^2}{4\kappa(t - \tau)} \right], \tag{A32} \\
\omega(t, \tau) &= \frac{1}{\sqrt{\pi(t - \tau)}} \left\{ \frac{1}{2\sqrt{\kappa}} \frac{R_d(t) + R_d(\tau)}{t - \tau} - \sqrt{\kappa} H(t) \right\}
\end{aligned}$$

$$\times \exp \left[ -\frac{(R_d(t) + (R_d(\tau))^2)}{4\kappa(t - \tau)} \right], \quad (\text{A33})$$

Functions  $\Omega(t, \tau)$  and  $\omega(t, \tau)$  are continuous for  $\tau \in [0, t]$ . Hence, the singularity  $1/\sqrt{t - \tau}$  of the kernel in Equation (A31) is presented in an explicit form.

We look for the solution of Equation (A31) for  $t \in [0, \hat{t}]$ , where  $\hat{t} \leq t_e$  is an arbitrary, but fixed positive constant. Let  $\Delta t = \hat{t}/N$  and  $t_n = n\Delta t$ , where  $N$  is the total number of time steps,  $n = 0, 1, \dots, N$  is the number of the current time step. Note that  $t_0 = 0$  and  $t_N = \hat{t}$ . Discretisation of Equation (A31) gives:

$$\nu(t_n) + \sum_{j=1}^n \int_{t_{j-1}}^{t_j} \nu(\tau) \left\{ \frac{\Omega(t_n, \tau)}{\sqrt{t_n - \tau}} + \omega(t_n, \tau) \right\} d\tau = 2\mu_0(t_n), \quad (\text{A34})$$

where  $n = 0, 1, \dots, N$ . Note that

$$\nu(t_0) = \nu(0) = 2\mu_0(0)$$

is the known constant derived in Appendix 5.

The first  $(n - 1)$  terms in the sum in Equation (A34) can be approximated as:

$$\begin{aligned} & \int_{t_{j-1}}^{t_j} \nu(\tau) \left\{ \frac{\Omega(t_n, \tau)}{\sqrt{t_n - \tau}} + \omega(t_n, \tau) \right\} d\tau \\ & \approx \frac{\nu(t_j) + \nu(t_{j-1})}{2} \left\{ \frac{\Omega(t_n, \tau_j)}{\sqrt{t_n - \tau_j}} + \omega(t_n, \tau_j) \right\} \Delta t, \end{aligned} \quad (\text{A35})$$

where  $j = 1, 2, \dots, n-1$ ;  $\tau_j = t_j - \frac{\Delta t}{2}$ . This approximation is valid since all functions in the integrand are continuous, and we look for the solution in the class of continuous functions ( $\nu(t)$  should be continuous for  $t \geq 0$ ). In this approximation the known functions are taken at the points  $\tau = \tau_j$  (middle of the time interval  $[t_{j-1}, t_j]$ ), while the unknown function is taken as an arithmetic mean of its values at the times  $t_{j-1}$  and  $t_j$ .

The last term in the sum in Equation (A34) has an integrable singularity  $1/\sqrt{t - \tau}$  when  $\tau \rightarrow t-0$  (recall that functions  $\Omega(t, \tau)$  and  $\omega(t, \tau)$  are continuous for  $\tau \in [0, t]$ ).

This allows us to approximate this term as:

$$\begin{aligned} & \int_{t_{n-1}}^{t_n} \nu(\tau) \left\{ \frac{\Omega(t_n, \tau)}{\sqrt{t_n - \tau}} + \omega(t_n, \tau) \right\} d\tau \\ & \approx \frac{\nu(t_n) + \nu(t_{n-1})}{2} \left[ \Omega(t_n, \tau_n) \int_{t_{n-1}}^{t_n} \frac{d\tau}{\sqrt{t_n - \tau}} + \omega(t_n, \tau_n) \Delta t \right] \\ & = \frac{\nu(t_n) + \nu(t_{n-1})}{2} \left[ 2\Omega(t_n, \tau_n) \sqrt{t_n - t_{n-1}} + \omega(t_n, \tau_n) \Delta t \right] = (\nu(t_n) + \nu(t_{n-1})) g_n, \end{aligned} \quad (\text{A36})$$

where

$$g_n = \Omega(t_n, \tau_n)\sqrt{\Delta t} + \frac{\omega(t_n, \tau_n)\Delta t}{2}.$$

Equations (A35) and (A36) allow us to rewrite Equation (A34) in the form:

$$\nu(t_n)(1 + g_n) + \nu(t_{n-1})g_n + \sum_{j=1}^{n-1} \frac{\nu(t_j) + \nu(t_{j-1})}{2} \left\{ \frac{\Omega(t_n, \tau_j)}{\sqrt{t_n - \tau_j}} + \omega(t_n, \tau_j) \right\} \Delta t = 2\mu_0(t_n), \quad (\text{A37})$$

where  $n = 1, 2, \dots, N$ ; Equation (A37) can be rewritten in an alternative form:

$$\begin{aligned} \nu(t_n) &= -\frac{\nu(t_{n-1})g_n}{1 + g_n} - \frac{1}{1 + g_n} \sum_{j=1}^{n-1} \frac{\nu(t_j) + \nu(t_{j-1})}{2} \\ &\quad \times \left\{ \frac{\Omega(t_n, \tau_j)}{\sqrt{t_n - \tau_j}} + \omega(t_n, \tau_j) \right\} \Delta t + \frac{2\mu_0(t_n)}{1 + g_n}. \end{aligned} \quad (\text{A38})$$

Note that  $g_n$  is a continuous function of  $\Delta t$ , and  $g_n \rightarrow 0$  when  $\Delta t \rightarrow +0$ . Hence,  $1 + g_n \neq 0$  for a sufficiently small time step  $\Delta t$ . For  $n = 1$  the sum in Equation (A38) is equal to zero and  $\nu(t_0)$  is a known constant (see above). This allows us to calculate  $\nu(t_1)$  in an explicit form from Equation (A38). As soon as the value of  $\nu(t_1)$  is found we can use Equation (A38) to find  $\nu(t_2)$  etc. At the  $n$ th time step, Equation (A38) is used for calculating  $\nu(t_n)$ , based on the values of  $\nu(t_0)$ ,  $\nu(t_1)$ , ...,  $\nu(t_{n-1})$  calculated at the previous time steps. At this stage all terms in the sum  $\sum_{j=1}^{n-1}$  are already known.

In the limiting case when  $R_d(t) = R_d(\tau) = R_d = \text{const}$ , functions  $\Omega(t, \tau)$  and  $\omega(t, \tau)$  are simplified to:

$$\Omega(t, \tau) = \frac{1}{\sqrt{\pi}} \sqrt{\kappa} H(t), \quad (\text{A39})$$

$$\omega(t, \tau) = \frac{1}{\sqrt{\pi(t - \tau)}} \left\{ \frac{R_d}{\sqrt{\kappa(t - \tau)}} - \sqrt{\kappa} H(t) \right\} \exp \left[ -\frac{R_d^2}{\kappa(t - \tau)} \right]. \quad (\text{A310})$$

## Appendix 4

### Numerical calculation of the improper integrals in Equations (3.11) and (3.23)

The integrals in Equations (3.11) and (3.23) have the same type of integrable singularity as the integral in Equation (3.5). The following analysis will focus on the

latter equation which will enable us to simplify the notation. Let us rewrite this equation as:

$$v(R, \hat{t}) = \sum_{j=1}^N \int_{t_{j-1}}^{t_j} \nu(\tau) G(\hat{t}, \tau, R) d\tau, \quad (\text{A41})$$

where  $\hat{t} = t_N$ ,  $t_n = n\Delta t$ ,  $n = 0, 1, 2, \dots, N$ ,  $\Delta t = \hat{t}/N$ . In all integrals we can replace  $\nu(\tau)$  with the average values over the corresponding time interval  $(\nu(t_{j-1}) + \nu(t_j))/2$ . Moreover, in all integrals, except the last one, we can replace  $G(\hat{t}, \tau, R)$  with  $G(\hat{t}, \tau_j, R)$ , where  $\tau_j = (t_{j-1} + t_j)/2$ . As a result, Equation (A41) can be presented in a more explicit form:

$$v(R, \hat{t}) = \sum_{j=1}^{N-1} \frac{\nu(t_{j-1}) + \nu(t_j)}{2} G(\hat{t}, \tau_j, R) \Delta t + \frac{\nu(t_{N-1}) + \nu(t_N)}{2} \int_{t_{N-1}}^{t_N} G(\hat{t}, \tau, R) d\tau. \quad (\text{A42})$$

Firstly we assume that an *a priori* chosen  $R$  is not equal to  $R_d(\hat{t})$ . In this case  $G(\hat{t}, \tau, R)$ , as defined by Equation (3.6), approaches 0, when  $\tau \rightarrow \hat{t} - 0$ . Hence the singularity in the integrand is not present and the last time step can be treated as in all the previous time steps. This allows us to simplify Equation (A42) to:

$$v(R, \hat{t}) = \sum_{j=1}^N \frac{\nu(t_{j-1}) + \nu(t_j)}{2} G(\hat{t}, \tau_j, R) \Delta t. \quad (\text{A43})$$

In the case when  $R = R_d(\hat{t})$  the first exponent in Equation (3.6) tends to 1 when  $\tau \rightarrow \hat{t} - 0$ . This leads to a singularity  $(\hat{t} - \tau)^{-1/2}$  in the integrand in Equation (A42).

As a result, the integral in this equation can be presented as:

$$\begin{aligned} \int_{t_{N-1}}^{t_N} G(\hat{t}, \tau_N, R) d\tau &= \frac{\sqrt{\kappa}}{2\sqrt{\pi}} \left\{ \exp \left[ -\frac{(R - R_d(\tau_N))^2}{4\kappa(\hat{t} - \tau_N)} \right] \int_{t_{N-1}}^{t_N} \frac{d\tau}{\sqrt{\hat{t} - \tau}} \right. \\ &\quad \left. - \exp \left[ -\frac{(R + R_d(\tau_N))^2}{4\kappa(\hat{t} - \tau_N)} \right] \frac{\Delta t}{\sqrt{\hat{t} - \tau_N}} \right\} \\ &= \frac{\sqrt{\kappa}}{\sqrt{2\pi}} \left\{ \sqrt{2} \exp \left[ -\frac{(R - R_d(\tau_N))^2}{2\kappa\Delta t} \right] - \exp \left[ -\frac{(R + R_d(\tau_N))^2}{2\kappa\Delta t} \right] \right\} \sqrt{\Delta t}. \end{aligned} \quad (\text{A44})$$

The latter equation allows us to simplify the equation for  $v(R, \hat{t})$  for  $R = R_d(\hat{t})$  to:

$$\begin{aligned} v(R, \hat{t}) &= \sum_{j=1}^{N-1} \frac{\nu(t_{j-1}) + \nu(t_j)}{2} G(\hat{t}, \tau_j, R) \Delta t \\ &\quad + \frac{(\nu(t_{N-1}) + \nu(t_N))\sqrt{\kappa}}{2\sqrt{2\pi}} \left\{ \sqrt{2} \exp \left[ -\frac{(R - R_d(\tau_N))^2}{2\kappa\Delta t} \right] \right. \\ &\quad \left. - \exp \left[ -\frac{(R + R_d(\tau_N))^2}{2\kappa\Delta t} \right] \right\} \sqrt{\Delta t}. \end{aligned} \quad (\text{A45})$$

## Appendix 5

### Derivation of the expression for $\mu_0(0)$

Having substituted Equation (3.20) into Equation (3.19) and integrating by parts we obtain:

$$\begin{aligned} U'_R(t, R) \Big|_{R=R_d(t)} &= \int_0^{R_{\text{eff}}} (\zeta T_{d0}(\zeta)) \frac{\partial G_1(t, R, \zeta)}{\partial \zeta} \Big|_{R=R_d(t)} d\zeta \\ &= (\zeta T_{d0}(\zeta)) [G_2(t, R_d(t), \zeta)] \Big|_{\zeta=R_{\text{eff}}} - \int_0^{R_{\text{eff}}} [G_2(t, R, \zeta)] \Big|_{R=R_d(t)} (\zeta T_{d0}(\zeta))'_\zeta d\zeta, \end{aligned} \quad (\text{A51})$$

where

$$\begin{aligned} G_2(t, R, \zeta) &= -\frac{1}{\kappa} [G_0(t, R(t) - \zeta) + G_0(t, R(t) + \zeta)] \\ &= -\frac{1}{2\sqrt{\pi\kappa t}} \left[ \exp\left(-\frac{(R - \zeta)^2}{4\kappa t}\right) + \exp\left(-\frac{(R + \zeta)^2}{4\kappa t}\right) \right]. \end{aligned}$$

One can see that the first term on the right hand side of Equation (A51) approaches zero when  $t \rightarrow +0$  (there is no singularity at  $t = 0$ ) since  $R_{\text{eff}} - R_{d0} > 0$ . Hence, remembering Equation (3.16), we obtain

$$U'_R(t, R) \Big|_{R=R_d(t)} \rightarrow (\zeta T_{d0}(\zeta))'_\zeta \Big|_{\zeta=R_{d0}} \quad (\text{A52})$$

when  $t \rightarrow +0$ .

Following the same approach and remembering Equation (3.16), we obtain:

$$U(t, R) \Big|_{R=R_d(t)} \rightarrow (\zeta T_{d0}(\zeta)) \Big|_{\zeta=R_{d0}} = R_{d0} T_{d0}(R_{d0}) \quad (\text{A53})$$

when  $t \rightarrow +0$ . Remembering Equations (A52) and (A53), we obtain Equation (3.22) as a limiting case of Equation (3.18) when  $t \rightarrow +0$ .

## Appendix 6

### Derivation of Equation (4.42)

Remembering that Solution (4.41) is applied to a very short time step, changes of  $\mu_0(\tau)$  in the integrand before the exponential term can be ignored. This allows us to simplify (4.41) to

$$\Theta_n(t) = q_n \exp \left[ -\frac{(-1)^{\delta_{n,0}} D_l t \lambda_n^2}{R_{d0} R_d(t)} \right] + f_n \mu_0(t) -$$

$$f_n \mu_0(0) \left[ (-1)^{\delta_{n,0}} D_l \lambda_n^2 \int_0^t \frac{1}{R_d(\tau)^2} \exp \left[ (-1)^{\delta_{n,0}} \frac{D_l \lambda_n^2}{\alpha R_{d0}} \left( \frac{1}{R_d(t)} - \frac{1}{R_d(\tau)} \right) \right] d\tau \right]. \quad (\text{A61})$$

$\mu_0(\tau)$  in the integrand of (4.41) is taken at the beginning of the time step.

Remembering that

$$d(R_d(\tau)^{-1}) = -\frac{R'_d}{R_d^2(t)} d\tau$$

we can rearrange the last term in (A61) to

$$\begin{aligned} & (-1)^{\delta_{n,0}} D_l \lambda_n^2 \int_0^t \frac{1}{R_d(\tau)^2} \exp \left[ (-1)^{\delta_{n,0}} \frac{D_l \lambda_n^2}{\alpha R_{d0}} \left( \frac{1}{R_d(t)} - \frac{1}{R_d(\tau)} \right) \right] d\tau = \\ & \frac{(-1)^{\delta_{n,0}} D_l \lambda_n^2}{R'_d} \exp \left[ (-1)^{\delta_{n,0}} \frac{D_l \lambda_n^2}{\alpha R_{d0}} \left( \frac{1}{R_d(t)} \right) \right] \int_0^t \frac{R'_d}{R_d(\tau)^2} \exp \left[ (-1)^{\delta_{n,0}} \frac{D_l \lambda_n^2}{\alpha R_{d0}} \left( -\frac{1}{R_d(\tau)} \right) \right] d\tau = \\ & \frac{(-1)^{\delta_{n,0}} D_l \lambda_n^2}{R'_d} \exp \left[ (-1)^{\delta_{n,0}} \frac{D_l \lambda_n^2}{\alpha R_{d0}} \left( \frac{1}{R_d(t)} \right) \right] \frac{\alpha R_{d0}}{(-1)^{\delta_{n,0}} D_l \lambda_n^2} \left( \exp \left[ (-1)^{\delta_{n,0}} \frac{D_l \lambda_n^2}{\alpha R_{d0}} \left( -\frac{1}{R_d(t)} \right) \right] - \right. \\ & \quad \left. \exp \left[ (-1)^{\delta_{n,0}} \frac{D_l \lambda_n^2}{\alpha R_{d0}} \left( -\frac{1}{R_d(0)} \right) \right] \right) \\ & = \left( 1 - \exp \left[ (-1)^{\delta_{n,0}} \frac{D_l \lambda_n^2}{\alpha R_{d0}} \left( \frac{1}{R_d(t)} - \frac{1}{R_d(0)} \right) \right] \right) = \left( 1 - \exp \left[ -(-1)^{\delta_{n,0}} \frac{D_l \lambda_n^2 t}{R_{d0} R_d(t)} \right] \right). \end{aligned} \quad (\text{A62})$$

When deriving (A62) we took into account (2.8).

Having substituted (A62) into (A61), we obtain (4.42).

## Appendix 7

### Derivation of Formula (5.9)

Introducing a new variable

$$u = (T - T_{g0}(R_g)) R$$

we can simplify Equation (5.1) and initial and boundary conditions (5.3) – (5.4) to:

$$\frac{\partial u}{\partial t} = \kappa \frac{\partial^2 u}{\partial R^2} + RP(t, R), \quad (\text{A71})$$

$$u|_{t=0} = -T_0 R \quad (\text{A72})$$

$$u|_{R=R_b^-} = u|_{R=R_b^+}, \quad k_b \left[ R_b u'_R - u \right] \Big|_{R=R_b^-} = k_g \left[ R_b u'_R - u \right] \Big|_{R=R_b^+}, \quad u|_{R=R_g} = 0, \quad (\text{A73})$$

where

$$T_0 \equiv T_0(R) = \begin{cases} T_{g0}(R_g) - T_{b0}(R) & \text{when } R \leq R_b \\ T_{g0}(R_g) - T_{g0}(R) & \text{when } R_b < R \leq R_g, \end{cases}.$$

Conditions (A73) need to be amended by the boundary condition at  $R = 0$ . Since  $T - T_{g0}$  is finite at  $R = 0$  then  $u|_{R=0} = 0$ .

We look for the solution of Equation (A71) in the form:

$$u = \sum_{n=1}^{\infty} \Theta_n(t) v_n(R), \quad (\text{A74})$$

where functions  $v_n(R)$  form the full set of non-trivial solutions of the eigenvalue problem:

$$\frac{d^2 v}{dR^2} + a^2 \lambda^2 v = 0 \quad (\text{A75})$$

subject to boundary conditions:

$$\left. \begin{aligned} v|_{R=0} &= v|_{R=R_g} = 0 \\ v|_{R=R_b^-} &= v|_{R=R_b^+} \\ k_b [R_b v'_R - v]|_{R=R_b^-} &= k_g [R_b v'_R - v]|_{R=R_b^+} \end{aligned} \right\}, \quad (\text{A76})$$

where

$$a = \frac{1}{\sqrt{\kappa}} = \begin{cases} \sqrt{\frac{c_b \rho_b}{k_b}} \equiv a_b & \text{when } R \leq R_b \\ \sqrt{\frac{c_g \rho_g}{k_g}} \equiv a_g & \text{when } R_b < R \leq R_g. \end{cases} \quad (\text{A77})$$

Note that  $\lambda$  has dimension  $1/\sqrt{\text{time}}$ . We look for the solution of Equation (A75) in the form:

$$v(R) = \begin{cases} A \sin(\lambda a_b R) & \text{when } R \leq R_b \\ B \sin(\lambda a_g (R - R_g)) & \text{when } R_b < R \leq R_g. \end{cases} \quad (\text{A78})$$

Function (A78) satisfies boundary conditions (A76) at  $R = 0$ . Having substituted function (A78) into boundary conditions (A76) at  $R = R_b$  we obtain:

$$A \sin(\lambda a_b R_b) = B \sin(\lambda a_g (R_b - R_g)), \quad (\text{A79})$$

$$A k_b [R_b \lambda a_b \cos(\lambda a_b R_b) - \sin(\lambda a_b R_b)] = B k_g [R_b \lambda a_g \cos(\lambda a_g (R_b - R_g)) - \sin(\lambda a_g (R_b - R_g))]. \quad (\text{A710})$$

Condition (A79) is satisfied when:

$$\left. \begin{aligned} A &= [\sin(\lambda a_b R_b)]^{-1} \\ B &= [\sin(\lambda a_g (R_b - R_g))]^{-1} \end{aligned} \right\}. \quad (\text{A711})$$

Having substituted Equations (A711) into (A710) we obtain:

$$k_b [R_b \lambda a_b \cot(\lambda a_b R_b) - 1] = k_g [R_b \lambda a_g \cot(\lambda a_g (R_b - R_g)) - 1]. \quad (\text{A712})$$

Remembering the definitions of  $a_b$  and  $a_g$ , Equation (A712) can be simplified to:

$$\sqrt{k_b c_b \rho_b} \cot(\lambda a_b R_b) - \sqrt{k_g c_{pg} \rho_g} \cot(\lambda a_g (R_b - R_g)) = \frac{k_b - k_g}{R_b \lambda}. \quad (\text{A713})$$

Equation (A713) allows us to find a countable set of positive eigenvalues  $\lambda_n$  which can be arranged in ascending order  $0 < \lambda_1 < \lambda_2 < \dots$ . Note that the negative solutions  $-\lambda_n$  also satisfy Equation (A713) as both sides of this equation are odd functions of  $\lambda$ .  $\lambda = 0$ , however, does not satisfy this equation. Having substituted these values of  $\lambda_n$  into Equation (A78) and remembering Equations (A711) we obtain the expressions for eigenfunctions  $v_n$  in the form:

$$v_n(R) = \begin{cases} \frac{\sin(\lambda_n a_b R)}{\sin(\lambda_n a_b R_b)} & \text{when } R \leq R_b \\ \frac{\sin(\lambda_n a_g (R - R_g))}{\sin(\lambda_n a_g (R_b - R_g))} & \text{when } R_b < R \leq R_g \end{cases}. \quad (\text{A714})$$

It can be shown (see Appendix 8) that functions  $v_n(R)$  are orthogonal with weight

$$b = \begin{cases} k_b a_b^2 = c_b \rho_b & \text{when } R \leq R_b \\ k_g a_g^2 = c_{pg} \rho_g & \text{when } R_b < R \leq R_g \end{cases}.$$

This means that:  $\int_0^{R_g} v_n(R) v_m(R) b dR = \delta_{nm} \|v_n\|^2$ , where

$$\delta_{nm} = \begin{cases} 1 & \text{when } n = m \\ 0 & \text{when } n \neq m \end{cases}.$$

The proof of completeness of this set of functions is much more complicated (it is based on the methods of functional analysis and properties of Banach spaces [132]). Implicitly, the fact that this set is complete, could be supported by the agreement between our results in the limit  $R_g = \infty$  and  $T_{g0} = \text{const}$  and those of Cooper [67].

The norm of  $v_n$  with weight  $b$  is calculated as:

$$\begin{aligned} \|v_n\|^2 &= \int_0^{R_g} v_n^2 b dR = \int_0^{R_b} \left[ \frac{\sin(\lambda_n a_b R)}{\sin(\lambda_n a_b R_b)} \right]^2 c_b \rho_b dR + \int_{R_b}^{R_g} \left[ \frac{\sin(\lambda_n a_g (R - R_g))}{\sin(\lambda_n a_g (R_b - R_g))} \right]^2 c_{pg} \rho_g dR \\ &= \frac{c_b \rho_b}{2 \sin^2(\lambda_n a_b R_b)} \left[ R_b - \frac{\sin(2\lambda_n a_b R_b)}{2\lambda_n a_b} \right] \\ &\quad + \frac{c_{pg} \rho_g}{2 \sin^2(\lambda_n a_g (R_b - R_g))} \left[ R_g - R_b + \frac{\sin(2\lambda_n a_g (R_b - R_g))}{2\lambda_n a_g} \right] \end{aligned}$$

$$= \frac{c_b \rho_b R_b}{2 \sin^2(\lambda_n a_b R_b)} + \frac{c_{pg} \rho_g (R_g - R_b)}{2 \sin^2(\lambda_n a_g (R_b - R_g))} - \frac{k_b - k_g}{2 R_b \lambda_n^2}. \quad (A715)$$

When deriving Equation (A715) we took into account Equation (A713). Since all functions  $v_n$  satisfy boundary conditions (A76), function  $u$  defined by expression (A74) satisfies boundary conditions (A73). Let us expand  $RP(t, R)$  in a series over  $v_n$ :

$$RP(t, R) = \sum_{n=1}^{\infty} p_n(t) v_n(R), \quad (A716)$$

where:

$$p_n(t) = \frac{1}{\|v_n\|^2} \int_0^{R_g} RP(t, R) v_n(R) b dR.$$

Remembering that  $P(t, R) = 0$  at  $R > R_b$  the latter formula can be simplified to:

$$p_n(t) = \frac{c_b \rho_b}{\|v_n\|^2} \int_0^{R_b} RP(t, R) v_n(R) dR.$$

Having substituted Equations (A74) and (A716) into Equation (A71) we obtain:

$$\sum_{n=1}^{\infty} \Theta'_n(t) v_n(R) = - \sum_{n=1}^{\infty} \Theta_n(t) \lambda_n^2 v_n(R) + \sum_{n=1}^{\infty} p_n(t) v_n(R). \quad (A717)$$

When deriving Equation (A717) we took into account that functions  $v_n(R)$  satisfy Equation (A75) for  $\lambda = \lambda_n$ . Equation (A717) is satisfied if and only if:

$$\Theta'_n(t) = -\lambda_n^2 \Theta_n(t) + p_n(t). \quad (A718)$$

The initial condition for  $\Theta_n(t)$  can be obtained after substituting Expression (A74) into initial condition (A72) for  $u$ :

$$\sum_{n=1}^{\infty} \Theta_n(0) v_n(R) = -T_0 R. \quad (A719)$$

Remembering the orthogonality of  $v_n$  with the weight  $b$ , we obtain from Equation (A719):

$$\begin{aligned} \Theta_n(0) &= \frac{1}{\|v_n\|^2} \int_0^{R_g} (-T_0 R) v_n(R) b dR. \\ &= -\frac{c_b \rho_b}{\|v_n\|^2 \sin(\lambda_n a_b R_b)} \int_0^{R_b} T_0(R) R \sin(\lambda_n a_b R) dR \\ &\quad - \frac{c_{pg} \rho_g}{\|v_n\|^2 \sin(\lambda_n a_g (R_b - R_g))} \int_{R_b}^{R_g} T_0(R) R \sin(\lambda_n a_g (R - R_g)) dR \end{aligned}$$

If  $T_{g0}(R) = T_{g0}(R_g) = \text{const}$ , and  $T_{b0}(R) = \text{const}$ , then

$$T_0 \equiv T_0(R) = \begin{cases} T_{g0}(R_g) - T_{b0}(R_b) & \text{when } R \leq R_b \\ 0 & \text{when } R_b < R \leq R_g, \end{cases}$$

and the expression for  $\Theta_n(0)$  can be further simplified to:

$$\Theta_n(0) = -\frac{c_b \rho_b T_0}{\|v_n\|^2 \sin(\lambda_n a_b R_b)} \int_0^{R_b} R \sin(\lambda_n a_b R) dR = \frac{T_0 \sqrt{k_b c_b \rho_b}}{\lambda_n \|v_n\|^2} \left[ R_b \cot(\lambda_n a_b R_b) - \frac{1}{\lambda_n a_b} \right]. \quad (\text{A720})$$

The solution of Equation (A718) subject to the initial condition (A720) can be written as:

$$\Theta_n(t) = \exp(-\lambda_n^2 t) \Theta_n(0) + \int_0^t \exp(-\lambda_n^2 (t - \tau)) p_n(\tau) d\tau. \quad (\text{A721})$$

Equation (5.9) follows from the definition of  $u$  and Equations (A74) and (A721).

## Appendix 8

### Proof of orthogonality of $v_n(R)$ with the weight $b$

Remembering Expressions (A714) for  $v_n(R)$  we can write for  $n \neq m$ :

$$\begin{aligned} I_{nm} &\equiv \int_0^{R_g} v_n(R) v_m(R) b dR = \frac{k_b a_b^2}{\sin(\lambda_n a_b R_b) \sin(\lambda_m a_b R_b)} \int_0^{R_b} \sin(\lambda_n a_b R) \sin(\lambda_m a_b R) dR \\ &+ \frac{k_g a_g^2}{\sin(\lambda_n a_g (R_b - R_g)) \sin(\lambda_m a_g (R_b - R_g))} \int_{R_b}^{R_g} \sin(\lambda_n a_g (R - R_g)) \sin(\lambda_m a_g (R - R_g)) dR \\ &= \frac{k_b a_b^2}{2 \sin(\lambda_n a_b R_b) \sin(\lambda_m a_b R_b)} \left[ \frac{\sin((\lambda_n - \lambda_m) a_b R_b)}{(\lambda_n - \lambda_m) a_b} - \frac{\sin((\lambda_n + \lambda_m) a_b R_b)}{(\lambda_n + \lambda_m) a_b} \right] \\ &\quad - \frac{k_g a_g^2}{2 \sin(\lambda_n a_g (R_b - R_g)) \sin(\lambda_m a_g (R_b - R_g))} \\ &\quad \times \left[ \frac{\sin((\lambda_n - \lambda_m) a_g (R_b - R_g))}{(\lambda_n - \lambda_m) a_g} - \frac{\sin((\lambda_n + \lambda_m) a_g (R_b - R_g))}{(\lambda_n + \lambda_m) a_g} \right] \\ &= \frac{1}{2(\lambda_n - \lambda_m)} \left[ \frac{k_b a_b \sin((\lambda_n - \lambda_m) a_b R_b)}{\sin(\lambda_n a_b R_b) \sin(\lambda_m a_b R_b)} - \frac{k_g a_g \sin((\lambda_n - \lambda_m) a_g (R_b - R_g))}{\sin(\lambda_n a_g (R_b - R_g)) \sin(\lambda_m a_g (R_b - R_g))} \right] \\ &+ \frac{1}{2(\lambda_n + \lambda_m)} \left[ -\frac{k_b a_b \sin((\lambda_n + \lambda_m) a_b R_b)}{\sin(\lambda_n a_b R_b) \sin(\lambda_m a_b R_b)} + \frac{k_g a_g \sin((\lambda_n + \lambda_m) a_g (R_b - R_g))}{\sin(\lambda_n a_g (R_b - R_g)) \sin(\lambda_m a_g (R_b - R_g))} \right] \\ &= \frac{[k_b a_b (\cot(\lambda_m a_b R_b) - \cot(\lambda_n a_b R_b)) - k_g a_g (\cot(\lambda_m a_b (R_b - R_g)) - \cot(\lambda_n a_b (R_b - R_g)))]}{2(\lambda_n - \lambda_m)} \\ &+ \frac{[-k_b a_b (\cot(\lambda_m a_b R_b) + \cot(\lambda_n a_b R_b)) + k_g a_g (\cot(\lambda_m a_b (R_b - R_g)) + \cot(\lambda_n a_b (R_b - R_g)))]}{2(\lambda_n + \lambda_m)} \end{aligned}$$

Remembering Equation (A713) we can write:

$$\begin{aligned} I_{nm} &= \frac{1}{2(\lambda_n - \lambda_m)} \left( \frac{k_b - k_g}{R_b \lambda_m} - \frac{k_b - k_g}{R_b \lambda_n} \right) - \frac{1}{2(\lambda_n + \lambda_m)} \left( \frac{k_b - k_g}{R_b \lambda_m} + \frac{k_b - k_g}{R_b \lambda_n} \right) \\ &= \frac{k_b - k_g}{2R_b \lambda_n \lambda_m} - \frac{k_b - k_g}{2R_b \lambda_n \lambda_m} = 0. \end{aligned}$$